

Universitätsklinik für Thorax-, Herz- und Gefäßchirurgie
Thorax-, Herz- und Gefäßchirurgie

**Absorbable Zinc-based alloy for craniomaxillofacial
osteosynthesis implants**

**Thesis submitted as requirement to fulfill the degree
Doctor of Philosophy (Ph.D.)**

**at the
Faculty of Medicine
Eberhard Karls University
Tübingen**

by

Li, Ping

2020

Dean: Professor Dr. I. B. Autenrieth

First reviewer: Professor Dr. J. Geis-Gerstorfer
Second reviewer: Professor Dr. K. Schenke-Layland

Date of oral examination: 19.12.2019

Table of Contents

1. Introduction	1
1.1. Craniomaxillofacial osteosynthesis implants	1
1.2. Absorbable osteosynthesis materials	3
1.3. Limitations at Zn-based CMF osteosynthesis implants	6
1.4. Objectives	9
2. Study I: Mechanical characteristics, <i>in vitro</i> degradation, cytotoxicity, and antibacterial evaluation of Zn-4.0Ag alloy as a biodegradable material	11
2.1. Introduction	11
2.2. Materials and methods	13
2.3. Results and discussion	18
2.4. Conclusions	30
3. Study II: Selection of extraction medium influences cytotoxicity of Zinc and its alloys	32
3.1. Introduction	32
3.2. Materials and methods	35
3.3. Results	41
3.4. Discussion	48
3.5. Conclusions	55
4. Study III: Response of human periosteal cells to degradation products of zinc and its alloy	56
4.1. Introduction	57
4.2. Materials and methods	59
4.3. Results	65
4.4. Discussion	74
4.5. Conclusions	79
5. Discussion	81
5.1. Evaluation of cytotoxicity	81
5.2. Determination of degradation behavior	84
5.3. Investigation of biofunctionality features	87

6. Summary.....	91
7. German summary	92
8. Bibliography	93
9. Declaration of contribution of others	107
Acknowledgements	110
Curriculum vitae	111

1. Introduction

1. Introduction

1.1. Craniomaxillofacial osteosynthesis implants

1.1.1. Osteosynthesis implants for craniomaxillofacial applications

Bone fracture is a significant challenge for health, affecting hundreds of millions of people worldwide. At least tens of millions of fractures occur worldwide annually, at which approximately 20% of cases were treated with rigid internal fixation with osteosynthesis implants, such as plates, screws and meshes [1, 2]. The demand for osteosynthesis implants is closely linked to the increasing cases of bone fractures caused by accidents or sports injuries [3, 4].

For bone fracture treatment, the principle of osteosynthesis is the anatomical repair and its functional restoration. Osteosynthesis implants are widely used for bone fixation, to fix and support the bone fragments and induce tissue remodelling and healing [1, 2]. Craniomaxillofacial (CMF) osteosynthesis implants, mainly including mini-plates, mini-screws and meshes, are frequently used in craniomaxillofacial surgery, such as internal fixation of fractures, orthognathic surgery and osteotomies [5, 6]. To achieve the function, the basic requirements of osteosynthesis materials have to meet are excellent biocompatibility and biomechanical properties, resistance to pressure load and deformation.

1.1.2. Main issues of bioinert implants

To date, bioinert osteosynthesis implants are commonly manufactured from titanium (Ti) and its alloys mainly due to excellent biocompatibility and superior strength [7, 8]. Nonetheless, bioinert materials are facing several disadvantages and issues for osteosynthesis applications.

Firstly, the strength mismatch between bone and metallic implant might cause stress shielding, leading to re-fracture especially in osteoporotic patients [9]. As listed in Table 1.1, the inhomogeneous stress transfer can be attributed to the higher Young's modulus of metallic materials (i.e. Ti, 316L SS and Co-Cr-Mo alloy) compared with that of the cortical bone, which also affects new bone growth and

1. Introduction

remodeling [10, 11]. Furthermore, several adverse side effects and postoperative complications for bioinert materials have been documented after long-term observation, such as the release of toxic metallic ions and particles, foreign body host response, interference with diagnostic imaging, metal hypersensitivity and thermal conductivity [12-14]. In addition, the clinical use of bioinert osteosynthesis implants is restricted for pediatric cases because they can lead to the possibility of growth disturbance [5]. Finally, the additional surgery to remove these implants may lead to postoperative complications and potential risks, including infection, re-fracture, neurovascular injury, etc. [15, 16]. Therefore, to overcome the disadvantages above, the development and investigation of novel absorbable materials have gained increasing attention.

Table 1.1. Mechanical properties of bone tissue and osteosynthesis materials.

Tissue/Materials	YS (MPa)	UTS (MPa)	Elongation (%)	Modulus (GPa)	Ref.
Cortical bone	-	164-240	1.0-2.1	7-30	[2, 8]
Bioinert materials					
As-rolled pure Ti	483	550	15	114	[17]
As cast Ti-6Al-4V	834	937	19	114	[18]
316L SS	190	490	40	193	[19]
Co-Cr-Mo alloy	500- 1500	900- 1540	-	240	[8]
Bioresorbable polymer					
PGA	-	60.0- 99.7	1.5-20	-	[20]
PLA	-	48-53	30-240	1.9-2.4	[8, 21]
Absorbable metals					
As-cast pure Mg	20	86	13	41	[8, 19]
WE43	195.2	280.6	10.3	-	[22]
Annealed pure Fe	140	205	25.5	-	[23]
As-cast pure Zn	10	18	0.3	-	[24]
As-rolled pure Zn	28	45	5.6	-	[24]
As-extruded pure Zn	32	61	3.5	-	[24]
Minimum requirements of orthopedic implant	230	300	15-18	7-30	[24, 25]

1. Introduction

1.2. Absorbable osteosynthesis materials

1.2.1. Bioresorbable polymers

Currently, absorbable CMF osteosynthesis implants fabricated from polymeric materials, mainly polyglycolic acid (PGA) and polylactic acid (PLA) or their copolymers, have been used in the craniomaxillofacial surgery [5]. These polymers come from the poly (α -hydroxy acids) (HOCHR-COOH) family. The clinical application of biodegradable polymers as osteosynthesis implants was early reported in maxillofacial surgery in the 1970s [26, 27]. To date, bioresorbable polymeric osteosynthesis implants, such as mini-plates and screws, are used mainly in pediatric patients or in non-loading areas with craniomaxillofacial bone fracture, mainly because the bioresorbable materials do not hinder the facial growth [27]. Nonetheless, current polymeric materials are still considered insufficient for most routine clinical applications.

In fact, principal limitations of polymeric osteosynthesis implants mainly include the poor mechanical strength, acidic degradation products and foreign body reactions, etc. [5, 27]. As shown in Table 1.1, it has been observed that the mechanical properties of bioresorbable polymers are significantly lower than those of metallic materials, indicating that the polymeric implants are insufficient for loading applications [2]. Additionally, the ideal degradation process of implants demands that the degradation products can completely disappear *in vivo* and are replaced by the respective tissues. However, previous studies reported that polymeric implants might not completely be replaced by the bone tissue [28, 29]. More importantly, a multicenter randomized controlled trial showed that the performance of biodegradable polymeric implants is inferior compared with that of titanium implants, causing high removal rates [30]. These disadvantages impede the wide application of polymeric osteosynthesis implants.

1.2.2. Absorbable metals

The term of absorbable metals (also named biodegradable metals) refers to metals that degrade safely within the body, mainly including magnesium (Mg), iron (Fe) zinc (Zn) and their alloys [7, 8, 19, 23, 31]. The generalized degradation mechanism is through a corrosion process in the specific physiological

1. Introduction

environment. As depicted in Figure 1.1, an absorbable metal contact with human body fluid can trigger the anodic reaction. Simultaneously, the generated electrons can be consumed by the cathodic reaction, corresponding to the water reduction for Mg-based alloys and the dissolved oxygen reduction for Zn-based alloys and Fe-based alloys. A degradation product layer ($\text{Metal}(\text{OH})_n$) is formed on the surface through the reaction with the release of metal ions and hydroxide. With progressing degradation time, phosphate- and carbonate- based apatite can be further deposited onto the $\text{Metal}(\text{OH})_n$ layer. In a physiological environment, the high concentration of chloride ions causes the breakdown of the degradation layers and accelerates the degradation process. According to the size of degradation particles, macrophages and/or fibrous tissue might enclose these degradation particles until the metal is completely degraded [7, 23].

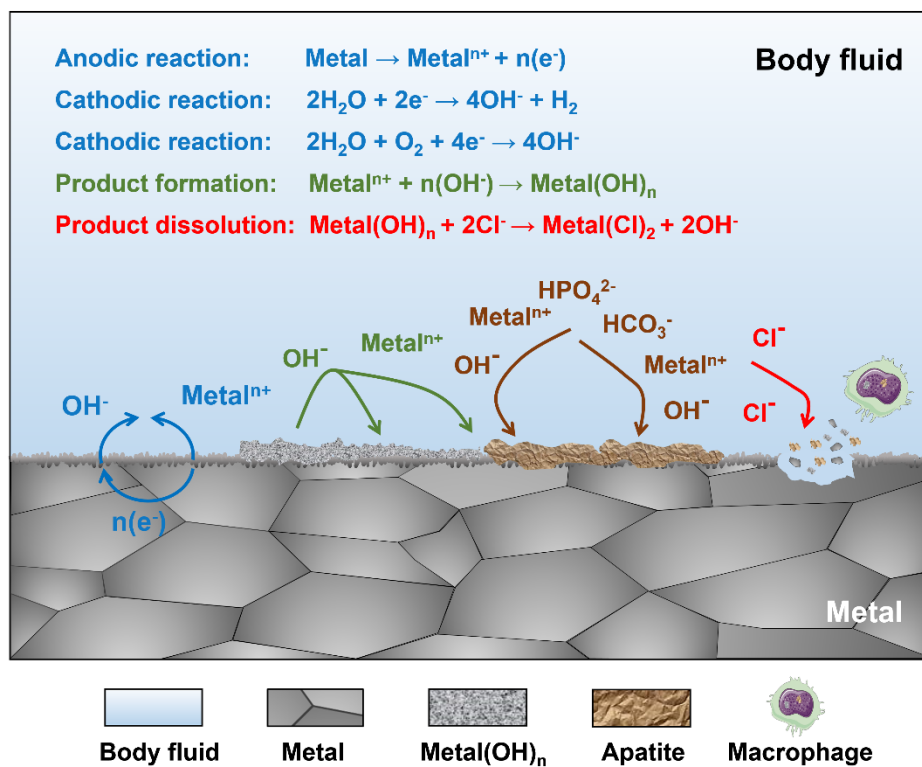


Figure 1.1. Schematic diagram of the degradation mechanism of absorbable metals (own image).

1.2.2.1. Magnesium-based osteosynthesis implants

To date, research on the development of absorbable CMF osteosynthesis metals

1. Introduction

has focused mostly on pure Mg and its alloys as a result of the excellent biocompatibility and mechanical properties [7, 8, 32]. As the main degradation product released from Mg-based alloys, the Mg ion is an essential mineral in the human body [7]. The elastic modulus of pure Mg is close to that of human cortical bone, probably preventing stress shielding, as shown in Table 1.1 [8, 19]. In fact, Mg-based osteosynthesis implants have been first proposed in 1900 [33]. However, lack of optimized corrosion behavior leads to rapid degradation of Mg-based implants along with extensive subcutaneous gas cavities, causing local swelling and pain, which limited widely application until much later [33]. Recently, the corrosion resistance of Mg and its alloys could be increased by refinement technology. Although commercially available Mg-based osteosynthesis system has been approved, large-scale controlled clinical pilot trials of Mg alloys are still under way [34]. For the CMF applications reported, magnesium-based alloy osteosynthesis implants have been used in craniomaxillofacial surgery [35, 36]. Nevertheless, the intrinsic corrosion characteristics of Mg and its alloys provoke water reduction in a physiological environment (Figure 1.1), probably leading to the extensive accumulation of hydrogen. Accordingly, subcutaneous gas cavities might cause wound healing disorders.

1.2.2.2. Iron-based osteosynthesis implants

Pure Fe and its alloys exhibit high mechanical strength, as listed in Table 1.1 [23]. Importantly, ionic Fe is a human essential element and the main component of metallic proteins [37]. An early study reported the results of iron-based stents implanted into descending aortas of rabbits. No local and systemic toxicity was observed, suggesting an excellent biocompatibility [38]. Nevertheless, pure Fe and its alloys implanted into the femur of rats demonstrated that the implants degrade too slowly. Degradation products are observed for a long time in healed tissue, indicating that Fe-based osteosynthesis implants might be questionable [39]. Herein, numerous studies focused on accelerating the Fe/Fe alloy degradation process [40-42].

1.2.2.3. Zinc-based osteosynthesis implants

Recently, Zn-based alloys have been considered as osteosynthesis materials

1. Introduction

mainly due to the excellent *in vivo* biocompatibility, suitable mechanical properties and appropriate degradation behavior [43-47], Admittedly, ionic Zn has been described as the ‘calcium of the twenty-first century’ due to its significant functional roles in physiological and biological systems [48]. Also, Zn ions have a dual mode of action on bone formation and resorption through stimulating osteoblastogenesis and suppressing osteoclastogenesis [49]. In principle, Zn has a moderate corrosion behavior between those of Mg and Fe because the standard corrosion potential of Zn (-0.76 V_{SCE}) is between Mg (-2.37 V_{SCE}) and Fe (-0.44 V_{SCE}) [23, 50, 51]. Importantly, a recent study reported that pure Zn stent was implanted into rabbit abdominal aorta for one-year, and Zn exhibited steady degradation behavior and its degradation products might be safely metabolized [52]. Similarly, Zn-based alloy pins implanted in mouse distal femurs can promote new bone formation [53]. Therefore, these advantages make Zn alloys potential materials as CMF osteosynthesis implants.

1.3. Limitations at Zn-based CMF osteosynthesis implants

1.3.1. Ideal criteria for CMF osteosynthesis materials

Biocompatibility, biomechanics, biodegradability and biofunctionalization must be taken into consideration for the ideal osteosynthesis materials, as illustrated in Figure 1.2. Without a doubt, biocompatibility is an essential prerequisite for implant materials on cellular as well as tissue level. For bone applications, potential materials need to have sufficient strength to maintain mechanical support in the reconstruction process. For a biodegradable material, the candidate should degrade safely within the body and gradually lose its mechanical integrity while the bone tissue is regenerated. Ideally, released degradation products not only induce bone tissue formation but also prevent bacterial infection.

1. Introduction

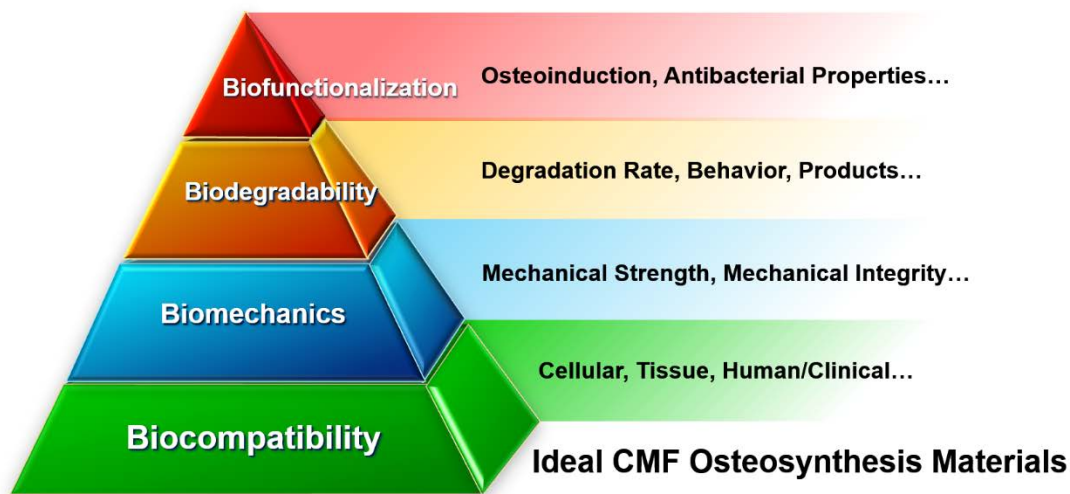


Figure 1.2. Key properties for ideal craniomaxillofacial osteosynthesis materials (own image).

Considering the defined ideal criteria, Zn is not without its issues. Herein, Zn and its alloys as CMF osteosynthesis materials have been questionable, mainly including inconsistent biocompatibility results, relatively low mechanical properties, uncertain degradation behavior and ambiguous biofunctionalization.

1.3.2. Biocompatibility

Excellent biocompatibility is an essential prerequisite of Zn-based materials for clinical applications. Numerous previous studies demonstrated that pure Zn and its alloys implanted *in vivo* indicated no obvious local and systemic toxicity, the implantation sites included abdominal aorta [52, 54-63], subcutaneous [64-66] and bony environment [45, 53]. For the *in vitro* evaluation, the standardized cytotoxicity test, which evaluates the ability of a biomaterial to destroy living cells, is used to predict and screen the Zn biocompatibility. In these tests, an extract test is most frequently used to assess the toxicity of released degradation products [67]. Nevertheless, there are conflicting reports on the cytotoxicity results of Zn and its alloys. Obvious toxic effects of Zn and Zn-based alloys were observed in undiluted extracts [24, 68]. Thus, the inconsistent results between *in vivo* and *in vitro* biocompatibility tests can interfere with the fast development of novel Zn and its alloys.

1. Introduction

1.3.3. Biomechanics

Accurate mechanical property requirements specific for CMF osteosynthesis implants are still lacking, due to the diversity of clinical cases. Whereas, as a reference for craniomaxillofacial implants, absorbable orthopedic implants need to possess the minimum mechanical requirements of yield strength > 230 MPa, tensile strength > 300 MPa, and an elongation > 15-18% [24, 25]. As shown in Table 1.1, mechanical strength of pure Zn is lower than that of metallic implants and part of polymeric implants. It is indicated that relatively poor mechanical properties of Zn are insufficient to the biomechanics requirements of CMF osteosynthesis implants. Therefore, the first step of development and research of materials is to improve the mechanical strength of pure Zn, in order to meet the requirement of clinical application. In our previous work, a Zn-4Ag alloy and a Zn-2Ag-1.8Au-0.2V (wt%) alloy with high mechanical properties was developed and fabricated, which is sufficient for most clinical applications [69].

1.3.4. Biodegradability

Biodegradability is a critical criterion for CMF osteosynthesis implants, which directly affects mechanical strength and even biocompatibility. An appropriate degradation behavior of implants determines the maintenance of mechanical integrity, and degradation products can directly influence the bone healing and remodeling [8, 23]. On the one hand, although previous outstanding studies have been performed to investigate the degradation mechanism of Zn *in vivo*, several aspects are not yet completely understood. For example, for osteosynthesis applications, it is uncertain whether the *in vivo* degradation rates of Zn-based alloys are suitable for the ideal degradation rates, e.g. 0.5 mm/year mentioned by [24]. On the other hand, buffered salt solutions like Hank's balanced salt solution have been most commonly used in previous *in vitro* corrosion tests, which can mimic *in vivo* physiological environment to only some extent. The influence of organic components such as serum on degradation behavior of Zn and its alloys remain obscure.

1.3.5. Biofunctionalization

Post-operative infection rates are up to 6.8% after CMF osteosynthesis

1. Introduction

implantation [70]. Antibacterial properties of osteosynthesis implant materials could prevent post-operative infections. Theoretically, some metal ions such as Ag, Cu and Zn have been considered as antibacterial agents [71, 72]. Previous studies demonstrated that Zn-based alloys had effective antibacterial activity towards *Staphylococcus aureus* (*S. aureus*) [73, 74]. Nevertheless, an intraoral surgical approach is the increasing trend for treatment in maxillofacial trauma, indicating an increase in the risk with oral bacteria [75]. In other words, the antibacterial properties of a craniomaxillofacial biomaterial must be effective against related microorganisms. For most transcutaneous surgery, the organisms most likely to cause infection are *S. aureus* from the skin. However, for transoral maxillofacial surgery, the most microorganisms include *Streptococci*, *anaerobic Gram-positive cocci* and *anaerobic Gram-negative rods* [76]. Herein, considering Zn-based alloys as CMF osteosynthesis materials, the antibacterial properties should be evaluated by the related microorganisms, such as *Streptococcus gordonii*.

Osteoinductivity refers to materials promoting the new bone formation. For physiological function, Zn ions play a significant role in bone formation, and they can not only stimulate bone growth and mineralization but preserve bone mass as well [77]. Admittedly, zinc-containing biomaterials such as zinc-based ceramic biomaterials also exhibited effects to promote new bone formation. The osteoinductivity of released Zn ions might be attributed to the inhibition of osteoclasts as well as the stimulation of osteoblastic differentiation [48, 49]. In addition, previous studies reported that Zn-based implants can induce new bone formation *in vivo*, implying the osteoinductivity of Zn-based alloys [53, 63]. Nonetheless, it is noteworthy to further investigate the effect of Zn degradation products on the adjacent cellular response, such as periosteal cells.

1.4. Objectives

Pure Zn provides principally an excellent biocompatibility and suitable degradation behavior observed in previous studies. Nevertheless, the mechanical properties of pure Zn are insufficient for osteosynthesis applications. Previously, we tested a newly developed Zn-4wt%Ag alloy with high strength [69].

1. Introduction

Therefore, the main objectives of the cumulative thesis include:

1. To evaluate *in vitro* degradation behavior, cytotoxicity and antibacterial properties of a novel Zn-4wt%Ag alloy with high strength (Study I).
2. To explore the effect of fetal bovine serum (FBS) on initial *in vitro* degradation behavior and the related cytotoxicity of Zn and its alloys (Study II).
3. To investigate the influence of the degradation products of Zn and Zn-4Ag alloy on cytotoxicity and osteoinduction of human periosteal cells (Study III).

2. Study I

2. Study I: Mechanical characteristics, *in vitro* degradation, cytotoxicity, and antibacterial evaluation of Zn-4.0Ag alloy as a biodegradable material

The part is a reprint of the following publication:

Ping Li, Christine Schille, Ernst Schweizer, Frank Rupp, Alexander Heiss, Claudia Legner, Ulrich E. Klotz, Jürgen Geis-Gerstorfer, Lutz Scheideler. Mechanical characteristics, *in vitro* degradation, cytotoxicity, and antibacterial evaluation of Zn-4.0 Ag alloy as a biodegradable material. International journal of molecular sciences, (2018) 19(3), 755.

Abstract:

Zn-based biodegradable metallic materials have been regarded as new potential biomaterials for use as biodegradable implants, mainly because of the ideal degradation rate compared with those of Mg-based alloys and Fe-based alloys. In this study, we developed and investigated a novel Zn-4 wt% Ag alloy as a potential biodegradable metal. A thermomechanical treatment was applied to refine the microstructure and, consequently, to improve the mechanical properties, compared to pure Zn. The yield strength (YS), ultimate tensile strength (UTS) and elongation of the Zn-4Ag alloy are 157 MPa, 261 MPa, and 37%, respectively. The corrosion rate of Zn-4Ag calculated from released Zn ions in DMEM extracts is approximately $10.75 \pm 0.16 \mu\text{g cm}^{-2} \text{day}^{-1}$, which is higher than that of pure Zn. *In vitro* cytotoxicity tests showed that the Zn-4Ag alloy exhibits acceptable toxicity to L929 and Saos-2 cells, and could effectively inhibit initial bacteria adhesion. This study shows that the Zn-4Ag exhibits excellent mechanical properties, predictable degradation behavior, acceptable biocompatibility, and effective antibacterial properties, which make it a candidate biodegradable material.

2.1. Introduction

Biodegradable metals (BMs) are regarded as the next revolutionary metallic biomaterials and have become a potential alternative to permanent biomaterials during the last decade [23, 51, 78]. Magnesium, iron, zinc and their related alloys

2. Study I

have been intensively investigated for their potential as BMs. However, the rapid corrosion rate accompanied by the accumulation of hydrogen in physiological environment impedes the clinical application of Mg-based alloys [79, 80]. Fe-based alloys, on the contrary, exhibit relatively slow degradation rates and excellent mechanical properties, but superior corrosion resistance may impede the desired replacement by newly formed tissue [81, 82].

In comparison with Mg and Fe, the standard corrosion potential of Zn ($-0.762 V_{SCE}$) is between Fe ($-0.440 V_{SCE}$) and Mg ($-2.372 V_{SCE}$) [23, 50, 51]. Bowen et al. [55] reported the biocompatibility and degradation of zinc wires implanted into the abdominal aorta of rats, and zinc wires exhibited moderate degradation rates *in vivo* for up to 6.5 months. Moreover, zinc is one of the essential nutrients in the human body, where it influences various normal physiological processes [83, 84]. Additionally, considering bio-safety, the recommended allowances for zinc element are estimated at 15 mg day^{-1} [23]. Besides its excellent corrosion and biocompatibility properties, Zn is also one of only a few metals with high magnetic resonance imaging compatibility, which is superior to that of Mg alloys and Fe alloys. The magnetic (volume) susceptibility of Zn, Mg and Fe are -15.7×10^6 , $+11.7 \times 10^6$ and $+0.2 \times 10^6$, respectively [85]. Therefore, these advantages make Zn-based alloys promising candidates for a new generation of BMs, especially for use as osteosynthesis materials and cardiovascular stents [43, 55].

Regarding the clinical requirements, the application of pure Zn in BMs is limited because of its weak strength, plasticity, and hardness. It has been investigated that the tensile strength of pure Zn is from 10 MPa to 110 MPa, the elongation is 0.32% to 36%, and the Vickers hardness is 38 HV1 to 39 HV1, being insufficient mechanical properties for most clinical applications [43, 86]. Thus, biodegradable Zn-based alloys with superior mechanical properties should be developed to meet the clinical requirements. Improvements in mechanical properties may be achieved by adding alloying elements and/or appropriate thermomechanical treatment such as extrusion, rolling, forging, annealing and so forth [87, 88]. In BMs, the biocompatibility of alloying elements must be carefully considered. In this work, Ag is proposed as an alloying element in Zn-based alloys, which could improve mechanical properties. According to the phase diagram (Figure 2.1) up

2. Study I

to 6 weight% Ag is solvable in Zn at temperatures of about 400 °C. As the solubility decreases upon cooling, ϵ -AgZn₃ precipitates form. Thus, dislocations are pinned by the precipitates resulting in improved hardness and strength (precipitation hardening). Zn-Ag binary alloys have been investigated and Ag has been proven to effectively improve the mechanical properties efficiently [89]. Moreover, the Ag ion shows antibacterial functions and has already been used as alloying element [90]. Adding Ag has shown promising antibacterial properties in Mg-based alloys while preserving the biocompatibility [90].

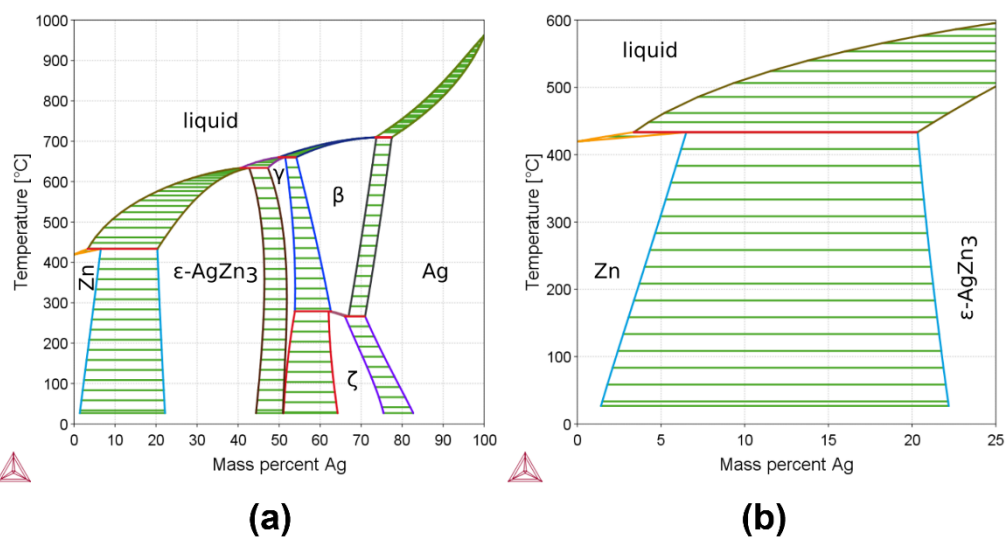


Figure 2.1. (a) Calculated Zn-Ag phase diagram using the Thermo-Calc software and the SNOB-3 database. (b) Detail of the phase diagram (a) manifesting that up to 6 wt% Ag can be solved in Zn. Upon cooling the composition enters the two-phase area, i.e. precipitations of ϵ -AgZn₃ in the Zn matrix occur. As this effect is generally accompanied by an increase in strength, it referred to as precipitation hardening.

In this study, the aim was to develop and investigate a Zn-4wt%Ag alloy as a novel biodegradable metal. The Zn-4Ag alloy was prepared, and thermomechanical treatment was applied to refine the microstructure and improve the mechanical properties. The microstructure, mechanical properties and corrosion behavior of the Zn-4Ag alloy were investigated. Furthermore, the cytotoxicity and antibacterial properties were also evaluated.

2.2. Materials and methods

2.2.1. Materials preparation

2. Study I

Alloys were prepared from high purity elements (> 99.9%) by induction melting (Indutherm VC 500 D, Germany) under 1 bar Argon in a graphite crucible. An oxide scavenger (Zincrex D85, Feuerungsbau Mutschler GmbH, Germany) was employed to clear the melt. The melt (750 °C) was cast into a cylindrical graphite mold of 15 mm diameter. During solidification the mold was vibrated resulting in a reduction in grain size from approximately 200 µm to about one tenth this size. All casting rods were homogenized at 300 °C for 1 h in a furnace under Ar protective gas and then left in the furnace for cooling. The moderate cooling rate allowed phase separation and grain growth which proved to be advantageous for the subsequent hot working. The rods were first machined to diameter of 10 mm and then swaged to 3 mm diameter wires. As the rods proved to be too brittle for swaging at room temperature, rods and tool were preheated to 200 °C. Subsequently, the wires were annealed at 390 °C for 15 minutes, quenched in water and finally precipitation hardened in an oil bath for 10 minutes at 100 °C. An inductively coupled plasma optical emission spectrometry (ICP-OES) analysis of the alloy confirmed composition.

For the corrosion tests and the biological tests, small plates with a dimension of (7 × 7 × 0.5) mm³ were prepared analogously to the wires by casting into a rectangular graphite mold with a thickness of 10 mm, homogenization at 300 °C for 1 h, hot rolling at 200 °C, annealing at 390 °C for 15 minutes and finally cutting. Samples were ground with SIC paper of P1200 (Buehler-Wirtz, Düsseldorf, Germany) using a grinding machine (Meta Serv, Buehler-Wirtz, Düsseldorf, Germany) and ultrasonically cleaned (Sonorex super RK102H, Bandelin, Berlin, Germany) with absolute ethanol for 10 min. Each side of the specimens was further sterilized by ultraviolet-radiation for at least 1 h in a sterile workbench (Lamin Air HB2472, Heraeus, Hanau, Germany) for corrosion test, cytotoxicity and antibacterial evaluation.

2.2.2. Microstructure observation and mechanical characteristic test

Metallographic cross sections of each processing step were prepared, etched with 2% Nital, a mixture of EtOH and HNO₃, and routinely subjected to a light microscopic investigation (Zeiss Axioplan 2, Germany). Vickers hardness

2. Study I

(diamond pyramid hardness), here denoted as HV1, was measured on metallographically polished cross sections using a load of 1 kg. Hardness is generally proportional to ultimate tensile strength (UTS) values, but it does not provide information about the ductility of alloy. 3 mm wires were subjected to tensile testing according to DIN EN ISO 10002-1 in a Zwick Z100HT universal testing machine (Zwick, GmbH, Germany) at a room temperature. The strain was measured until fracture using a strain gauge on a starting length of 15 mm. The testing speed was 1.5 mm/min until the yield strength was surpassed and then increased to a strain controlled strain rate of 0.0025 s^{-1} . The values for 0.2% yield strength ($YS_{0.2}$), ultimate tensile strength (UTS) and elongation (ϵ_f) were determined.

Prior to an investigation in the scanning electron microscope (SEM), all cross sections were subjected to an broad argon ion beam polishing procedure (BIB, sample rotation, 3° incident angle, 6 kV, 2.2 mA, 15 cycles: 2 min beam on, 15 min rest) using a Bal-Tec RES 101 (now Leica Microsystems GmbH, Germany). The SEM investigations were conducted with a Zeiss Auriga 60 (Carl Zeiss Microscopy GmbH, Germany) equipped with a field emission gun and a 80 mm^2 SDD EDX-Detector (X-Max 80, Oxford Instruments, UK).

A Bruker D8 GADDS diffractometer (Bruker AXS GmbH, Germany) equipped with a Vântec-500 2D detector (Bruker AXS) was employed for X-ray diffraction (XRD) based phase analysis. The x-ray beam ($\lambda(\text{Cu K}\alpha) = 1.54 \text{ \AA}$) was adjusted using a Göbel mirror and a 1 mm collimator. Acquired diffraction rings were translated (by integration) to 1 dimensional diffraction pattern using the GADDS and MERGE software packages. Pattern analysis relied on the software DIFFRAC.EVA 2 (Bruker) and the database (ICDD-PDF-2).

2.2.3. Extracts preparation

The extracts of Zn-4Ag alloy and pure Zn were prepared in DMEM (Dulbecco's modified Eagle medium; Gibco-Life Technologies, Gaithersburg, MD, USA) containing 10% fetal calf serum (FCS; PAA Lab, GmbH, Linz, Austria), 1% 200 mM L-glutamine (PAA Labor GmbH, Linz, Austria), and 1% penicillin 10 mg/ml (Gibco-Life Technologies, Darmstadt, Germany) and McCoy's 5A (Sigma-Aldrich

2. Study I

Chemie GmbH, Steinheim, Germany) supplemented with 15% FCS , 1% 200 mM L-glutamine and 1% penicillin 10 mg/ml at 37 °C in 5% CO₂ for 24 h. The ratio of surface area (cm²) to solution volume (ml) was set to 3 cm² ml⁻¹ for all samples, according to ISO 10993-12:2012 [91]. Thereafter, series of dilution of the extracts were performed with four extract concentrations, namely 10% extracts (dilution factor 1 : 10), 16.7% extracts (dilution factor 1 : 6), 33.3% extracts (dilution factor 1 : 3) and 100% extracts, according to the recommendation in Ref [92]. The extracts were further used for corrosion rate determination and cytotoxicity evaluation.

2.2.4. Corrosion rate determination

The estimated corrosion rates were calculated from released ions in the extracts according to the previous studies [93-95]. An ICP-OES (Optima 4300 DV, Perkin Elmer, Rodgau, Germany) was employed to detect released Zn and Ag ions in the extracts. Measured extracts were diluted triple prior to the measurement. Released Zn and Ag ions were measured at 2 different wavelengths with three-time repetition. The corrosion rate was calculated from released Zn ions using the following formula, according to the Ref [96]:

$$\text{Corrosion rate } (\mu\text{g cm}^{-2} \text{ day}^{-1}) = (C \times V) / (S \times T) \quad (1)$$

where C is the released Zn ions concentration in $\mu\text{g/ml}$, V is the solution volume in ml, S is the sample surface area in cm², T is the incubation time in days. The surface morphology and chemical composition of the corrosion products on the surfaces after immersion were also observed using a scanning electron microscope equipped with an energy dispersive X-ray spectrometer (SEM-EDX; LEO 1430, Zeiss, Oberkochen, Germany).

2.2.5. Cytotoxicity tests

The cytotoxicity evaluation of Zn-4Ag was performed via extract test, according to ISO 10993-5: 2009 [97]. L929 fibroblasts (Mouse fibroblast cell line, DSMZ GmbH, Braunschweig, Germany) and Saos-2 osteoblasts (Human primary osteosarcoma cell line, DSMZ GmbH, Braunschweig, Germany) were used. Cytotoxicity was tested for two biological endpoints: metabolic activity (Roche

2. Study I

Cell Proliferation Kit II, XTT assay) and cell proliferation (Roche cell proliferation ELISA, BrdU assay). Ti-6Al-4V alloy (Camlog, Wimsheim, Germany) was used as negative control. L929 fibroblasts were cultured in 24 ml DMEM medium and Saos-2 osteoblasts were cultured in 10 ml McCoy's 5A. Both cell types were grown in 75 cm² culture flasks (Costar, Corning, Tewksbury, MA, USA) at 37 °C in a humidified atmosphere of 5% CO₂.

For the tests, L929 fibroblasts and Saos-2 osteoblasts were seeded in 96-well plates (200 µl/well) at a cell density of 1 × 10⁴ cells per well and pre-incubated overnight. Thereafter, 150 µl of the respective extract dilutions replaced the cell medium (4 parallel wells per dilution). After 24 h incubation with these extracts, 50 µl XTT reagent was added to each well for 2 h. Subsequently, the formazan formation was determined photometrically using an ELISA Reader (Biotek, Bad Friedrichshall, Germany) at the wavelengths of 450/620 nm. Proliferative activity of L929 and Saos-2 was determined in the logarithmic growth phase between 24 h and 48 h after seeding by BrdU assay. 15 µl BrdU labeling reagent were added to each well 24 h after seeding. Additional cell cultures without BrdU-label were used as background controls. Culture medium without cells containing BrdU and Anti-BrdU-POD was used as blank controls. Afterwards, the cells were fixed, and Anti-BrdU-POD was added according to manufacturer's instructions. The absorbance of the samples was measured using an ELISA Reader at 450/690 nm.

2.2.6. Antibacterial effect evaluation

For determining bacterial adhesion, Zn-4Ag samples were inoculated with *Streptococcus gordonii* strain DL1 (*S. gordonii*) and adhering bacteria were determined using a crystal violet staining assay (0.5% crystal violet in 20% methanol) and a green fluorescent nucleic acid stain (Live/Dead BacLight Bacterial Viability Kit, Invitrogen, L13152, USA). Bacteria were grown as a stationary suspension culture in Schaedler medium (Beckton Dickinson GmbH, Heidelberg, Germany) overnight at 37 °C. Thereafter, 4 ml *S. gordonii* suspension were added to each sample in 6-well plates and cultivated for 12 h at 37 °C. After incubation for 12 h, *S. gordonii* suspension was carefully removed and samples

2. Study I

were immersed in 3 ml crystal violet solution for 20 min. After staining, the samples were rinsed 3 times with deionized water. Subsequently, the samples were observed and photo-documented under a photomicroscope (Wild M 400, Wild, Heerbrugg, Switzerland) equipped with a remote control DSLR (Nikon 550D, Japan). For live/dead test, the samples were rinsed two times with Hanks' salt solution (Biochrom AG, Germany). Live/dead staining was used to evaluate the live/dead state of bacteria on the surface, following the manufacturer's instructions. The biofilm formation and adherent bacteria were examined with a fluorescence microscope (Optiphot-2, Nikon, Tokyo, Japan) equipped with a remote control DSLR. Ti-6Al-4V samples were selected as a reference.

2.2.7. Statistical methods

The inhibition of metabolic activity of the cells (XTT) was determined in three independent experiments, and the proliferation tests (BrdU-incorporation) were performed twice. The combined results of the respective cytotoxicity tests are given as mean values \pm standard deviation. Statistical significance of differences between groups was tested by Student's t-test. Differences of p-values < 0.05 were considered statistically significant.

2.3. Results and discussion

2.3.1. Microstructure and mechanical properties

The evolution of microstructure was investigated by light and scanning electron microscopy. A heat treatment (homogenization, 300 °C for 1h) induced a transformation of the dendritic as-cast microstructure (Figure 2.2a) to large globular grains. After the thermomechanical treatment, i.e. swaging, annealing (390 °C for 15 min) and quenching, bright grains corresponding to the ϵ -AgZn₃ phase are visible (Figure 2.2b). Subsequent precipitation hardening (100 °C for 10 min) led only to slightly larger grains but did not further affect the microstructure (Figure 2.2c).

2. Study I

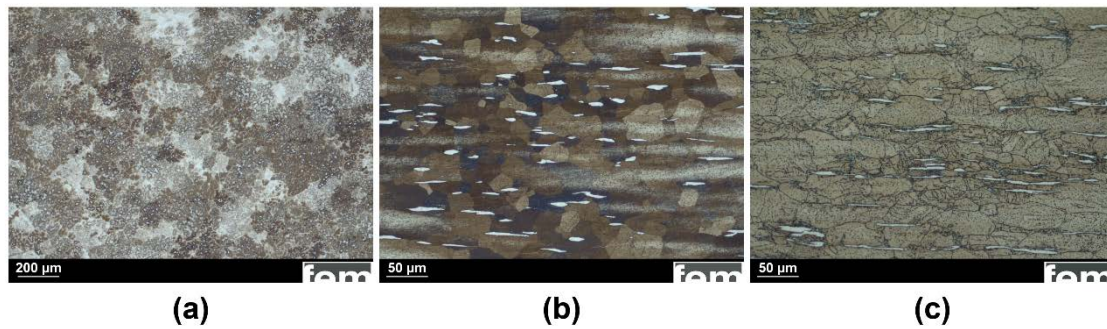


Figure 2.2. Optical micrograph of (a) the as-cast Zn-4Ag dendritic microstructure. (b) Longitudinal sections after thermomechanical treatment (homogenization, swaging and solution annealing) and after (c) precipitation hardening showing globular grains. Large ϵ -AgZn₃ grains (bright) can be identified on the cross sections.

Table 2.1. Assessment of mechanical properties by tensile testing and Vickers hardness tests.

Alloy / processing	Mechanical Properties				References
	Yield Strength (YS _{0.2}) (MPa)	Ultimate Tensile Strength (UTS) (MPa)	Elongation to failure (%)	Hardness (HV1)	
Zn-4Ag*	157	261	37	73	In this study
Zn-4Ag**	149	215	24	82	In this study
WE43 / extruded	195	280	10	-	[98]
Zn / cast	10	18	0.32	38	[51]
Zn / extruded	35	60	3.5	-	[51]
Zn / hot rolled	30-110	50-140	5.8-36	39	[51]
Zn-2.5Ag / extruded	147	203	35	-	[89, 99]
Zn-5Ag / extruded	205	253	36	-	[89, 99]
Zn-7Ag / extruded	236	287	32	-	[89]

* Thermomechanical treatment; ** Additional precipitation hardening. While the aspired precipitation hardening essentially resulted only in a slight increase in hardness, yield strength and ultimate tensile tended to decrease. This is due to the fact that that precipitates had formed beforehand (see next paragraphs).

Concerning thermomechanical treatment and precipitation hardening, the resulting mechanical properties are compiled in Table 2.1. A minor modification of the Mg alloy WE43 is already used for bioresorbable stents. The material

2. Study I

exhibits reasonable mechanical properties, but the corrosion rate is high, a controversial issue among experts [100]. Bowen et al. [54] investigated the qualification of metallic zinc for bioresorbable stents. They concluded that the comparably slow corrosion rate and the low toxicity of the resulting products make zinc a promising candidate for bioresorbable stents. However, the authors acknowledge the insufficient mechanical properties of pure zinc, excluding a straight-forward application, and discuss putative additives. A recent publication shows that the addition of Ag results in considerably improved mechanical properties [89], which is in good agreement with the data presented here. Zn-4Ag shows good mechanical properties. Subsequent precipitation hardening (100 °C for 10 min) did not improve the mechanical properties. While the hardness slightly increases, YS and UTS both slightly decrease. This minor loss of strength is probably due to grain growth. Nevertheless, a sufficiently large window between YS (157 MPa) and UTS (261 MPa) as well as an elongation of 37% represents an excellent starting point for future material developments.

The missing aging effect of this heat treatment might be explained by the fact that the precipitates predominantly had formed beforehand. XRD analysis of the thermomechanically treated state confirmed the presence of the two expected phases, Zn and ϵ -AgZn₃ (Figure 2.3).

A micrograph acquired by surface sensitive secondary electron (SE) imaging at an accelerating voltage of 6 kV is shown in Figure 2.4a. Despite the gentle BIB polishing procedure, the surface is characterized by a certain grain orientation dependent topography and surface roughness, respectively. Submicron sized, Ag enriched ϵ -AgZn₃ particles were identified along the Zn grain boundaries by EDX mapping (Figure 2.4a, blue colouring). Nucleation and growth of the ϵ -AgZn₃ particles led on the other hand to a Ag depleted zone. Moreover, small precipitates inside the Zn grains were detected by backscatter electron imaging (BSE) at 20 kV (Figure 2.4b).

2. Study I

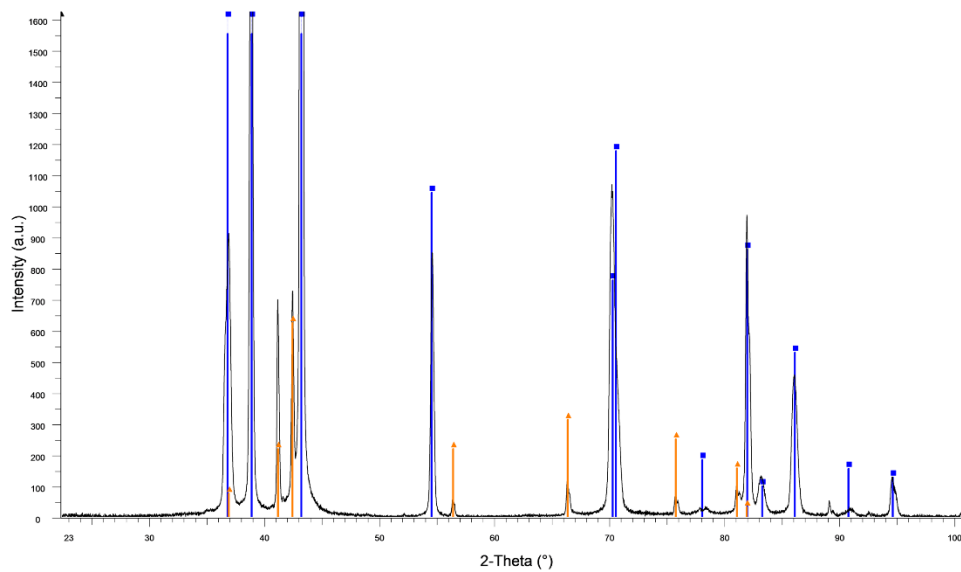
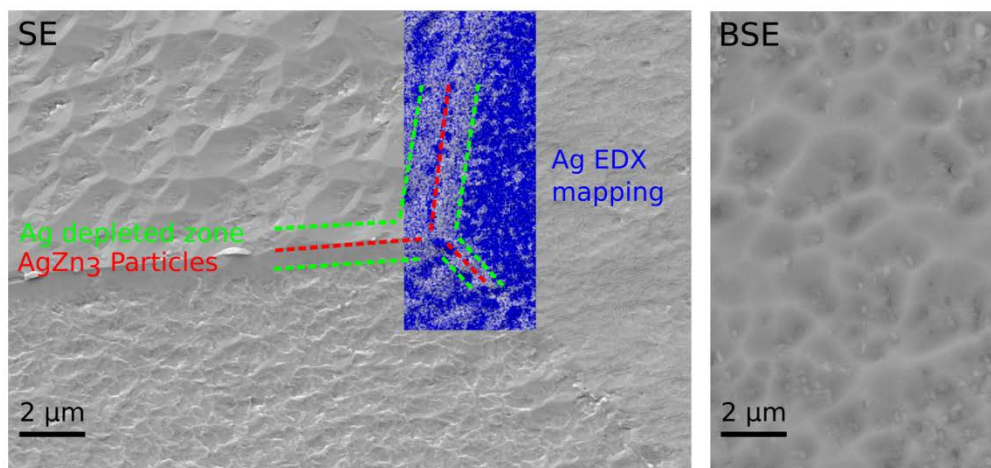


Figure 2.3. XRD pattern (black) of Zn-4Ag after thermomechanical treatment. The phases Zn (03-065-3358, blue) and ϵ -AgZn₃ (00-025-1325, orange) were identified.



(a)

(b)

Figure 2.4. SEM investigation of the microstructure after thermomechanical treatment. (a) For the sake of resolution, SE imaging of the BIB polished surface as well as the corresponding EDX analysis were performed at 6 kV. The overlay shows that ϵ -AgZn₃ particles have formed along the grain boundaries while the proximity is Ag depleted. (b) 20 kV BSE imaging revealed the presence of ϵ -AgZn₃ precipitates within the Zn grains.

2.3.2. Corrosion properties

In this study, corrosion rates of Zn-4Ag alloy and pure Zn were calculated from released Zn ions in the cell medium extracts (Figure 2.5), which correspond to

2. Study I

the cytotoxicity of the Zn-4Ag alloy and pure Zn. The cell media used, DMEM and McCoy's 5A, consist both of inorganic ions and organic components with concentrations equal to those in human plasma, as shown in Table 2.2. The use of extraction media with concentrations of buffering agents and glucose similar to those of human plasma is critical for predicting *in vivo* corrosion rate [101]. In these tests using cell culture medium instead of simple salt solutions, the extract conditions are more closely related to the physiological environment in the body, although extraction time is only for 24 h. However, *in vitro* corrosion rates from long-term immersion tests in simulated body fluid should be further investigated.

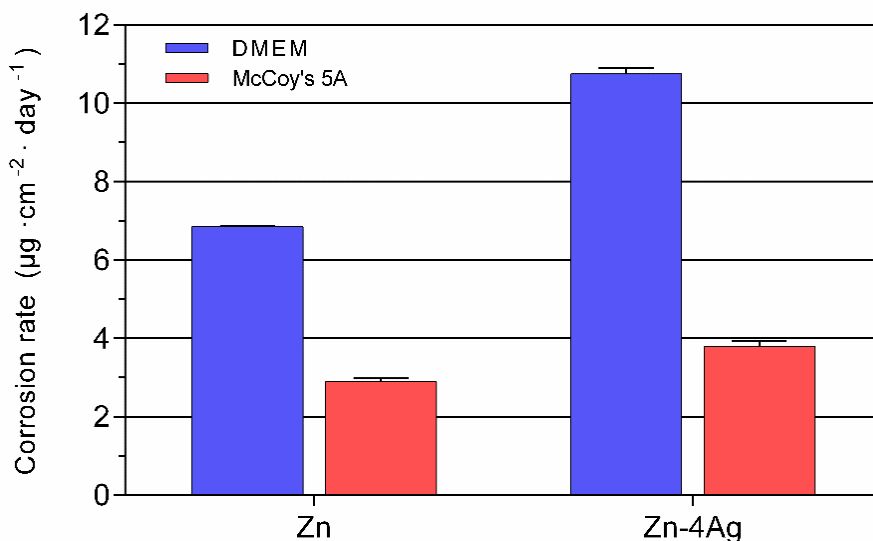


Figure 2.5. Corrosion rates of pure Zn and Zn-4Ag in DMEM and McCoy's 5A calculated from released Zn ions.

As shown in Figure 2.5, corrosion rates of Zn-4Ag in DMEM and McCoy's 5A were $(10.75 \pm 0.16) \mu\text{g cm}^{-2} \text{ day}^{-1}$ and $(3.80 \pm 0.14) \mu\text{g cm}^{-2} \text{ day}^{-1}$, respectively, which is higher than the counterpart of pure Zn, $(6.85 \pm 0.02) \mu\text{g cm}^{-2} \text{ day}^{-1}$ and $(2.89 \pm 0.08) \mu\text{g cm}^{-2} \text{ day}^{-1}$. It is clearly evident that higher corrosion rates in DMEM in comparison to McCoy's 5A were also observed. The difference can be ascribed to the different composition of DMEM and McCoy's 5A. One reason could be the higher (15%) concentration of FCS which was used in McCoy's 5A. It is known that the proteins in FCS can decrease corrosion rates, which was also observed in the case of Mg alloys [102].

2. Study I

Table 2.2. Composition of the blood plasma, DMEM and McCoy's 5A [101, 103, 104] .

	Blood plasma	DMEM	McCoy's 5A
Inorganic ions (mmol l⁻¹)			
Na	142	127.3	141.0
K	5.0	5.3	5.4
Mg	1.5	0.8	0.8
Cl	103.0	90.8	117.2
Ca	2.5	1.8	1.2
HPO ₄	1.0	0.9	4.2
SO ₄	0.5	0.8	0.8
HCO ₃	27.0	44.1	26.2
Organic components			
Protein (g l ⁻¹)	63-80	-	-
Glucose (mmol l ⁻¹)	3.6-5.2	4.5	16.6
Amino acids (g l ⁻¹)	Variable	1.6	0.4
Concentrations of buffering agents (mmol l⁻¹)	43.5-45.5	70	30.4

In most previous studies, *in vivo* corrosion rates of Zn alloys were estimated by *in vitro* long-term immersion tests and electrochemical tests [51, 103]. However, standardized *in vitro* methods for the corrosion rate determination which are able to mimic the degradation behavior of Zn alloys in the complex body physiologic environment are still lacking. In this study, the *in vitro* corrosion rate determination of Zn alloys was estimated from released Zn ions in DMEM for 24 h, as reported in previous studies [93-95]. Kubásek et al. [93] reported the corrosion rate of Zn-0.8Mg in DMEM was $(13.4 \pm 0.3) \mu\text{g cm}^{-2} \text{ day}^{-1}$. This value is close to the calculated value of $(10.75 \pm 0.16) \mu\text{g cm}^{-2} \text{ day}^{-1}$ in our present study. Jablonská et al. [94] reported a corrosion rate of Zn-1.5Mg calculated by released ions in extracts of $(52 \pm 10) \mu\text{g cm}^{-2} \text{ day}^{-1}$ for an untreated control under a CO₂ atmosphere, which is higher than the corrosion rate of Zn-4Ag in our study. The difference could be attributed to a different surface to volume ratio in the two studies and the fact that in the study of Jablonská et al. the solid corrosion products were dissolved by addition of ultrapure HNO₃ prior to determination of the released ions.

2. Study I

In our study, adding Ag as alloying element to pure-Zn clearly increased the corrosion rate of the Zn-Ag binary alloy, which is consistent with previous findings [89]. Sikora-Jasinska et al. [89] reported that the corrosion rates of Zn-2.5Ag, Zn-5.0Ag and Zn-7.0Ag alloys are from 79 to 84 $\mu\text{m year}^{-1}$ in Hanks' modified solution, which is higher in comparison to pure Zn. This might be related to the formation of the $\epsilon\text{-AgZn}_3$ phase, inducing micro-galvanic corrosion, which finally leads to a decreased corrosion resistance of Zn-Ag alloys.

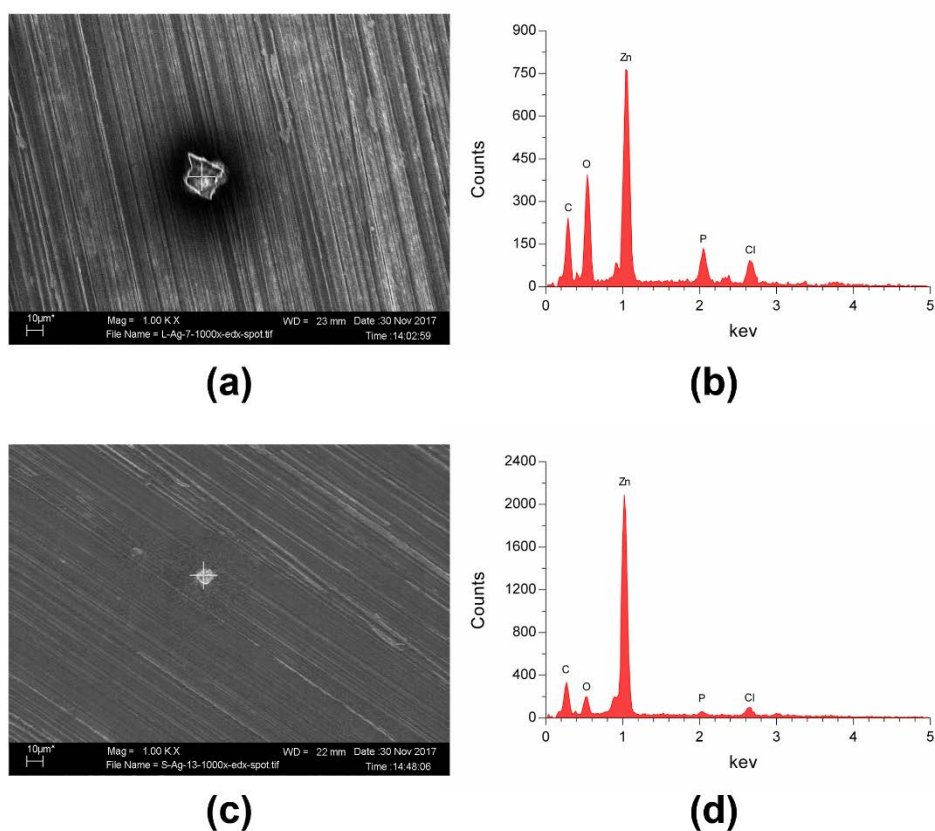


Figure 2.6. The SEM-EDX analysis of the Zn-4Ag alloy after immersion in DMEM / McCoy's 5A for 24 h: (a) SEM images of Zn-4Ag alloy in DMEM (magnification 1000 \times), (b) EDX result of the degradation products in (a), (c) SEM images of Zn-4Ag alloy in McCoy's 5A (magnification 1000 \times), (d) EDX result of the degradation products in (c).

Figure 2.6 shows the surface morphologies detected by SEM and the EDX analyses of corrosion products on the surface of Zn-Ag alloy after immersion for 24 h. The degradation products of Zn-4Ag were mainly similar as those of pure Zn. Only a small amount of white degradation products were distributed on the surface, and round particles formed on the surface were observed at high

2. Study I

magnification (Figure 2.6a and Figure 2.6c), which is consistent with previous studies [89, 105]. The EDX analysis (Figure 2.6b and Figure 2.6d) shows that these degradation products of Zn-4Ag alloy were mainly composed of Zn, O, P, C and Cl, suggesting that these particles could be mainly composed of hydroxides, phosphate, carbonate compounds and chloride salt formation, as reported in previous studies [43, 88, 106].

2.3.3. Cytocompatibility

Table 2.3 shows the mean Zn ion concentration after incubation of pure Zn and Zn-4Ag alloy in DMEM / McCoy's 5A to correlate the ion concentrations to the results of the cytotoxicity tests (Figure 2.7 and Figure 2.8). Analysis of the mean Zn ion concentration revealed that the highest concentration was determined for Zn-4Ag alloy of 100% extract in DMEM with 493.4 μM . Furthermore, the mean Zn ion concentration in DMEM extracts is higher than the counterpart in McCoy's 5A. In addition, the mean Ag ion concentration in Zn-4Ag extracts was below the detection limit of the instrument, indicating a very limited release of Ag element into cell medium, although some Ag ions may be bound in the corrosion products.

Table 2.3. The mean Zn ion concentration in pure Zn and Zn-4Ag alloy extracts.

Cell medium	Samples	Zn ion concentration ($\mu\text{mol/l}$)			
		100% extracts	33.3% extracts	16.7% extracts	10% extracts
DMEM	Pure Zn	314.4	107.4	55.5	34.7
	Zn-4Ag	493.4	167.2	85.4	52.6
McCoy's 5A	Pure Zn	132.8	51.5	31.1	22.9
	Zn-4Ag	174.4	65.4	38.0	27.0

2. Study I

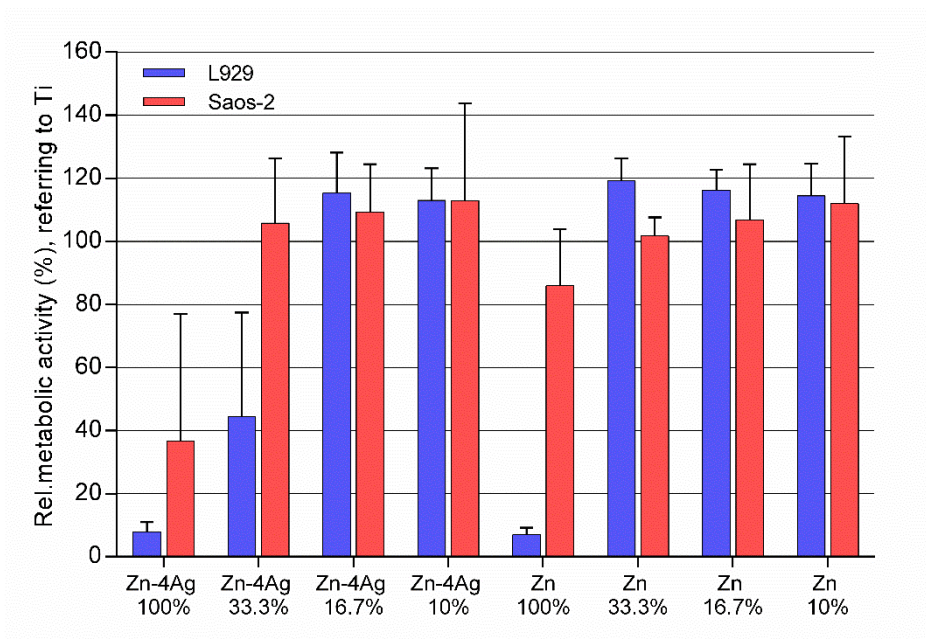


Figure 2.7. Effect of different concentrations of Zn-4Ag alloy and pure Zn extracts on the cell metabolic activity of L929 and Saos-2 determined by XTT assay. Ti-6Al-4V alloy was used as negative control and was set to 100%. Means of three independent experiments are shown with respective standard deviations.

Figure 2.7 shows the metabolic activity of L929 and Saos-2, respectively, cultured in 100%, 33.3%, 16.7% and 10% extracts of Zn-4Ag for 24 h; pure Zn served as a control. According to ISO 10993-5: 2009, a decrease of cell viability higher than 30% is considered as a toxic effect. For the Zn-4Ag alloy, L929 cells and Saos-2 cells cultured in 100% Zn-4Ag extracts showed a much lower metabolic activity, below 40% of the control. Thus, these undiluted extracts possess clearly cytotoxicity. In the 33% Zn-4Ag extract, the cell viability of Saos-2 already approached 100%. L929 cells, on the contrary, reached approximately 40%. For 10% and 16.7% diluted extracts of Zn-4Ag, the metabolic activities of L929 cells and Saos-2 cells were always reaching 100%, and there was no statistically significant difference between Zn and Zn-4Ag groups ($p > 0.05$). Therefore, the Zn-4Ag alloy tested showed a certain degree of toxicity for L929 cells and Saos-2 cells based on the cytotoxicity results in our test systems.

2. Study I

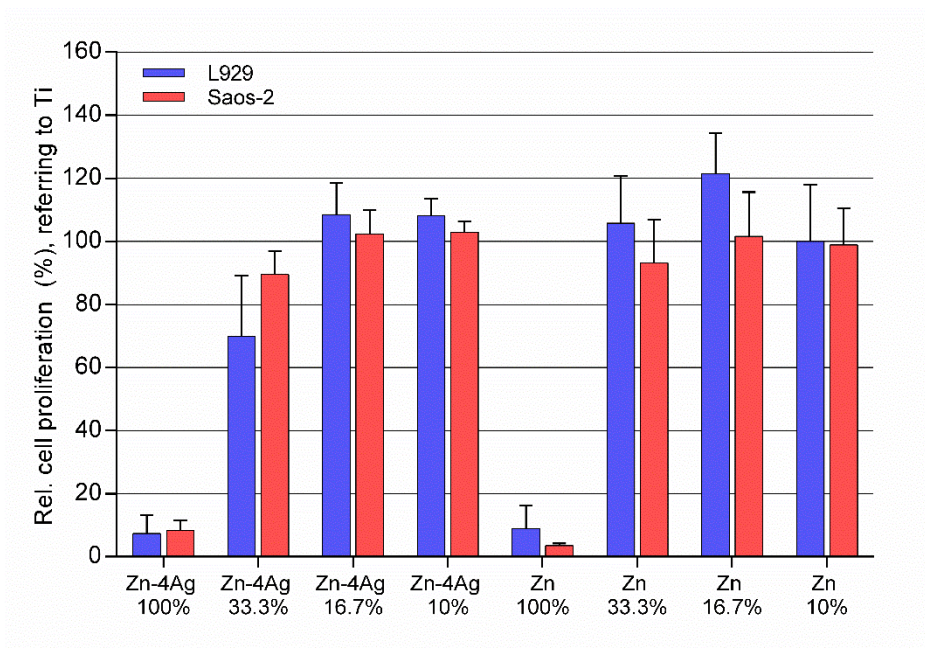


Figure 2.8. Influence of different concentrations of Zn-4Ag alloy and pure Zn extracts on the cell proliferation of L929 and Saos-2 determined by BrdU assay. Ti-6Al-4V alloy was used as negative control and was set to 100%. Means of two independent experiments are shown with respective standard deviations.

Figure 2.8 shows the cell proliferation of L929 cells and Saos-2 cells cultured in 100%, 33.3%, 16.7% and 10% extracts of Zn-4Ag and pure-Zn for 24 h determined by BrdU incorporation. *In vitro* cytotoxicity can be easily evaluated with tetrazolium-salt-based assays. However, XTT assay and Cell Counting Kit-8 (CCK-8; Dojindo Molecular Technologies, Kumamoto, Japan) in our preliminary experiments were influenced by the degradation products of Zn-based alloys, for reasons which are probably similar to Mg-based alloys [107]. In contrast to the tetrazolium-salt-based XTT-assay, the BrdU incorporation is a direct measure for proliferative activity. An additional advantage is that the BrdU assay is not prone to the interference of the released Zn ions with tetrazolium-based assays [107]. In 100% extracts of Zn-4Ag alloy and pure Zn, both cell types showed an almost total inhibition at proliferation ability, which was different compared to the results of the metabolic activity. In different diluted extracts of Zn-4Ag alloy and pure Zn, the proliferation activities of L929 and Saos-2 exhibited similar results as with the metabolic activities.

As a potential biodegradable material, the biocompatibility of the degradable Zn-4Ag alloy should be considered. In fact, the significance of Zn in human nutrition

2. Study I

has been widely acknowledged. Zn is the second most abundant transition metal in the human body and an essential element for numerous biological functions [108, 109]. The recommended intake for an adult is estimated at 15 mg day^{-1} [23, 51]. Also, the human tolerance level silver is estimated from $0.4 \text{ } \mu\text{g day}^{-1}$ to $27 \text{ } \mu\text{g day}^{-1}$ [110]. The effects evaluated by the extract test for the biodegradable Zn-based alloy is mainly attributed to the released corrosion products during the degradation process. In this study, a considerable released Zn ion concentration in extracts was found, while the Ag ion concentration was below the detection limit, indicating that the Zn ion concentration mainly determined the toxicity of the Zn-4Ag alloy. As far as systemic toxicity is concerned, the daily released Zn ions of the Zn-4Ag alloy are far below the above-allowed value. With the Zn ion concentration decreased in the diluted extracts, the cytotoxic effect also decreased, which is consistent with several studies [111, 112]. It is worth noting that significant differences in Zn ion concentrations were determined between both cell media under the same extraction conditions, which is obviously related to the different composition of the media.

Concerning cell sensitivity to zinc, Kubásek et al. [93] reported the Zn^{2+} safety concentrations for L929 and U-2 OS cell being $80 \text{ } \mu\text{M}$ and $120 \text{ } \mu\text{M}$, respectively. In this present work, results similar to the above study were found. The mean Zn ion concentrations in 100% Zn-4Ag extract of DMEM and McCoy's 5A were $493.4 \text{ } \mu\text{M}$ and $174.4 \text{ } \mu\text{M}$, respectively. These values are higher than the safety concentrations. In our study, metabolic activity, determined by XTT assay, was less decreased by cytotoxic effects of the experimental alloy than proliferation determined by BrdU assay. This may be caused by the fact that metabolic activity of the cells is less sensitive to the cytotoxic action of the released Zn ions. However, interference of these ions with tetrazolium salts in the XTT assay may contribute this effect.

For extract tests, most studies have found that only diluted extracts of biodegradable Zn-based alloys exhibited good cell viability [50, 88, 93], although even undiluted extracts have shown no cell toxicity in few studies [87, 113]. The difference observed might be caused by different cell lines and different experimental Zn-based alloys. It is already been discussed that the current ISO

2. Study I

10993 standards for *in vitro* cytotoxicity tests (10993-5: 2009 and 10993-12: 2012) have only limited value for the evaluation of biodegradable metallic materials [91, 97]. Wang et al. [92] suggested that a maximal tenfold dilution (10% extracts) to a minimal sixfold dilution (16.7% extracts) of extracts for *in vitro* cytotoxicity tests were recommended for screening potential Mg-based alloys. According to this suggestion, the Zn-4Ag alloy in this study would have no potential cytotoxicity, according to the results of the 10% and 16.7% extracts. However, it is critical to perform *in vivo* systematic toxicity evaluation in future studies.

2.4.4 Antibacterial evaluation

The antibacterial properties of Zn-4Ag alloy to inhibit biofilm formation and initial bacterial adhesion was evaluated by crystal violet staining and live/dead staining, as shown in Figure 2.9. After 12 h incubation with *S. gordonii*, the surface of the Ti-6Al-4V alloy showed an intense violet staining and green fluorescence (Figure 2.9a and Figure 2.9b), respectively, which means a high level of biofilm formation and a significant amount of adherent *S. gordonii*. In comparison, Zn-4Ag alloy presented point-like violet staining and a thin layer of green fluorescent vital bacterial chains (Figure 2.9c and Figure 2.9d), indicating the inhibition of initial *S. gordonii* adhesion and less biofilm formation compared with the Ti-6Al-4V alloy.

Postoperative infection is a common complication in surgical implants, and the infection rate ranges from 1% to 4.5% for dental implant surgery [114]. The postoperative infection not only leads to implants failure but also delays tissue remodeling. In the present work, Zn-4Ag alloy could effectively inhibit bacterial adhesion and biofilm formation in comparison to Ti-6Al-4V alloy, indicating a good antibacterial effect. It is well known that Zn and Ag ions possess excellent antibacterial functions, and especially Ag has been used as effective antimicrobial agents incorporated into all kinds of biomaterials, such as metals, polymers, ceramics and glasses [115, 116]. The exact mechanism of Zn and Ag action on bacteria has not been completely understood but may probably include interference with electron transport binding to DNA and interaction with the membrane [115, 117]. Hu et al. [118] reported that Zn-incorporated TiO₂ coatings on titanium by plasma electrolytic oxidation could greatly inhibit the growth of both

2. Study I

Staphylococcus aureus (*S. aureus*) and *Escherichia coli* (*E. coli*). Moreover, the antibacterial effects of Ag ions in biodegradable Mg-Ag alloys have also been studied. Increased Ag addition (from 2% to 6%) showed a 74% to 79% reduction of bacterial viability and a 50% to 75% reduction of adherent bacteria [90]. Therefore, the novel developed Zn-4Ag alloy could prevent or at least diminish postoperative infection.

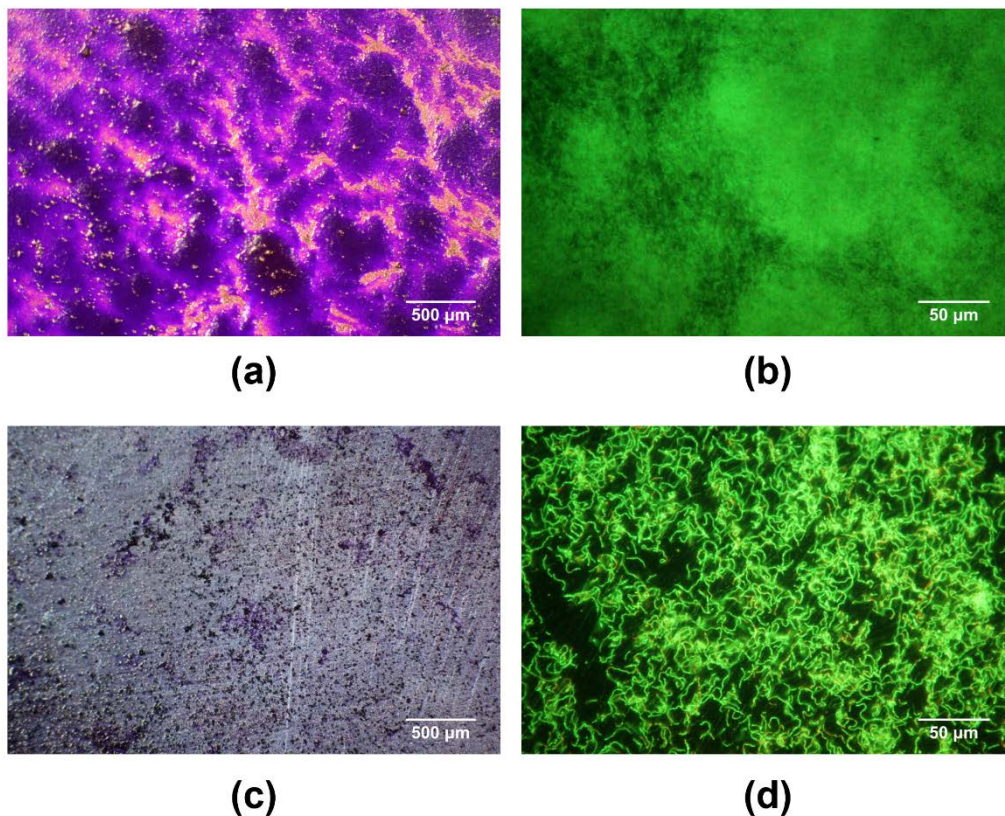


Figure 2.9. Biofilm formation and initial bacterial adhesion on Ti-6Al-4V alloy (a,b) and Zn-4Ag alloy (c,d) after incubation with *S. gordonii* for 12 h. a and c by crystal violet staining (magnification 32×); b and d by live/dead staining (magnification 400×).

2.4. Conclusions

A Zn-4Ag alloy was developed as a novel biodegradable Zn-based alloy, and thermal treatment was applied to improve its mechanical properties and to refine the microstructure. The *in vitro* degradation behavior, cytotoxicity and antibacterial evaluation were also investigated. Based on the limitations of the *in vitro* study, the following conclusions can be drawn:

2. Study I

1. After thermomechanical treatment, the yield strength (YS), ultimate tensile strength (UTS) and elongation of the alloy are 157 MPa, 261 MPa and 37%, respectively, rendering this alloy a promising material for bioresorbable stents. Future alloy development will focus on the optimization of the microstructure in order to ensure a safe application.
2. The corrosion rate of Zn-4Ag calculated from released Zn ions in DMEM extract was approximately $(10.75 \pm 0.16) \mu\text{g cm}^{-2} \text{ day}^{-1}$, which is higher than the that of pure Zn.
3. A cytotoxic effect decreasing viability and proliferation of L929 and Saos-2 cells was observed, but only in the undiluted extracts of the Zn-4Ag alloy. However, this finding should not be overestimated, since the suitability of the used ISO 10993-5 standard method has to be discussed for degradable materials, according to each application.
4. *In vitro* antibacterial evaluation showed the Zn-4Ag alloy has the potential to inhibit initial *S. gordonii* adhesion.

Therefore, the biodegradable Zn-4Ag alloy exhibits excellent mechanical properties, predictable degradation behavior, acceptable cytotoxicity and effective antibacterial property *in vitro*, which make it a promising candidate for biodegradable implants. It should be investigated by further *in vitro* and *in vivo* studies.

3. Study II

3. Study II: Selection of extraction medium influences cytotoxicity of Zinc and its alloys

The part is a reprint of the following publication:

Ping Li, Christine Schille, Ernst Schweizer, Evi Kimmerle-Müller, Frank Rupp, Alexander Heiss, Claudia Legner, Ulrich E. Klotz, Jürgen Geis-Gerstorfer, Lutz Scheideler. Selection of extraction medium influences cytotoxicity of zinc and its alloys. *Acta Biomaterialia* (2019) DOI: 10.1016/j.actbio.2019.03.013

Abstract:

Zinc (Zn) alloys have been considered as promising absorbable metals, mainly due to their moderate degradation rates ranging between magnesium alloys and iron alloys. The degradation behavior depends on the specific physiological environment. Released metallic ions and corrosion products directly influence biocompatibility. The initial contact of orthopedic implants or vascular stents after implantation will be with blood. In this study, fetal bovine serum (FBS) was used as a model system of blood components. We investigated the influence of FBS on *in vitro* degradation behavior and cytotoxicity of pure Zn, and Zn-4Ag and Zn-2Ag-1.8Au-0.2 V (wt%) alloys. The initial degradation rates in FBS were assessed and compared with the degradation and toxicity in four other common physiological model systems: DMEM cell culture medium ± FBS and McCoy's 5A medium ± FBS. Test samples in pure FBS showed the highest initial degradation rates, and accordingly, FBS supplemented media accelerated the degradation process as well. Moreover, an extract test according to ISO 10993-5 and -12 with L929 and Saos-2 cells was performed to investigate the role of FBS in the extraction medium. The cytotoxic effects observed in the tests were correlated with FBS-mediated Zn²⁺ release. These findings have significant implications regarding the selection of appropriate media for *in vitro* degradation and cytotoxicity evaluation of Zn and its alloys.

3.1. Introduction

Absorbable metals (also named biodegradable metals) refer to metals or their

3. Study II

alloys that degrade safely within the body [19, 51, 77, 119]. Three major metals, such as magnesium (Mg), iron (Fe), zinc (Zn), have been considered for medical applications. To date, Zn and its alloys have been proposed as promising metallic biomaterials due to their degradation behavior. Compared with Mg and Fe, the intrinsic standard corrosion potential of Zn ($-0.76 V_{SCE}$), which determines the corrosion rate, is between Mg ($-2.37 V_{SCE}$) and Fe ($-0.44 V_{SCE}$) [3]. Nevertheless, pure Zn possesses relatively poor mechanical properties, which are insufficient for the majority of clinical applications. Zn-based alloys with superior strength have been fabricated by adding alloying elements, further improvements have been achieved by thermomechanical treatment [1, 2]. The mechanical properties of both Zn alloys investigated in this study roughly meet the generally acknowledged minimal requirements for implant materials, i.e. UTS > 250 MPa and elongation > 15%. Most importantly, previous *in vivo* studies found that the degradation products of pure Zn can be tolerated and metabolized, indicating that pure Zn can exhibit excellent biocompatibility [52, 57]. From the perspective of metallic biomaterials, the degradation behavior of alloys in the body affects their mechanical integrity and even directly influences biocompatibility and bioactivity via degradation products [13, 23]. Thus, it is critical to investigate the degradation behavior of Zn and Zn alloys in the specific physiological environment or the desired implantation site.

For absorbable Zn alloys, proposed clinical applications mainly include cardiovascular stents and osteosynthesis materials [43, 53, 73, 119]. The local degradation environment for cardiovascular stents will be the bloodstream, and they will be in contact with the human blood until a neointima, a hyperplastic region of the vascular wall having histological characteristics of both intima and normal artery cells, has formed on the surfaces [19]. In addition, the ambient conditions of osteosynthesis materials are physically and chemically much more complicated and hard to predict. Nevertheless, the initial local environment after implantation will be a blood-filled cavity, mainly comprising a mixture of blood and interstitial fluid [102]. Thus, the initial contact both of stents and orthopedic implants after implantation will be with blood. However, the composition of human blood is much more complex compared to the artificial standard salt solutions

3. Study II

used in corrosion tests. In our previous studies, the initial degradation behavior of absorbable Mg alloys in whole human blood has been investigated. It is self-evident and has been confirmed in several studies that simulated body fluids, such as phosphate-buffered saline (PBS), are insufficient to mimic the *in vivo* degradation behavior of Mg alloys in *in vitro* test systems [80, 120]. Except for the ionic component, the significant difference is that the blood contains large amounts of serum proteins compared to the standard salt solutions. These proteins will come into direct contact with implants in the initial stage and influence the degradation behavior. Fetal bovine serum (FBS) representing the cell and coagulation factor depleted fraction of fetal blood, is readily available in controlled quality. Therefore, FBS was widely employed to investigate the degradation behavior and cytotoxicity of Mg alloys in previous studies [102, 121]. However, the effect of FBS on Zn degradation behavior is widely unexplored.

It is noteworthy that obvious cytotoxic effects of absorbable Zn alloys have been observed in extract tests based on the current ISO standards for cytotoxicity testing (ISO 10993-5 and 10993-12) [73, 74, 93, 122-124]. However, the excellent biocompatibility of pure Zn and Zn alloys observed in *in vivo* studies is indisputable [52, 53, 57]. The general discrepancy between *in vitro* and *in vivo* biocompatibility tests might limit the relevance of *in vitro* tests. Routinely, an extract test with a cell medium is used to investigate the cytocompatibility related to degradation products released from test materials. One of the advantages is that the extraction vehicle can be chosen to mimic the specific human body fluids. It can be assumed that the degradation behavior of alloys in the different extraction vehicles directly influences the results of cytotoxicity [67]. Previously, we reported that a high concentration of serum used in the extraction vehicle for Mg alloys, as a roughly blood-like environment, significantly affects the results of cytotoxicity in the extract test. This might be explained by the “protective” phenomenon of serum components forming a protective layer on Mg alloys, increasing corrosion resistance, and thus reducing the cytotoxicity of Mg alloys [102]. However, the influence of FBS on cytotoxicity of Zn alloys is not yet well understood.

3. Study II

In this study, the first objective was to investigate the role of FBS in the initial degradation behavior of pure Zn and its alloys using an immersion test under cell culture conditions. The second objective was to compare the influence of different extraction media with and without FBS on the cytotoxicity of pure Zn and its alloys.

3.2. Materials and methods

3.2.1. Sample preparation

Two zinc-based alloys, a Zn-4Ag and a Zn-2Ag-1.8Au-0.2V (wt%) (denoted as Zn-Ag-Au-V) alloys were investigated. Details of the fabrication and characteristics of the alloys have been described in previous studies [69, 122]. The age hardened 0.5 mm thick sheets of Zn alloys were cut into the dimension of 30 mm × 10 mm. Likewise, pure Zn sheets were cut into 30 mm × 10 mm × 1 mm in size. The entire surface of the samples was mechanically ground with silicon carbide abrasive papers up to grit 600 (CarbiMet P1200, Buehler, Düsseldorf, Germany) using a manual polisher (Metaserv, Buehler, Düsseldorf, Germany), immediately followed by ultrasonic cleaning in absolute ethanol in an ultrasonic water bath (Sonorex K102H, Bandelin, Berlin, Germany) for 10 min. Prior to tests, all specimens were further disinfected with ultraviolet (UV) radiation for 1 h in a workbench (Lamin Air HB2472, Heraeus Instruments Co., Hanau, Germany). To avoid interference of the native oxidation layer of pure Zn and Zn alloys, the procedure of polishing, cleaning and disinfection was performed within 6 hours prior to all tests.

3.2.2. Immersion test

To correlate between initial degradation behavior and cytotoxicity, we used an extraction method adapted from previously established procedures [74, 93, 122]. The immersion tests were performed with a ratio of surface area to extraction medium volume of 3.0 cm²/mL, according to ISO 10993-12: 2012 [91]. All samples in the media were processed in parallel using standard 6-well culture plates (Cellstar; Cat# 657160; Greiner Bio-One, Frickenhausen, Germany) under standard cell culture conditions (95% relative humidity, 37 °C and 5% CO₂) for 24 ± 1 h.

3. Study II

To further investigate the effect of FBS on degradation of Zn and Zn alloys, five different extraction media were prepared as follows: heat-inactivated fetal bovine serum (FBS; Cat# 10500-064; South American origin; Life Technologies Co., Grand Island, USA), Dulbecco's modified Eagle medium (DMEM; Cat# 21063-029; Life Technologies Co. Paisley, UK), DMEM supplemented with 10% FBS, McCoy's 5A (Cat# M8403; Sigma-Aldrich Chemie GmbH, Steinheim, Germany) and McCoy's 5A supplemented with 15% FBS, respectively. For comparison with human extracellular fluid, the compositions of DMEM, McCoy's 5A and FBS are presented in Table 3.1 [101, 104, 125, 126]. Additionally, the composition of fetal bovine serum, as provided by Life Technologies Co., is listed in Table 3.2.

Table 3.1. Main composition of DMEM, McCoy's 5A and FBS, compared to the human extracellular fluid

Composition	Human extracellular fluid		DMEM	McCoy's 5A	FBS
	Blood plasma	Interstitial fluid			
Inorganic ions (mM)					
Na ⁺	142.0	139.0	127.3	141.0	137.0
K ⁺	4.2	4.0	5.3	5.4	11.2
Mg ²⁺	0.8	0.7	0.8	0.8	n.m.
Ca ²⁺	1.3	1.2	1.8	1.2	3.4
Cl ⁻	106.0	108.0	90.8	117.2	103.0
SO ₄ ²⁻	0.5	0.5	0.8	0.8	n.m.
HPO ₄ ²⁻	2.0	2.0	0.9	4.2	n.m.
HCO ₃ ⁻	24.0	28.3	44.1	26.2	n.m.
Organic components					
Protein	1.2 (mM)	0.2 (mM)	-	-	38.0 (g/L)
Glucose (mM)	5.6	5.6	4.5	16.6	6.9
Amino acids	2.0 (mM)	2.0 (mM)	1.6 (g/l)	0.4 (g/l)	n.m.
Concentrations of buffering agents (mM)					
HCO ₃ ⁻	24.0	28.3	44.1	26.2	n.m.
HPO ₄ ²⁻	2.0	2.0	0.9	4.2	n.m.
HPr	16.0-18.0*	-	-	-	n.m.
Tris-HCl	-	-	25.0	-	n.m.
Total	42.0-44.0	30.3	70.0	30.4	n.m.
Reference	[101, 125]	[125]	[101]	[104]	[126]

* Data are given from the Ref in [101]; n.m., not mentioned in the reference literature.

3. Study II

Table 3.2. The main composition of fetal bovine serum*

Component	Units	Mean	Range	Component	Units	Mean	Range
Total Protein	g/dL	4.2	4.0-4.3	Globulin (total)	g/dL	1.3	1.1-1.5
pH	units	7.3	6.7-7.3	Alkaline Phosphatase	U/L	262	2-319
Osmolality	mosm/kg	314	290-335	GG-Transpeptidase	U/L	5.0	0-7.0
Glucose	mg/dL	130	107-144	SGOT	U/L	60.4	28-161
Hemoglobin	mg/dL	14.2	5.8-23.0	Lactate Dehydrogenase	U/L	559	262-1010
Bilirubin	mg/dL	0.2	0.1-0.4	Cholesterol	mg/dL	34.2	19-54
Uric Acid	mg/dL	3.2	2.6-3.5	Low Density Lipoprotein	mg/dL	2.8	0-7.0
Urea Nitrogen	mg/dL	14.4	15-18	High Density Lipoprotein	mg/dL	6.5	5.0-9.0
Creatinine	mg/dL	3.1	2.8-3.3	Triglycerides	mg/dL	219.5	73-1720
Sodium	meq/L	134	131-137	Growth Hormone	ng/mL	131	126-138
Potassium	meq/L	15.1	12.9-14.2	Insulin	uIU/mL	4.3	2.9-5.5
Calcium	mg/dL	14.6	14.3-15.0	Estradiol	pg/mL	13.8	11.2-17.5
Chloride	meq/L	104.9	102-108	Progesterone	ng/mL	0.03	0.01-0.06
Phosphorus (inorg.)	mg/dL	11.2	10.0-14.0	Testosterone	ng/mL	0.40	0.38-0.45
Iron (total)	ug/dL	195	189-204	T4 (Thyroxine)	ug/dL	14.8	13.9-15.8
Albumin	g/dL	2.6	1.3-2.9	T3	ng/mL	1.2	0.9-1.4

* Data are provided from the Life Technologies Corporation.

3.2.3. Determination of degradation behavior

The initial degradation rate was calculated by the concentrations of released metallic ions in the different media. For each respective measurement, six specimens of each sample were immersed in the different media, respectively. After incubation for 24 h, the pH value of the extracts was measured at room temperature using a 766 Calimatic pH-meter (Knick, Berlin, Germany). After that, the extracts were diluted with deionized water to a final volume of 10 mL. Subsequently, released metallic ion concentrations (Zn^{2+} , Ag^{2+} , Au^{2+} and V^{2+}) were determined by using an inductively coupled plasma optical emission spectrometer (ICP-OES, Perkin-Elmer Optima 4300 DV, Rodgau, Germany). Three-time repetitions for each element were performed at two different wavelengths. Based on released metallic ion concentrations, the degradation rate (DR) was expressed as $\mu g\ cm^{-2}\ day^{-1}$ using the following Eq. (1):

3. Study II

$$\text{Degradation rate} = ((C_{\text{test}} - C_{\text{blank}}) \times V) / (S \times T) \quad (1)$$

Here, C_{test} ($\mu\text{g/mL}$) is the released metallic ion concentration in the extraction media, C_{blank} ($\mu\text{g/mL}$) is the mean metallic ion concentration in the original media, V (mL) is the measured solution volume, S (cm^2) is the specimen surface area, and T (day) is the incubation time. Afterward, a LEO 1430 scanning electron microscope (SEM) equipped with an energy dispersive X-ray (EDX) spectrometer (Carl Zeiss GmbH, Oberkochen, Germany) was used to detect the surface morphology of the samples and to analyze the chemical composition of the corrosion products after extracts preparation.

3.2.4. Cytotoxicity test

According to ISO 10993-5: 2009, an extract test was performed for cytotoxicity evaluation. A mouse fibroblast cell line (L929) and a human osteosarcoma cell line (Saos-2) were used [97]. Cytotoxicity evaluation was performed via two assays: cell viability and morphology were qualitatively analyzed by live/dead fluorescence staining with fluorescein diacetate (FDA) and ethidium bromide (EB), and cell metabolic activity was quantitatively analyzed by Cell Counting Kit-8 (CCK-8). Ti-6Al-4V disks were used as negative control, and pure Cu foils were used as positive control.

3.2.4.1. Cell culture and extract preparation

L929 fibroblasts (DSMZ GmbH, Braunschweig, Germany) were cultured in 24 mL DMEM containing 10% FBS, 1% GlutaMAX (Cat# 35050-038; Life Technologies Co. Paisley, UK) and 1% penicillin/streptomycin (Cat# 15140-122; Life Technologies Co., Grand Island, USA). Saos-2 osteoblasts (DSMZ GmbH, Braunschweig, Germany) were cultured in 10 mL McCoy's 5A supplemented with 15% FBS, 1% GlutaMAX and 1% penicillin/streptomycin. Both cells were grown in 75 cm^2 cell culture flasks (Cat# 430641U; Corning Co., Tewksbury, USA) under standard cell culture conditions, and cells were passaged after reaching approximately 80% confluency.

To further investigate the role of FBS in extract tests of Zn and its alloys, four different extraction vehicles were respectively prepared: DMEM, DMEM + 10%

3. Study II

FBS, McCoy's 5A and McCoy's 5A + 15% FBS, as described in Section 3.2.2. Before transferring to cell cultures, all alloy extracts of unsupplemented DMEM and McCoy's 5A were supplemented with FBS to provide comparable culture conditions (FBS-supplemented media) in all groups. Figure 3.1 illustrates the procedure of DMEM extract preparation in a schematic diagram. 10% FBS was added to the DMEM extracts (without FBS) prior to incubation of the cells with the extracts for 24 h. To maintain the same dilution factor in the corresponding, FBS-supplemented extraction medium (DMEM + 10% FBS), the same amount of liquid in form of DMEM + 10% FBS was added to these extracts. The extracts of McCoy's 5A medium were prepared likewise, using the same procedure. The extracts of McCoy's 5A were supplemented with 15% FBS. Afterward, the metallic ion concentration detected by ICP-OES were further calculated.

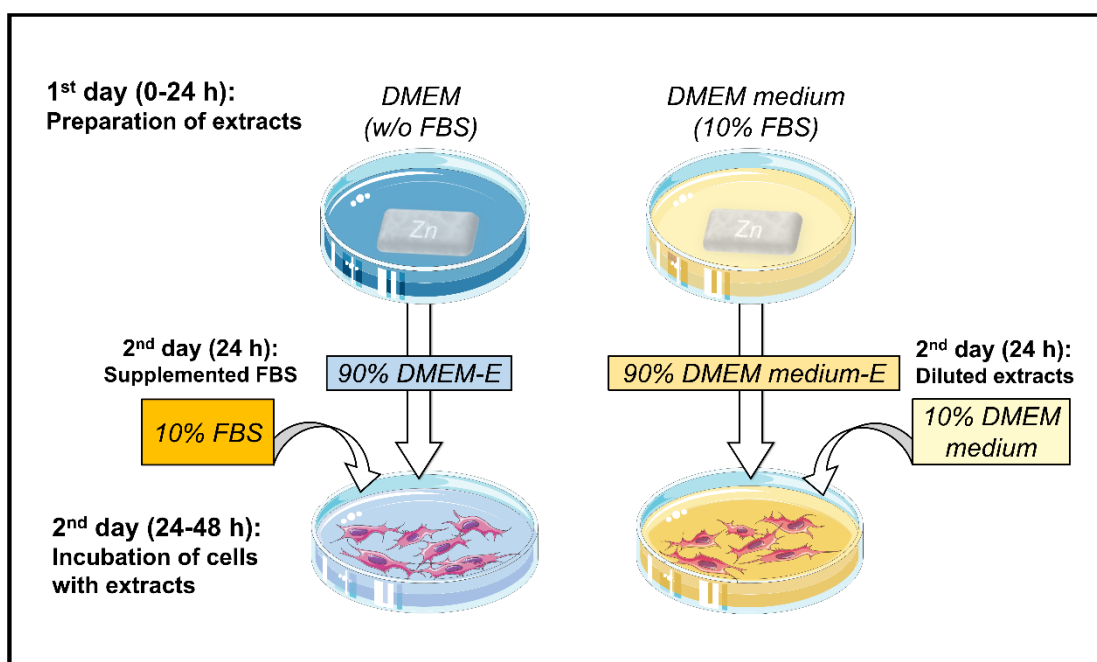


Figure 3.1. Schematic diagram showing the experimental set-up for the investigation of the effect of FBS on extract test results. On the onset of the test, the extraction vehicles were chosen: pure DMEM and DMEM medium containing 10% FBS. After incubation for 24 h, the extracts of pure DMEM were supplemented 10% FBS. For maintaining the same dilution factor, the extracts of DMEM medium were diluted 0.9-fold with fresh DMEM medium.

3.2.4.2. Live/dead fluorescence staining

The cell morphology and viability of L929 and Saos-2 cultured in sample extracts

3. Study II

were qualitatively evaluated by live/dead fluorescence staining, using Hank's balanced salt solution (HBSS, Biochrom AG, Berlin, Germany) containing 25 µg/mL FDA and 1.25 µg/mL EB (Sigma-Aldrich Chemie GmbH, Taufkirchen, Germany). L929 fibroblasts and Saos-2 osteoblasts were respectively inoculated in 12-well culture plates (Costar; Cat# 3512, Corning Costar Co., NY, USA). The cell seeding density was set to 3×10^4 cells/cm². L929 suspension and Saos-2 suspension were adjusted to a density of 5×10^4 cells/mL, and then 2.4 mL of the suspensions were respectively seeded to each well and pre-cultivated overnight. Cell media were then replaced with the respective sample extracts. After 24 h the L929 and Saos-2 morphologies cultured in the different extracts were observed and photographed using a CK2 inverted microscope (Olympus, Tokyo, Japan) equipped with a 550D DSLR camera (Canon, Tokyo, Japan). Subsequently, sample extracts were removed, and the cells were gently rinsed with HBSS. Afterward, 1.5 mL staining solution was added to each test well and samples were stained for 10 min in darkness. After rinsing with HBSS, the cells were observed with an Optiphot-2 fluorescence microscope (Nikon, Tokyo, Japan) equipped with a 550D DSLR camera. Representative areas of the cell layer were photographed to document the amount of living and dead cells, stained by FDA and EB into green and red, respectively.

3.2.4.3. Cell counting kit-8 assay

The inhibition of the metabolic activity of L929 and Saos-2 cells in different sample extracts was quantitatively analyzed using the CCK-8 assay (Dojindo Laboratories Co., Kumamoto, Japan). Corresponding to the experiments with live/dead fluorescence staining, the cell seeding density was also set to 3×10^4 cells/cm². For tests, 200 µL of L929 and Saos-2 suspensions (5×10^4 cells/mL) were respectively seeded in 96-well culture plates (Cellstar; Cat# 655180; Greiner Bio-One, Frickenhausen, Germany) and cultured overnight. Subsequently, the cell medium was replaced by 150 µL sample extracts. After incubation for 24 h, extracts were replaced by 100 µL fresh medium without FBS to avoid interference of Zn alloy degradation products and serum with the tetrazolium-based assay. Afterward, 10 µL of CCK-8 reagent was added to each

3. Study II

test well and the cultures were incubated for 2 h, following manufacturer's instructions. The optical density (OD) was measured at 450 nm in a Tecan F50 microplate ELISA reader (Tecan Austria GmbH, Grödig, Austria). To calculate relative metabolic activity compared to the negative control, the following formula was used:

$$\text{Relative metabolic activity (\%)} = ((\text{OD}_{\text{test}} - \text{OD}_{\text{blank}}) / (\text{OD}_{\text{negative}} - \text{OD}_{\text{blank}})) \times 100\% \quad (2)$$

Here, OD_{test} is the mean OD value of the test groups, and $\text{OD}_{\text{negative}}$ is the mean OD value of the negative control, OD_{blank} is the mean OD values of the cell culture media with the CCK-8 reagent. As described ISO 10993-5: 2009 [25], a cytotoxic effect was defined as a metabolic activity of cells subjected to extracts of test materials below 70% of the negative control.

3.2.5. Statistical analysis

All data were tested for normal distribution by Shapiro-Wilk normality test and homogeneous variance by Levene test. Data sets with abnormal distribution (non-parametric data sets) were analyzed using the Kruskal-Wallis test followed by the Nemenyi post hoc test. Parametric data sets were analyzed using one-way analysis of variance (ANOVA) with extraction medium as an independent factor, followed by the Tukey highest significant difference post hoc test. Parametric data sets with heterogeneous variance were analyzed using one-way ANOVA (homogeneous variance not assumed) followed by the Games-Howell post hoc test. Statistical analyses were analyzed using SPSS version 22.0 software (IBM, Armonk, USA) and statistical significance was considered at P -value < 0.05 .

3.3. Results

3.3.1. Degradation properties

To determine the effect of FBS on the initial degradation rate, samples were immersed in different media under cell culture conditions for 24 h. The initial degradation rate was assessed by metallic ion release detected by ICP-OES, as shown in Figure 3.2. Due to other metallic ion concentrations (Ag^{2+} , Au^{2+} and V^{2+}) being below the detection limit ($< 50 \mu\text{g/L}$), only Zn ion concentration in the

3. Study II

different media was quantified. According to the measurement of Zn ion release, all samples immersed in FBS showed the highest degradation rates. A comparison of degradation rates in media with and without FBS supplement confirmed the corrosion-promoting effect of FBS: the degradation rates of all samples in DMEM + 10% FBS (or McCoy's 5A + 15% FBS) respectively were higher than their counterparts in unsupplemented DMEM (or McCoy's 5A). ANOVA (without homogeneous variance) confirmed the statistically significant difference in the degradation rate. Games-Howell post hoc pairwise comparisons confirmed a significantly higher degradation rate ($p < 0.05$) for Zn-4Ag ($16.29 \pm 6.28 \mu\text{g cm}^{-2} \text{day}^{-1}$) and Zn-Ag-Au-V ($16.10 \pm 5.88 \mu\text{g cm}^{-2} \text{day}^{-1}$) in DMEM + 10% FBS in comparison to Zn-4Ag ($2.99 \pm 0.68 \mu\text{g cm}^{-2} \text{day}^{-1}$) and Zn-Ag-Au-V ($3.70 \pm 0.57 \mu\text{g cm}^{-2} \text{day}^{-1}$) in unsupplemented DMEM. Likewise, post hoc pairwise comparisons showed that the degradation rates were significantly increased ($p < 0.05$) for Zn-4Ag ($9.01 \pm 5.21 \mu\text{g cm}^{-2} \text{day}^{-1}$) and Zn-Ag-Au-V ($6.72 \pm 3.05 \mu\text{g cm}^{-2} \text{day}^{-1}$) in McCoy's 5A + 15% FBS, compared to their counterparts of Zn-4Ag ($0.18 \pm 0.07 \mu\text{g cm}^{-2} \text{day}^{-1}$) and Zn-Ag-Au-V ($0.23 \pm 0.14 \mu\text{g cm}^{-2} \text{day}^{-1}$) in unsupplemented McCoy's 5A, respectively. As predicted, the initial degradation rates of Zn alloys in DMEM and McCoy's 5A were increased by supplementation with FBS in this test setup.

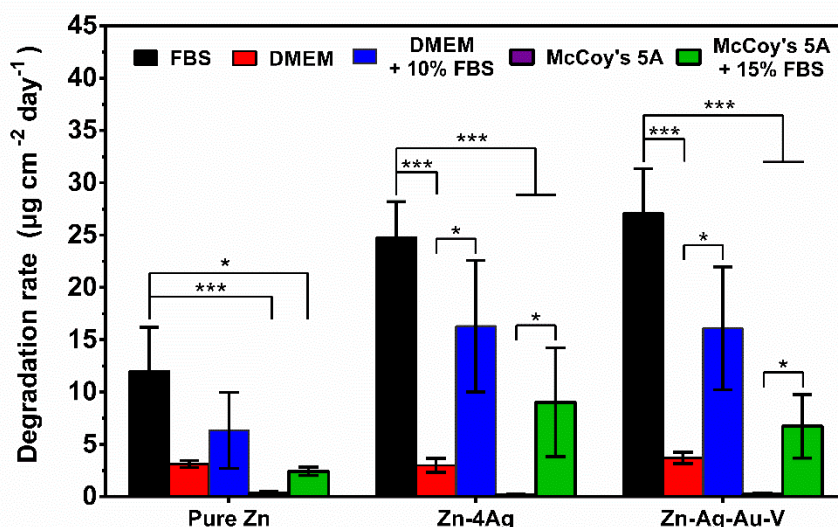


Figure 3.2. Initial degradation rates of pure Zn, Zn-4Ag and Zn-Ag-Au-V alloys calculated from released Zn ion concentration in different media under cell culture conditions for 24 h. Values are mean \pm SD, $n = 6$; Significant differences are marked by asterisks

3. Study II

(significance level * $p < 0.05$, *** $p < 0.001$).

Figure 3.3 demonstrates the SEM-EDX analysis of the surface morphology and elemental composition analysis of pure Zn and Zn alloys after immersion in different media. Visible to the naked eye, inhomogeneous thin degradation layers were formed on the surfaces of samples after immersion. SEM micrographs showed no obvious corrosion layers covering the whole surfaces, only a small amount of irregular tiny degradation particles distributed on the surfaces was detected. EDX analysis revealed the presence of the elements Zn, O, C, Cl, Ca, P and S in these degradation particles.

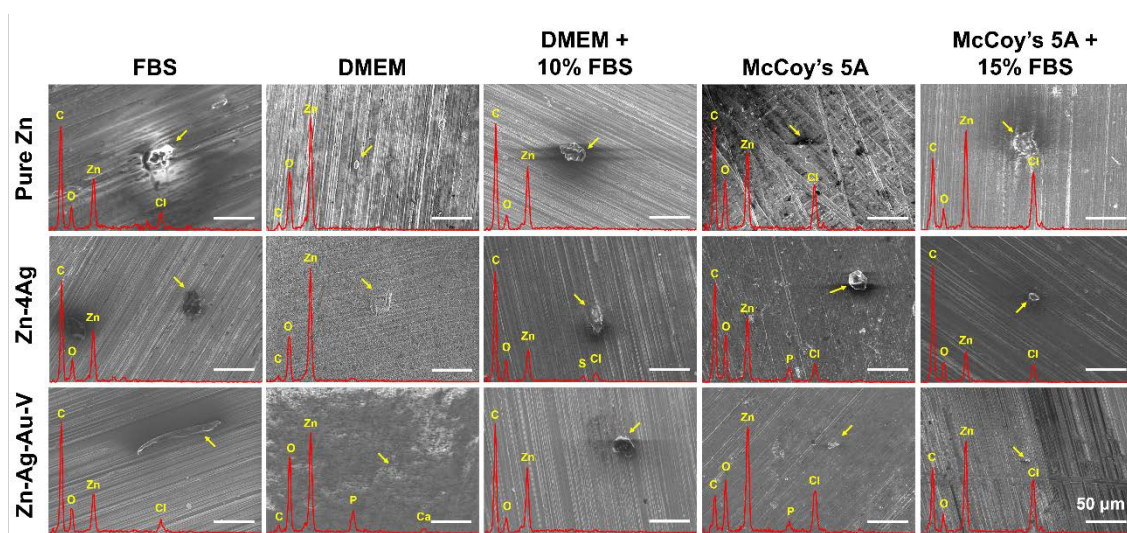


Figure 3.3. The SEM-EDX analysis of pure Zn and Zn alloys after immersion in different media under cell culture conditions for 24 h. Representative SEM images of degradation products on the surfaces (scale bar = 50 μm). The EDX spectrum (inset red line) indicates the elemental composition of degradation products, corresponding to points marked with a yellow arrow (energy range between 0.0 keV and 5.0 keV).

3.3.2. Analysis of alloy extracts

Table 3.3 illustrates the pH values of sample extracts after 24 h. The pH value of all extracts stayed in the range of 8.0-8.5, no dramatic changes were observed. Although pH values of McCoy's 5A media were higher than of DMEM media, the pH tended in the opposite direction, indicating more hydroxide ion release in the DMEM-based media. Prior to the cytotoxicity test, sample extracts were further prepared as described in Section 3.2.4.1. The mean Zn ion concentration of sample extracts is summarized in Table 3.3. ANOVA (without homogeneous

3. Study II

variance) was employed to confirm statistically significant differences. Specifically, post hoc pairwise comparisons indicated statistically higher Zn ion concentrations in the extracts of DMEM + 10% FBS for Zn-4Ag ($688.21 \pm 264.87 \mu\text{M}$) and Zn-Ag-Au-V ($679.89 \pm 248.17 \mu\text{M}$) when compared with the DMEM-extracts of Zn-4Ag ($129.19 \pm 28.69 \mu\text{M}$) and Zn-Ag-Au-V ($159.11 \pm 23.89 \mu\text{M}$) ($p < 0.05$). In addition, ANOVA confirmed statistically significant differences of Zn alloys in the extracts of McCoy's 5A with or without FBS. Post hoc pairwise comparisons showed that the Zn ion concentrations in the extracts of McCoy's 5A + 15% FBS for Zn-4Ag ($365.03 \pm 207.63 \mu\text{M}$) and Zn-Ag-Au-V ($273.96 \pm 121.37 \mu\text{M}$) were significantly higher than their counterparts in the extracts of McCoy's 5A for Zn-4Ag ($11.49 \pm 2.87 \mu\text{M}$) and Zn-Ag-Au-V ($13.46 \pm 5.63 \mu\text{M}$) ($p < 0.05$). Nevertheless, the Kruskal-Wallis showed no statistically significant differences for the Zn ion release from pure Zn in media with or without FBS ($p > 0.05$). Still, the overall tendency clearly indicated that the Zn ion concentration was increased by the presence of FBS in the extraction media.

Table 3.3. The pH value and released Zn ion concentration of sample extracts.

	DMEM	DMEM + 10% FBS	McCoy's 5A	McCoy's 5A+ 15% FBS
pH value				
Initial	7.69	7.66	8.20	8.15
Pure Zn	8.12 ± 0.09	8.08 ± 0.03	8.38 ± 0.02	8.23 ± 0.01
Zn-4Ag	8.17 ± 0.03	8.13 ± 0.01	8.50 ± 0.05	8.33 ± 0.02
Zn-Ag-Au-V	8.21 ± 0.03	8.16 ± 0.01	8.49 ± 0.01	8.38 ± 0.02
Zn ion concentration (μM)				
Pure Zn	134.27 ± 14.30^a	267.98 ± 153.04^a	17.55 ± 7.19^A	102.75 ± 16.21^A
Zn-4Ag	129.19 ± 28.69^a	688.21 ± 264.87^b	11.49 ± 2.87^A	365.03 ± 207.63^B
Zn-Ag-Au-V	159.11 ± 23.89^a	679.89 ± 248.17^b	13.46 ± 5.63^A	273.96 ± 121.37^B

Different superscript letters within a row indicate statistical significance of Zn ion concentration between media with and without FBS ($p < 0.05$)

3.3.3. Cell morphology and viability

To investigate the effect of FBS on cytotoxicity, cell morphologies of L929 and

3. Study II

Saos-2 cultured in the specified extracts for 24 h were documented by light microscope. Exemplary images of the respective cultures are shown in Figure 3.4. The cell morphology of L929 cultured in DMEM extracts with FBS exhibited an irregular circular shape, and a fraction of the cells was floating in the extracts, which is consistent with the positive (toxic) control group. Although some L929 cells were also suspended in the DMEM extracts without FBS, another part of the cells was adhering. These cells showed a spindle shape and clear cellular outlines, which was obviously different from the corresponding cultures in DMEM extracts with FBS. Furthermore, the optical images of Saos-2 osteoblasts incubated in McCoy's 5A extracts without FBS showed predominantly regular shaped morphologies with intact outlines, which is in agreement with the negative control group. In contrast, most Saos-2 osteoblasts in the McCoy's 5A extracts with FBS tended to lose their attachment resulting in a spherical shape, similar to the positive control group.

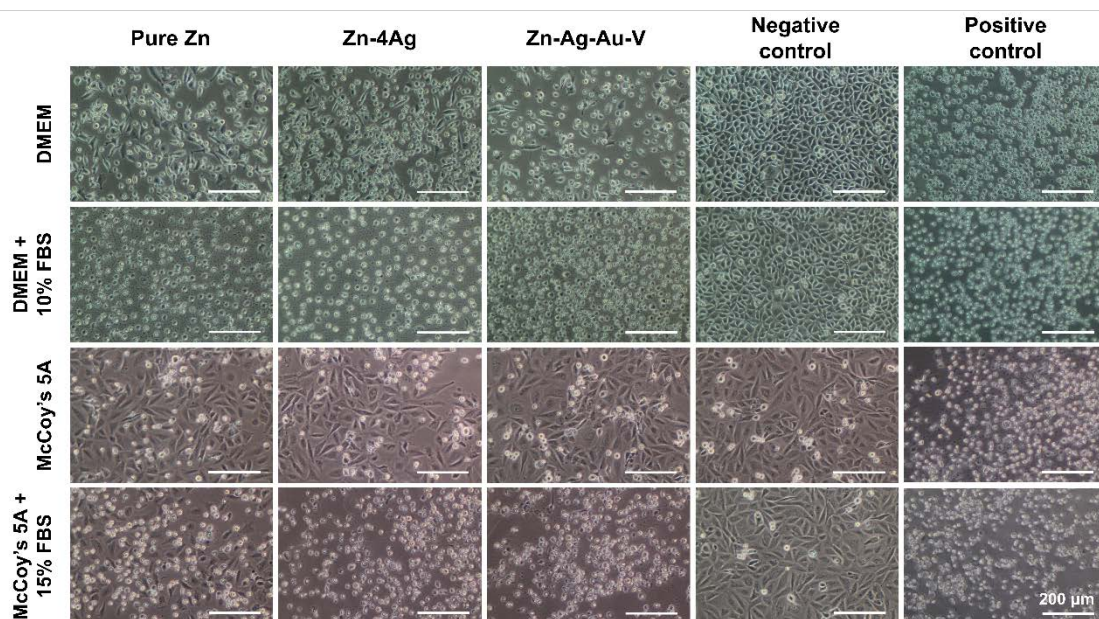


Figure 3.4. Representative optical images of L929 fibroblasts incubated with sample extracts of DMEM and DMEM + 10% FBS, and Saos-2 osteoblasts incubated with sample extracts of McCoy's 5A and McCoy's 5A + 15% FBS for 24 h (magnification 160 \times ; scale bar = 200 μ m). Ti-6Al-4V alloy was used as negative control and pure Cu foil as positive control.

Figure 3.5 shows live/dead fluorescence microscopy images of L929 fibroblasts and Saos-2 osteoblasts after incubation with the different extracts for 24 h. The

3. Study II

L929 fibroblasts were nonviable in the DMEM extracts with FBS, indicated by almost total red staining, comparable with the positive control. On the contrary, some green fluorescent L929 cells existed in the extracts without FBS, indicating that part of the cells survived. Thus, it can be inferred that cell viability inversely correlates with FBS supplementation. In addition, Saos-2 osteoblasts in the extracts of McCoy's 5A without FBS appeared more viable and spread. Although the density of living osteoblasts in these groups was slightly less than the density in the negative control group, dead cells were rarely observed. Regarding the extracts supplemented with FBS, the results of the Saos-2 cells corresponded to those observed with L929 cells, i.e. the cell viability was notably decreased. Again, according to the qualitative analysis based on fluorescence images, the presence of FBS in the extraction media inversely correlates with the viability of both cell lines used in this study.

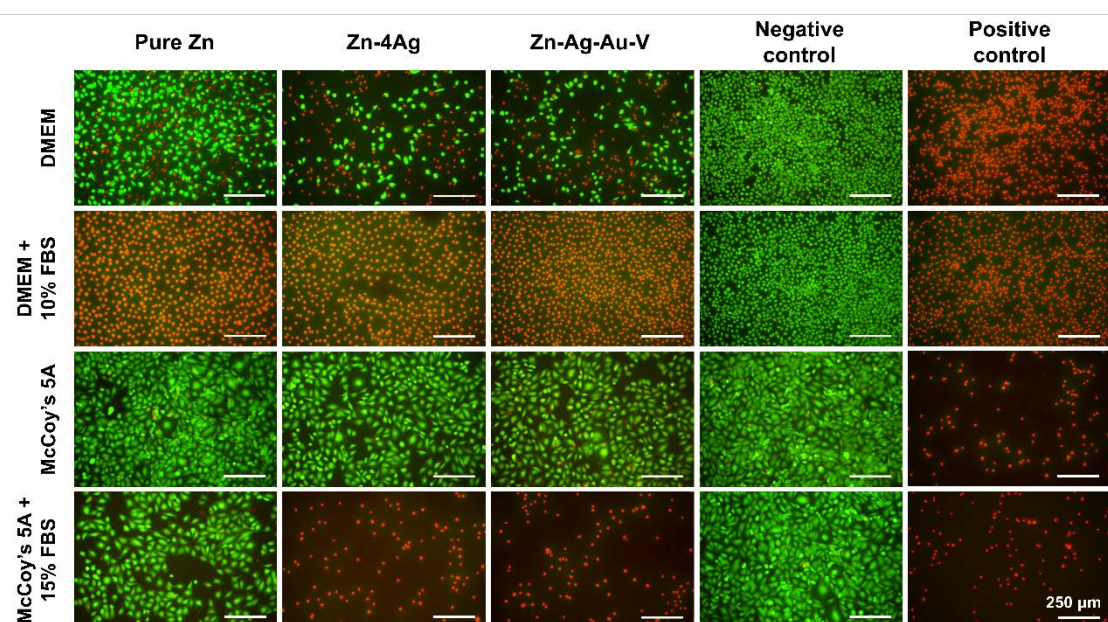


Figure 3.5. Representative fluorescence microscopy images of L929 fibroblasts incubated with sample extracts of DMEM and DMEM + 10% FBS, and Saos-2 osteoblasts incubated with sample extracts of McCoy's 5A and McCoy's 5A + 15% FBS for 24 h. Ti-6Al-4V alloy was used as negative control and pure Cu as positive control. Cells were stained by live/dead fluorescence staining using FDA & EB, where the green fluorescence represents live cells stained by FDA and the red fluorescence represents dead cells stained by EB (magnification 100 \times ; scale bar = 250 μ m).

3.3.4. Relative metabolic activity

3. Study II

To quantitatively determine the effect of FBS on cytotoxicity, an extract test was performed, measuring the relative metabolic activity of L929 and Saos-2 in different extracts for 24 h in comparison to the negative control, as shown in Figure 3.6. The results of the extract test showed that L929 fibroblasts exposed to the FBS-containing extracts from all samples displayed an extremely low relative metabolic activity (almost 0% of the negative control). The Kruskal-Wallis test confirmed statistically significant differences in the relative metabolic activity. Post hoc pairwise comparisons showed that L929 viability in all extracts without FBS was statistically increased compared to the respective counterparts with FBS ($p < 0.001$). Interestingly, L929 in the DMEM extracts without FBS of pure Zn had a relative mean metabolic activity above 70% of the control (less than 30% inhibition), which is considered as non-cytotoxic according to ISO 10993-5: 2009. Furthermore, Saos-2 osteoblasts cultured in the extraction media without FBS exhibited a relatively high metabolic activity of above 70% for all materials tested. In contrast, obvious reductions of those values (below 40% of the control) were observed for the extraction medium with FBS. The Kruskal-Wallis test followed by the Nemenyi post hoc test indicated generally significantly different relative metabolic activities for Saos-2 cells in extraction media with and without FBS ($p < 0.001$), respectively. Hence, the effect of FBS on cytotoxicity determined by relative metabolic activity is consistent with the results of the live/dead fluorescence staining.

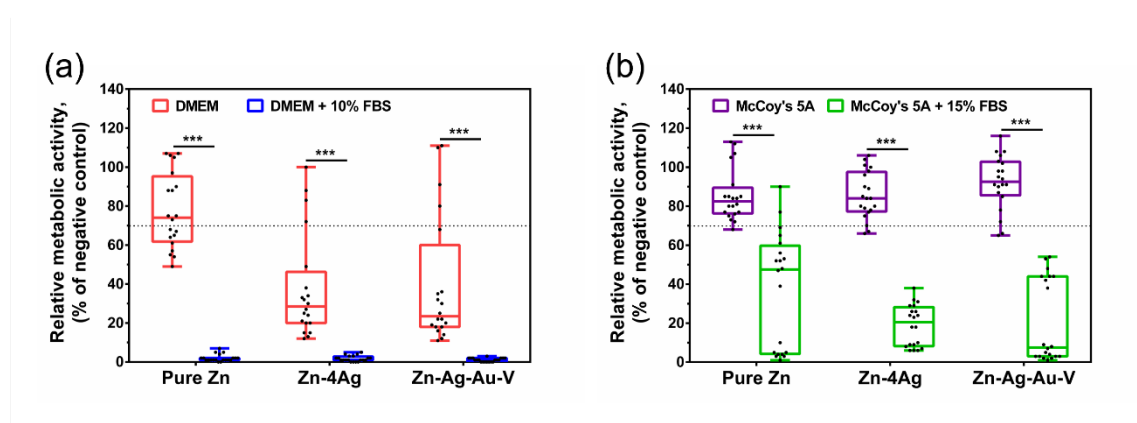


Figure 3.6. Box-and-whisker plot of relative metabolic activity of (a) L929 fibroblasts and (b) Saos-2 osteoblasts after 24 h incubation with extracts, determined by CCK-8 assay. Ti-6Al-4V alloy was used as negative control and set to 100%. Dashed lines represent 70% of control, which is a cut-off line between toxic and nontoxic effects. The data of five independent experiments are shown as the box-and-whisker plot (maximum, 75th, 50th,

3. Study II

and 25th percentiles and minimum) and black dots for each measurement (n = 20); Significant differences are marked by asterisks (Significance level *** p < 0.001).

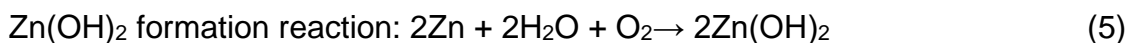
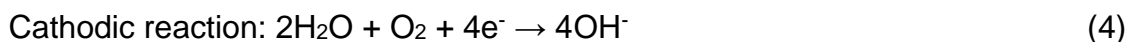
3.4. Discussion

3.4.1. Initial degradation behavior

A standardized *in vitro* approach for biocorrosion studies for absorbable metallic implant materials like Zn alloys is still lacking. Standard corrosion experiments in buffered salt solutions like PBS or artificial saliva do not correspond to the clinical situation. Absorbable Mg- or Zn-based alloys are proposed as materials for orthopedic implants or stents. These implants are inserted either into a blood-filled implant site or the blood system itself. The initial postoperative environment, affecting the corrosion behavior of these implants, therefore is blood. In the present study, to mimic the initial implantation environment, FBS has been chosen as an *in vitro* model of blood. In this model, the influence of FBS on the initial degradation behavior of pure zinc, Zn-4Ag and Zn-Ag-Au-V was investigated in an immersion test model performed under cell culture conditions, i. e. in cell culture media at 37 °C in an incubator. It has already been shown that the degradation behavior of Mg alloys under cell culture conditions is closer to the physiological environment [127, 128]. Based on the previous studies, the immersion test in this study was performed with cell culture medium as extraction vehicle, to enable the correlation between degradation behavior and cytotoxicity evaluation [93, 94, 122].

Considering the degradation mechanism, the degradation behavior of pure Zn in the body is intrinsically determined by a corrosion process that generally proceeds via an electrochemical reaction [23]. Generally, physiological body fluids exhibit a neutral to slightly alkaline pH (i.e., human interstitial fluid, or blood plasma, etc.), except for some partly acidic environments (i.e., gastric juice, or urine, etc.). Pure Zn has the tendency to be passivated in the nearly neutral physiological environment (pH value of human plasma: 7.35-7.45), according to the Pourbaix diagram. Thus, the initial degradation reactions were involved in the following anodic dissolution of the metal and the cathodic reduction of oxygen, as shown in from Eq. (3) to Eq. (5) [51, 77, 119]:

3. Study II



In our experiments, pure Zn and Zn alloys are immersed in different extraction media. Initially, the interaction between the electrolyte-containing aqueous media and the Zn surfaces causes Zn^{2+} and OH^{-} release based on the Eq. (3) and Eq. (4). Moreover, some corrosion particles on the Zn surface were formed, and EDX analysis revealed the presence of several elements such as Zn, C, O, Cl, Ca, P and S. It can be assumed that these elements found in the degradation particles derive mainly from chemical reactions with components of the different media, as listed in Table 3.1. Thus, these degradation particles might be mainly composed of zinc carbonates, zinc hydroxides and zinc phosphates, as reported in previous studies [89, 106, 129].

According to the determined degradation rates, it is obvious that FBS accelerates the initial degradation of pure Zn, Zn-4Ag and Zn-Ag-Au-V alloys. However, the underlying mechanisms of FBS mediated acceleration of Zn alloy degradation are unclear due to the complex nature of the interactions. Usually, apart from the corrosion properties of the alloy itself, the degradation rate mainly depends on the composition of the media used in the different *in vitro* tests [103, 127]. The factors influencing the degradation behavior are not only the inorganic ingredients but also the buffering system and organic components. As listed in Table 3.2, the composition of FBS is complex and variable, because serum is derived from individuals and differently processed. In fact, FBS is a mixture of various physiological components and contains serum proteins, polypeptides, fats, growth factors, hormones and required nutrients, etc. [130]. Serum proteins, as one of the main constituents, are in the range from 32 g/L to 70 g/L, with bovine serum albumin (BSA) being the major fraction and amounting from 20 g/L to 36 g/L [126]. Törne et al. [131] demonstrated that rapid protein adsorption on Zn surfaces immersed in whole blood prevents the initial passivation of the surface by a protective zinc-phosphate layer, leading to an increased initial corrosion rate. Thus, one of the assumptions for this study was that the initial degradation rate

3. Study II

of the tested alloys might be influenced by serum protein.

To our knowledge, only few studies have investigated the interaction between FBS and the corrosion behavior of Zn and its alloys. In most previous studies, FBS has been used to provide serum protein in simulated body fluids to investigate corrosion behavior of metals, such as Mg alloys [121, 132, 133]. Nonetheless, studies of the influence of the FBS on corrosion behavior of Mg alloys have also produced diverging results, and the corrosion mechanisms are not fully understood. For pure Mg, Yamamoto et al. [132] reported additional FBS might form a diffusion barrier on the surface of pure Mg, which decreases the degradation rate of pure Mg. Meanwhile, Liu et al. [133] also demonstrated that bovine serum albumin might elicit a 'protective effect' decreasing corrosion of the AZ91 magnesium alloy. Nevertheless, the effect of proteins on the corrosion of Mg alloys might depend on the surface characteristics of the samples or alloy composition. Gu et al. [134] found that the corrosion rate of a Mg-Ca alloy increased in DMEM with FBS whereas the AZ91 alloy showed the opposite tendency. Also, Johnson et al. [121] reported that the degradation rate of a Mg-Y alloy with an oxidized surface was reduced in the presence of FBS, but the degradation rate of the same alloy without an oxidized surface was increased by FBS. These varying trends imply that the influence of proteins on corrosion is more complicated than the simplistic adsorption hypothesis model. Importantly, for *in vitro* biodegradation tests of Zn alloys, the addition of FBS in the solution is essential to bridge the gap between simple ionic solutions and the more complicated physiological fluids in the body. However, the mechanisms of FBS on the degradation behavior of Zn alloys are still not fully understood and require further basic studies.

3.4.2. Cytotoxicity evaluation

As a potential candidate for biomaterials, biocompatibility and feasibility of different Zn alloys have been investigated by several previous studies [19, 51, 77, 119]. However, the correlation between *in vitro* and *in vivo* biocompatibility results is poor. Specifically, the biocompatibility evaluation of Zn alloys in most previous studies exhibits an obvious toxic effect for the original undiluted extracts in

3. Study II

standardized cytotoxicity tests according to ISO standards 10993-5 and -12. The significant difference can be attributed to the fact that the current ISO standards were originally designed for screening the biocompatibility of non-absorbable materials. Due to the simplicity and feasibility of the experimental methodology, and to the worldwide acceptance of these harmonized standards by regulatory authorities, these standards were most commonly adopted for screening novel absorbable alloys [67, 135]. Considering the basic principles of the extract test, cytotoxicity was influenced by degradation products released from alloys via extraction with different extraction vehicles. Thus, the results were directly affected by three main factors: alloy properties, cell lines used and extraction conditions.

In this study, one of the objectives was a comparison of the presence or absence of FBS in the extraction medium on the results of extract testing of Zn and Zn alloys. According to the analysis of alloy extracts (Table 3.3), the main degradation product released from the alloys was free Zn^{2+} ions in the media. Due to buffering agents in the media, no dramatic changes of pH value were detected, and pH values stayed in the range of 8.0-8.5, implying that hydroxide ion release is limited. The previous study demonstrated no obvious decrease in cell viability of L929 cells when $pH < 9$ in the cell medium [136]. That means released Zn^{2+} ions in the extracts are mainly responsible for the observed toxic effect. In this study, cytotoxicity was assessed using different assays based on qualitative evaluation of cell viability and morphology, and quantitative measurement of cell metabolic activity. Qualitative and quantitative results proved to correlate very well. As shown in Figure 3.6, when media with FBS were used as extraction vehicle, mean relative metabolic activities below 70% were found for the Zn alloys, indicating more than 30% inhibition, which is the threshold for obvious cytotoxic effects in the abovementioned ISO standards. This indicates that the released Zn^{2+} concentration is beyond the cellular tolerance limit of L929 and Saos-2. For instance, in extracts of McCoy's 5A with FBS, the Zn ion concentration of Zn-4Ag and Zn-Ag-Au-V was $365.03 \pm 207.63 \mu M$ and $273.96 \pm 121.37 \mu M$, respectively. A comparison with the literature revealed that the range of Zn ion concentration in these extracts was far beyond most cellular tolerance limits, e.g., for L929

3. Study II

fibroblasts ($< 80 \mu\text{M}$) [93], human primary osteosarcoma cells U-2 OS ($< 120 \mu\text{M}$) [93], primary human coronary artery endothelial cells ($< 100 \mu\text{M}$) [137] and vascular smooth muscle cells ($< 80 \mu\text{M}$) [138]. The Ag concentration in the extracts was under the detection limit of OCP (approx. $0.5 \mu\text{M}$). This is about factor 10 under the reported tolerance limit, indicating that Ag does not contribute to the toxic effects observed here [139].

The metabolic activity of both cell types tested was less decreased when media without FBS were used as extraction vehicle. For Saos-2 osteoblasts cultured in the extracts of McCoy's 5A without FBS, no obvious cytotoxic effects were observed for all test samples because all relative metabolic activities in the cultures were exceeding 70%. This finding corresponds also to the fact that the Zn^{2+} ion concentrations of Zn-4Ag ($11.49 \pm 2.87 \mu\text{M}$) and Zn-Ag-Au-V ($13.46 \pm 5.63 \mu\text{M}$) in McCoy's 5A were lower than the maximum safe concentrations of Zn^{2+} for the Saos-2 osteoblasts.

The results for the metabolic activity of L929 in the extracts of DMEM without FBS differed, especially for the Zn-4Ag and Zn-Ag-Au-V alloy, as shown in Figure 3.6a. One possible explanation can be that the Zn ion concentration in the extracts of DMEM with Zn-4Ag ($129.19 \pm 28.69 \mu\text{M}$) and Zn-Ag-Au-V ($159.11 \pm 23.89 \mu\text{M}$) is not much higher than the reported cellular tolerance of L929 for the Zn ion concentration ($< 80 \mu\text{M}$) [93].

Indeed, few studies have reported the absence of cytotoxic effects in original undiluted extracts of Zn-based alloys used in extract tests, as summarized in Table 3.4 [53, 87, 88, 113, 140-143]. Interestingly, the studies by Li et al. [53] have found no obvious cytotoxicity for ECV304 and MG63 cells in original extracts of Zn-1Mg, Zn-1Ca and Zn-1Sr alloys. Similarly, Xiao et al. [144] investigated the cytotoxicity of a Zn-0.05Mg alloy with an extract test and demonstrated cytotoxicity of Zn-0.05Mg extracts was in Grade 0 and Grade 1, indicating no or weak cytotoxic effects. It is worthwhile to note that the above studies used serum-free cell culture media as an extraction medium, without explaining why an extraction medium without serum was chosen. In contrast, Kubásek et al. [93] investigated the cytotoxicity of a Zn-0.8Mg alloy and demonstrated an obvious

3. Study II

toxic effect for L929 fibroblasts and U-2 OS osteoblasts with the original extracts of the Zn-0.8Mg alloy, when cell media containing 5% FBS were used as an extraction medium. Likewise, previous work by Jablonská et al. [94] has demonstrated that the extracts prepared from untreated Zn-1.5Mg caused obvious cytotoxicity in L929 cells. Apart from the different alloys and cell lines, these discrepancies are probably explained by the fact that the cytotoxicity of Zn-Mg alloys was increased by the presence of FBS in the extraction medium, which is principally in agreement with our results. Another reason for the differing outcomes in several investigations are the different surface to volume ratios used in the extraction tests. In our study we used $3 \text{ cm}^2 / \text{ml}$, which results in a more than twofold higher concentrated extract compared to $1.25 \text{ cm}^2 / \text{ml}$ as used in other studies.

A critical issue regarding the extract test is the choice of an appropriate extraction vehicle. The current ISO standard for cytotoxicity testing (10993-5:2009) suggests three types of extraction vehicles, namely a) culture medium with serum, b) physiological salt solution or c) other suitable media. Culture medium with serum is explicitly recommended because it is able to extract polar and non-polar components as well and promotes cell culture viability. The standard also demands that the solvent selected as the extraction vehicle should simulate the conditions during clinical application as good as possible [97]. In general, the incubation of test surfaces with serum containing culture medium instantly leads to the formation of a layer consisting mainly of albumin and fibronectin. The layer acts as a diffusion barrier at the material interface, limiting the release of possible toxic components [135]. Likewise, as pointed out in our previous study concerning a biocompatibility screening of Mg alloys, this serum protein layer will also be formed after implantation and thus mimics the initial physiological situation *in vivo* to a certain extent [102]. Obviously, using an extraction medium with FBS can mimic the complex changes of the implant environment in the long-term clinical situation only to a limited extent. For instance, osseous implants come into contact with serum due to the injury set by the implantation and subsequent blood coagulation, but serum is not the long-term physiological environment of these implants *in vivo*. For absorbable osseous implants

3. Study II

consisting of Zn alloys, therefore, developing a suitable extraction vehicle for a long-term extraction test simulating clinical conditions is still an issue which should be further investigated to better predict and evaluate biocompatibility.

Table 3.4. Summary of the absence of cytotoxic effect in original undiluted extracts of absorbable Zn-based alloys used in extract test according to ISO 10993-5 and -12.

Alloys (wt%)	Cell lines*	Extract conditions			Relative cell viability (%)**	Ref.
		Medium	SA:V (cm ² /mL)	Time (h)		
Zn-1Mg Zn-1Ca Zn-1Sr	VSMC, ECV304, MG63	Serum-free cell culture medium	1.25	72 h	ECV304 in all alloys extracts: > 80% ^a VSMC in all alloys extracts: 60-80% ^a MG63 in all alloys extract: 100-120% ^a	[53]
As-cast Zn- 1.2Mg	MG63	Cell medium	1.25	72 h	MG63 in as-cast Zn-1.2Mg extracts: 80-90% ^b	[88]
Zn-0.05Mg	L929	Serum-free DMEM medium	1.25	72 h	L929 in the extracts: > 85%	[140]
Zn-1Mg Zn-1Mg-0.5Ca	Saos-2	DMEM with FBS	1.25	24 h	Saos-2 in Zn-1Mg and Zn- 1Mg-0.5Ca extracts: > 100%	[141]
Zn-1Mg-Ca Zn-1Mg-1Sr Zn-1Ca-1Sr	MG63	n.m.	n.m.	n.m.	MG63 in all alloys extracts: > 100%	[87]
Zn-3Cu-0.5Mg Zn-3Cu-1Mg	EA.hy92 6	DMEM	1.25	72 h	EA.hy926 in Zn-3Cu-0.5Mg and Zn-3Cu-1Mg extracts: 80-100%	[142]
Zn-0.5Al Zn-0.5Al-0.1Mg Zn-0.5Al-0.3Mg Zn-0.5Al-0.5Mg	MC3T3- E1	n.m.	n.m.	n.m.	MC3T3-E1 in all alloys extracts: 80-110% ^c	[113]
Zn-0.5Al-0.5Mg Zn-0.5Al- 0.5Mg-XBi where X = 0.1, 0.3, 0.5	MC3T3- E1	n.m.	1.25	24	MC3T3-E1 in all alloys extracts: 80-110% ^d	[143]

*Rodent vascular smooth muscle cells (VSMC), human umbilical vein endothelial cells (ECV304), human osteosarcoma cells (MG63), murine fibroblast cells (L929), human osteosarcoma cells (Saos-2), human endothelium-derived cells (EA.hy926) and murine calvarial preosteoblasts (MC3T3-E1).

**Relative cell viability (%) presents cell viability in original alloy extracts after incubation for 24 h,

3. Study II

compared to negative control.

n.m., not mentioned in the reference literature.

a Data gathered from the figure (Figure 5) in the literature [53].

b Data gathered from the figure (Figure 6a) in the literature [88].

c Data gathered from the figure (Figure 4e) after incubation for 2 days in the literature [113].

d Data gathered from the figure (Figure 10) after incubation for 2 days in the literature [143].

3.5. Conclusions

In this study, the degradation rates of pure Zn, Zn-4Ag and Zn-Ag-Au-V alloys were evaluated in FBS, DMEM, McCoy's 5A, DMEM + 10% FBS, and in McCoy's 5A + 15% FBS, respectively. The results demonstrate that the degradation rates of the test samples were affected by the composition of the media. Samples extracted in FBS showed the highest initial degradation rates, and supplementation of DMEM or McCoy's 5A with FBS notably accelerated the initial degradation process. Analysis of the released Zn ion concentration in the extracts showed that the decreased cytotoxicity observed in the extract media without FBS was obviously caused by the lower concentration of released Zn ions in these extracts. Therefore, besides tests with salt solutions, as used in standard corrosion tests, the influence of the serum components on the corrosion mechanism of Zn alloys should be further investigated. Likewise, selecting an appropriate extraction medium for cytotoxicity evaluation of Zn alloys should still be further studied based on the current standards.

4. Study III

4. Study III: Response of human periosteal cells to degradation products of zinc and its alloy

The part is a reprint of the following manuscript:

Ping Li, Jingtao Dai, Ernst Schweizer, Frank Rupp, Alexander Heiss, Ulrich E. Klotz, Jürgen Geis-Gerstorfer, Lutz Scheideler, Dorothea Alexander. Response of human periosteal cells to degradation products of zinc and its alloy. *Materials Science and Engineering: C*, manuscript under revision.

Abstract:

Zinc (Zn) and its alloys are proposed as promising resorbable materials for osteosynthesis implants. Detailed studies should be undertaken to clarify their properties in terms of degradability, biocompatibility and osteoinductivity. Degradation products of Zn alloys might affect directly adjacent cellular and tissue responses. Periosteal stem cells are responsible for participating in intramembranous ossification in fracture healing. The present study aims at examining possible effects emanating from Zn or Zn-4Ag (wt%) alloy degradation products on cell viability and osteogenic differentiation of a human immortalized cranial periosteal cell line (TAg cells). Therefore, a modified extraction method was used to investigate the degradation behavior of Zn and Zn-4Ag alloys under cell culture conditions. Compared with pure Zn, Zn-4Ag alloy showed almost fourfold higher degradation rates under cell culture conditions, while the associated degradation products had no adverse effects on cell viability. Osteogenic induction of TAg cells revealed that high concentration extracts significantly reduced calcium deposition of TAg cells, while low concentration extracts enhanced calcium deposition, indicating a dose-dependent effect of Zn ions. Our results indicate that the observed cytotoxicity effects were determined by the released degradation products of Zn and Zn-4Ag alloys, rather than by degradation rates calculated by weight loss. Extracellular Zn ion concentration determined the effect of osteogenic differentiation of TAg cells. These findings provide significant implications and guidance for the development of Zn-based alloys with an optimized degradation behavior for Zn-based osteosynthesis

4. Study III

implants.

4.1. Introduction

Absorbable zinc (Zn) and its alloys have been considered as potential materials for osteosynthesis implants [43-47]. Indeed, Zn-based alloys can address main drawbacks of current osteosynthesis materials, such as non-degradability issues caused by bioinert implants [13], low strength of polymeric implants [5], and unsuitable degradation behavior of magnesium-based or iron-based implants [145]. Most notable is the fact that Zn-based materials possess biocompatible, biodegradable, osteoinductive and antibacterial properties [48, 63]. The ionic zinc, as the main degradation product of Zn-containing chemical bonds or biomaterials, is one of the essential elements in the human body since it represents the metallic part of numerous proteins [48]. Moreover, the ionic zinc possesses superior osteoinduction and promotes new bone formation [49]. Nonetheless, pure Zn exhibits relatively low strength, insufficient for the most clinical requirements. By adding alloying elements, mainly including Mg, Cu, Ag, Ca, Sr, Al, Li and Mn, etc., to pure Zn mechanical strength can be enhanced substantially [145]. Previous studies reported that the Zn-Ag alloy exhibits superior mechanical properties compared with those of pure Zn [62, 89, 122]. Additionally, Zn-Ag based stents implanted into porcine iliofemoral arteries showed excellent biocompatibility and constant degradation behavior [62]. Meanwhile, incorporation of Ag ions into implants is beneficial for antibacterial properties and does not interfere or even disturb the process of bone regeneration [49]. However, it is not trivial to investigate the correlation between the degradation behavior within specific physiological environments and the impact of the resulting degradation products on biocompatibility.

As potential osteosynthesis materials, the degradation products of Zn and its alloys not only directly participate in the adjacent cellular reaction but affect bone tissue regeneration as well. In general, bone fracture healing consists of a complex series of physiological responses, and the exact mechanism of the respective cells mediating bone healing is still unknown [146]. Admittedly, periosteal stem cells play an important role in callus formation and participate in

4. Study III

intramembranous bone formation in the bone healing process [147, 148]. Compared to other skeletal stem cells, periosteal stem cells can directly form bone tissue via the intramembranous pathway, and are also capable to induce endochondral ossification after trauma [148]. For bone regeneration therapies in the oral and maxillofacial surgery, jaw periosteal cells could represent the most suitable stem cell source. In previous and present works, we characterized this cell type in detail and optimized culturing conditions to advance step by step towards clinical use [149-152]. Zn-based alloys pins (Zn-1Mg, -1Ca, -1Sr) implanted into a non-fracture femora cavity induced new bone formation emanating from periosteum, indicating that zinc might induce periosteum-mediated new bone formation [53]. Although the osteoinductive properties of Zn ions and Zn-containing biomaterials have been reported previously, the effect of degradation products of Zn and its alloys on cellular response of periosteal osteoprogenitor cells remains obscure.

Biocompatibility of implant materials mainly depends on their degradation behavior in the body. Nevertheless, the suitability of current *in vitro* cytocompatibility tests for absorbable metallic materials has been controversially discussed [135, 153]. According to the ISO standards, a direct contact test is suggested to evaluate the cell response directly on the material interface. Obviously, for absorbable Mg and Zn alloys, various tested cells were not able to grow on the *in vitro* dynamic interface for long-term periods [154, 155]. In general, an extract test should investigate possible effects of degradation products of materials caused by the cell culture medium on cellular response [67, 156]. In most studies, performed tests cover only the initial degradation stage [67, 157, 158]. Previously, we reported about a developed extraction method which correlates between initial degradation behavior and cytotoxicity of Zn and its alloys. The results indicated that cytotoxicity of Zn and its alloys is influenced by released Zn ion concentrations [122, 156]. In fact, during the degradation process of Zn and its alloys, various Zn degradation products, soluble (i.e., Zn^{2+} and OH^-) or complex insoluble products (i.e., zinc phosphate) are produced, synergistically participating to the physiological response *in vivo* [44, 45, 52]. Herein, the influence of the long-term degradation products of Zn and its alloys on

4. Study III

cytocompatibility should be further investigated.

In our study, a modified extraction method was used to investigate the degradation behavior of pure Zn and Zn-4.0 wt% Ag alloy (Zn-4Ag) under cell culture conditions. The paper also focuses on the effect of associated degradation products on cellular function of human immortalized cranial periosteal cells (TAg cells). The use of TAg cells was chosen due to their genetic and phenotypic similarity to the primary cells from which they derive. The immortalized cells seem to possess a higher osteogenic capacity compared to the parental cells, as reported previously [159]. Thus, our study is a comprehensive investigation of (i) the *in vitro* degradation behavior of Zn and Zn-4Ag under cell culture conditions; (ii) the effects of associated degradation products on cell viability and osteogenic differentiation of TAg cells; (iii) the respective effects of pH and Zn ion concentrations on TAg cell response and (iv) the establishment of a modified extraction method to correlate *in vitro* long-term degradation behavior with the cellular response, offering a suitable screening method for the testing of absorbable Zn-based alloys.

4.2. Materials and methods

4.2.1. Materials preparation

A Zn-4Ag (wt%) alloy was fabricated via conventional casting followed by a series of thermochemical treatments and pure Zn was prepared as a control, as described previously [122]. Subsequently, the ingots of Zn and Zn-4Ag were cut into 1.5 mm thick sheets. The as-produced pure Zn and Zn-4Ag sheets were cut into 23 mm × 8 mm × 1.5 mm in size. Prior to all tests, samples were ground with SiC abrasive paper up to grit 600 (CarbiMet P1200, Buehler, Germany), ultrasonically cleaned for 10 min in absolute ethanol, individually weighted with sensitivity of 0.1 mg, and immediately disinfected under ultraviolet radiation for 1 h each side (Lamin Air HB2472, Heraeus, Germany).

4.2.2. Experimental design

To correlate between *in vitro* degradation behavior and cytocompatibility, we modified an extraction method (as illustrated in Figure 4.1) based on previously

4. Study III

established methods [93, 94, 122, 156]. In order to collect extract medium, Zn and Zn-4Ag sheets were incubated in DMEM/F-12 for 28 days under continuous medium change. Every other day, extract medium was collected and added to TAg cells in different concentrations (100%, 50%, 25%, 10%, 5% and 2% extracts, respectively). Cytocompatibility was evaluated at different time points: cell metabolic activity at day 2, 6 and 12, gene expression pattern at day 14 and osteogenic potential at day 21 and 28. Additionally, Zn extracts were analyzed in terms of metallic ion concentration, pH values and insoluble products. At the end of the experiment (day 28), surface characterization after immersion test was analyzed and degradation rates were calculated by weight loss.

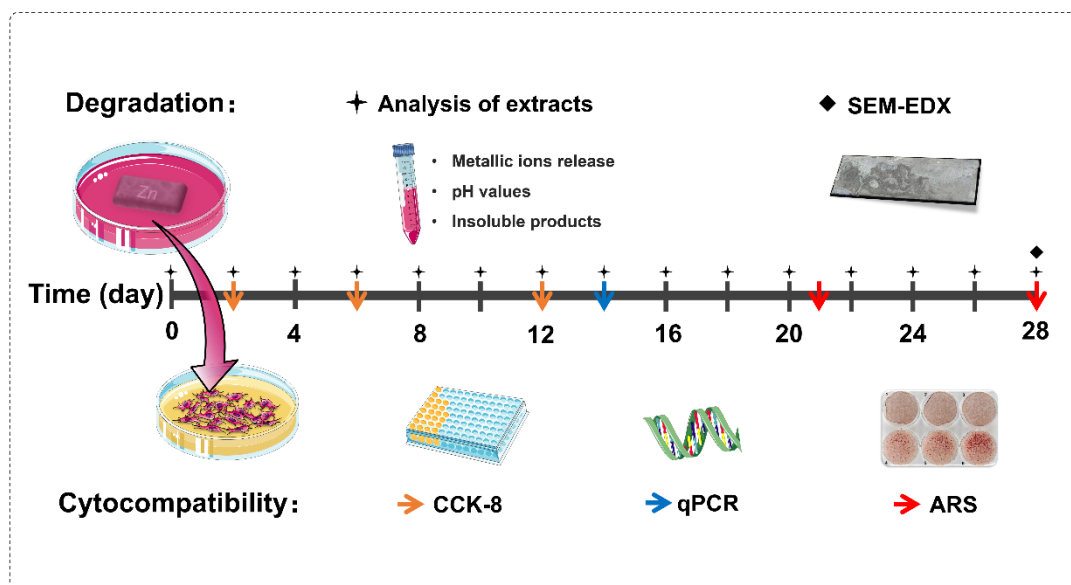


Figure 4.1. Draft of the experimental procedure with a time line (day) of performed experiments. Samples were incubated in DMEM/F-12 for 28 days. Sample media were exchanged every 48 h (plus signs) and the old ones were used for TAg cell cultivation at different concentrations. Extraction media were additionally used for the analysis of ion concentrations, pH values and the insoluble products. In order to visualize surface degradation of the samples, scanning electron microscopy (SEM) and element analysis (EDX) were performed at day 28. Cytocompatibility of Zn/Zn-4Ag alloys was assessed in terms of cell viability (cell counting kit-8 (CCK-8) at day 2, 6 and 12, orange arrows), gene expression (qPCR, at day 14, blue arrows) and osteogenic potential of TAg cells (Alizarin Red staining, ARS, at day 21 and 28, red arrows).

4.2.3. *In vitro* degradation test

All samples were immersed in pure Dulbecco's modified Eagle's medium/nutrient mixture F-12 (DMEM/F12; Life Technologies, Paisley, UK) and incubated under

4. Study III

standard cell culture conditions (37 °C, 95% rel. humidity, 5% CO₂ and 20% O₂) for 28 days. The surface area to medium volume ratio was set to 1.25 cm²/mL, according to ISO 10993-12: 2012 [91]. The media were refreshed every 48 h to simulate a semi-static immersion test. For analysis of sample extracts, pH values were recorded at each time point, and released metallic ion concentrations (Zn²⁺ and Ag²⁺) were detected by an inductively coupled plasma atomic emission spectroscopy (ICP-OES; Optima 4300DV, Germany). To determine the insoluble products, the extracts at 28 days immersion were collected and centrifuged at 170 g for 5 min. The visible insoluble products were analyzed by using a scanning electron microscope (SEM) equipped with an energy dispersive X-ray (EDX) spectrometer at 10 kV (LEO 1430, Carl Zeiss GmbH, Germany).

At the end of the immersion period, the degradation products on the sample surfaces were removed by incubation in 250 g/L glycine (NH₂CH₂COOH) for 10 min, according to ISO 8407: 2009 [160]. Afterwards, the degradation rates were calculated by weight loss and expressed as μm/year, according to ASTM G31-12a [161]. Degradation rate (DR) was calculated as $DR = (8.76 \times 10^7 \times W) / (A \times D \times T)$, namely, *W* is the weight loss (g); *A* is the surface area (cm²); *D* is the density (g/cm³) and *T* is the immersion time (h). In addition, surface morphologies and chemical composition after immersion and removal of degradation products were analyzed by SEM-EDX.

4.2.4. Cytocompatibility test

4.2.4.1. Cell culture and extract preparation

A human SV40 T-antigen immortalized cranial periosteal cell line (TAg cells) as described previously was used for cytocompatibility evaluation [159]. TAg cells were cultured in complete DMEM/F-12 supplemented with 10% fetal bovine serum (FBS, Sigma-Aldrich, Germany), 1% penicillin/streptomycin (P/S, Lonza, Switzerland), 1% amphotericin B (Biochrom, Germany), 0.25 mg/mL immortalization maintenance dose of G418 (Biochrom, Germany). TAg cells were cultured in either normal (Co) or osteogenically induced conditions (Ob) throughout the experiments. Osteogenic medium of TAg cells contained complete DMEM/F-12 medium supplemented with 100 μM L-ascorbic acid 2-

4. Study III

phosphate, 4 μ M dexamethasone and 10 mM β -glycerophosphate (Sigma-Aldrich, Germany).

To further correlate between degradation and cytocompatibility, the respective 48 h extracts were used as cell culture media supplement, as described in Section 4.2.3. Prior to transferring to cell culture, all extracts were further supplemented with 10% FBS, 1% P/S, 1% amphotericin B and 0.25 mg/mL G418-BC to adjust TAg cell culture conditions. For evaluation of the osteogenic potential, extracts were added to the normal and osteogenic medium, respectively. The original extracts under both conditions were diluted by the respective complete media to different concentrations (50%, 25%, 10%, 5% and 2% extracts, respectively).

4.2.4.2. Cell counting kit-8 assay

Cell counting kit-8 (CCK-8) assay was used to evaluate a potential inhibition of metabolic activities of TAg cells cultured under normal and osteogenic conditions containing sample extracts, according to ISO 10993-5: 2009 [97]. TAg cells were seeded in 96-well culture plates at a density of 3×10^3 cells cm^{-2} . After 24 h, the medium was removed and replenished by gradient sample extracts containing normal and osteogenic medium, and respective normal and osteogenic media were used as the negative controls, respectively. After incubation for 2, 6, and 12 days, sample extracts were replaced by 100 μ L fresh DMEM/F-12 and 10 μ L CCK-8 reagent (Dojindo Laboratories, Japan) was added to each well. After incubation for 2 h, optical density was measured by a microplate reader (Tecan, Austria) at a wavelength of 450 nm and relative metabolic activities were calculated, as described before [156].

4.2.4.3. Alizarin red staining

TAg cells were seeded in 6-well culture plates at a density of 3×10^3 cells cm^{-2} and pre-cultivated overnight. TAg cells were induced osteogenically for 28 days in the presence of 48 h sample extracts. After osteogenic induction for 21 and 28 days, TAg cells were fixed with 4% formalin for 20 min. After washing with DPBS, cell monolayers were stained with alizarin dye solution (40 mM, Sigma-Aldrich, Germany) for 20 min and washed 4 times with deionized water. A colorimetric assay was carried out to quantitate the calcium phosphate precipitates according

4. Study III

to the instructions of the manufacturer (Osteogenesis Quantitation Kit, Merck Millipore, Germany). Briefly, Alizarin red dyes were dissolved from the monolayers over a period of 30 min by the addition of 10% acetic acid solution. The monolayers were detached from the well bottom by scraping. The samples were vortexed for 30 s and heated at 85 °C for 10 min, cooled on ice for 5 min, and then centrifuged at 20.000 g for 20 min. After neutralization of the supernatants by adding 10% ammonium hydroxide, quantification of calcium precipitates was performed using an ELx800 plate reader (BioTek Instruments GmbH, Germany) at a wavelength of 405 nm.

4.2.4.4. Gene expression analysis

RNA isolation from TAg cells was carried out at day 14 of osteogenic stimulation in the presence of Zn extracts, according to the manufacturer's instructions using the NucleoSpin RNA kit (Macherey-Nagel, Germany). The isolated RNA was photometrically measured and quantified (GE Healthcare, Germany). cDNA synthesis was performed using 200 ng of RNA and the SuperScript VILO kit (Invitrogen, USA), according to the manufacturer's instructions. The real-time LightCycler System (Roche Diagnostics, Germany) was used to quantify mRNA levels of Runt-related transcription factor-2 (RUNX2), alkaline phosphatase (ALP), osteocalcin (OCN) and the alpha-1 chain of type I collagen (COL1A1), respectively. The DNA Master Sybr Green 1 (Roche Diagnostics, Germany) and the commercial primer kits (Search LC, Germany) were used for 40 cycles of PCR amplification. Transcript levels of target genes were normalized to those of the housekeeping gene glyceraldehyde 3-phosphate dehydrogenase (GAPDH, Serach LC, Germany). Calculated ratios in control groups were set as 1 (control) and induction indices in relation to this control were calculated.

4.2.5. Effects of alkaline pH values and different Zn ion concentration on cell viability

To evaluate the effect of alkaline media conditions induced by Zn degradation on cell viability, TAg cells were seeded in 96-well culture plates at a density of 3×10^3 cells cm^{-2} and pre-cultivated overnight. Subsequently, the medium was replaced by normal complete DMEM/F-12 (Co) and osteogenic complete medium

4. Study III

DMEM/F-12 (Ob) of pH values intentionally adjusted to 8, 9, 10, 11 and 12, and the normal culture media as a negative control. After incubation for 24 h, the relative metabolic activities were determined by CCK-8 assay, as described above.

To identify which Zn ion concentration modulated cell viability and osteogenic differentiation of TAg cells, separate experiments evaluating the effects of different concentrations of extracellular Zn ions were carried out. The normal complete DMEM/F-12 (Co) and osteogenic complete DMEM/F-12 (Ob) were adjusted to the respective Zn ion concentration gradient (2-100 μM) using a ZnCl_2 solution (Sigma-Aldrich, Germany). Cell culture media without supplemented Zn solution was used as a negative control. TAg cells were seeded in 96-well plates at a density of 3×10^3 cells cm^{-2} for 24 h. Subsequently, the medium was replaced by media containing various Zn ion concentrations and refreshed every other day. The relative cell metabolic activities were analyzed at day 2, 6, and 12, respectively, as described above. After initial testing of various Zn concentrations on cell vitalities, typical low (2 μM) and typical high (40 μM) Zn ion concentrations were further used to investigate a potential influence on the osteogenic differentiation of TAg cells. Mineral deposition and osteogenesis-related gene expression were analyzed using qPCR as described above.

4.2.6. Statistical analysis

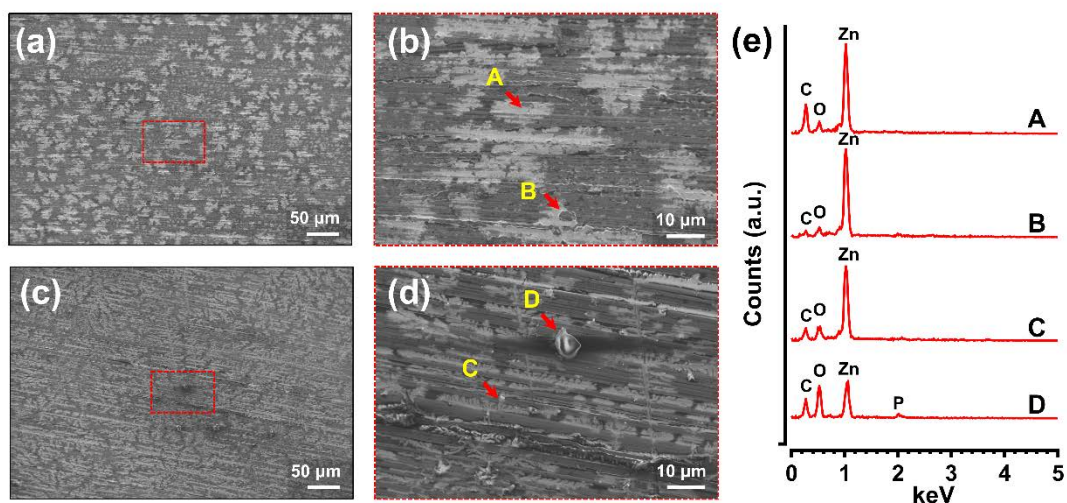
All data were presented as mean and corresponding standard deviations. All assays were repeated at least three times to ensure reproducibility. Where applicable, all data sets were first analyzed concerning their normal distributions by the Shapiro-Wilk test. For comparisons between two groups, a Student's t-test was performed. Mann-Whitney U-tests were analyzed if normality tests failed. For comparisons of three or more groups, parametric data sets were analyzed by one-way analysis of variance (ANOVA), followed by Tukey's multiple comparisons test. Non-parametric data sets were analyzed by the Kruskal-Wallis test followed by Dunn's multiple comparisons test. Statistical analyses were analyzed using GraphPad PRISM (version 6.01, GraphPad Software, Inc., San Diego, US). A P-value < 0.05 was considered as statistically significant.

4. Study III

4.3. Results

4.3.1. *In vitro* degradation behavior of Zn and Zn-4Ag sheets

In vitro degradation behavior was evaluated in DMEM/F-12 under cell culture conditions for 28 days. The degradation rates of Zn and Zn-4Ag alloy calculated by weight loss were $4.80 \pm 0.82 \mu\text{m}/\text{year}$ and $17.38 \pm 0.78 \mu\text{m}/\text{year}$, respectively. A Student's t-test was used to confirm the statistically significant difference between both groups ($p < 0.001$). As already macroscopically visible, all samples showed after the respective immersion period a dark blackish surface without obvious bulk degradation products. Furthermore, the surface morphology and chemical composition of Zn and Zn-4Ag sheets after immersion for 28 days are shown in Figure 4.2. The degradation precipitations dispersed on sample surfaces are visible under two different magnifications. Compared with Zn-4Ag surfaces, less structures of white appearance were formed on Zn surfaces. SEM images at higher magnification showed that some tiny degradation particles were distributed on the surfaces but no obvious thick degradation layers covering the whole surfaces were visible. As shown in Figure 4.2e, EDX analysis indicated that Zn, C, O and P were identified as elemental composition of degradation products on the surfaces. Additionally, Figure 4.3 illustrates sample surfaces after removal of the degradation products. The surfaces of Zn and Zn-4Ag showed a relatively uniform degradation morphology, without extensive localized corrosion spots.



4. Study III

Figure 4.2. Representative SEM-EDX analysis of samples after immersion in DMEM/F-12 for 28 days. SEM images showing (a,b) pure Zn and (c,d) Zn-4Ag alloy. The spots highlighted as red rectangles are shown in a higher magnification in b and d. (e) Representative EDX results from spots arrowed with yellow letters A/B and C/D in (b) and (d).

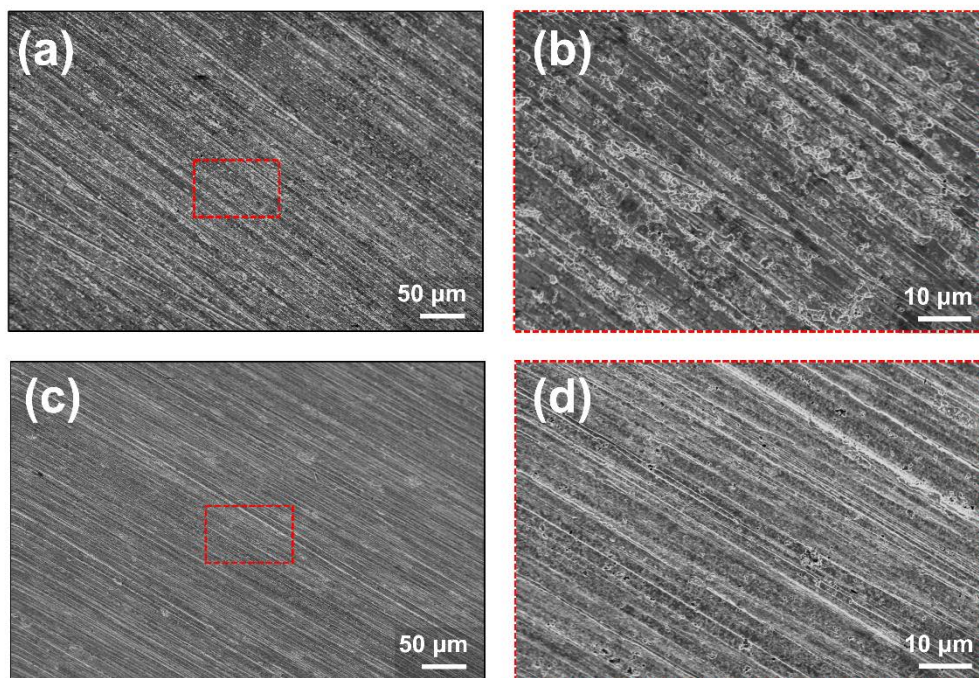


Figure 4.3. Representative SEM images of pure Zn and Zn-4Ag alloy after removal of degradation products. SEM images showing (a,b) pure Zn and (c,d) Zn-4Ag alloy. The red rectangles correspond to the magnified degradation morphologies of (b) pure Zn and (d) Zn-4Ag alloy.

4.3.2. Analysis of sample extracts during the 28-day period of immersion

Figure 4.4 shows the metallic ion release of pure Zn and Zn-4Ag alloy in DMEM/F-12 as well as the pH values of the respective extracts for the 28 day period of immersion. According to ICP-OES measurements, only Zn ions released from the Zn-4Ag sheets could be detected in DMEM/F-12. Released Ag ion concentrations were shown to be under the detection limit ($< 50 \mu\text{g/L}$). At all analyzed time points, the mean Zn ion release from samples was below $6.5 \mu\text{g/mL}$ (approximately $100 \mu\text{M}$). The tendency of Zn ion release was generally consistent between pure Zn and Zn-4Ag alloy (Figure 4.4a). As a simple calculation, the cumulative Zn ion release amount of pure Zn ($81.7 \pm 1.87 \mu\text{g/mL}$) was slightly, but significantly higher than that of Zn-4Ag ($79.1 \pm 0.99 \mu\text{g/mL}$) for the 28 day-period of immersion

4. Study III

($p = 0.015$), independent of degradation rates calculated by weight loss. The evolution of pH values during immersion is illustrated in Figure 4.4b. Pure Zn and Zn-4Ag showed a similar trend of pH changes during immersion in DMEM/F-12. A rapid increase in pH values was detected at initial time points, thereafter constantly decreasing pH values were measured. All mean pH values measured were in the range from 8.4 to 8.9, so all pH changes were below 0.8 compared to the respective initial values. At the end of the 28-day period, mean pH values of 8.42 and of 8.47 were measured for Zn-4Ag and Zn sheets respectively.

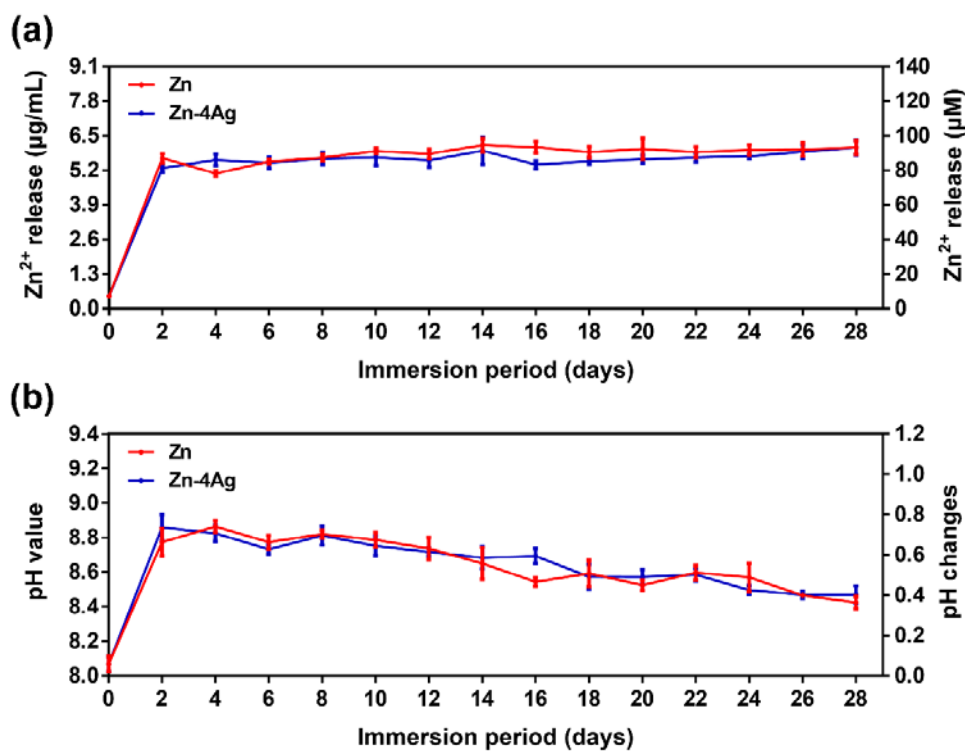


Figure 4.4. Analysis of sample extracts during the 28 day-period of immersion. (a) Zn ion release ($\mu\text{g/mL}$ and μM respectively) of pure Zn and Zn-4Ag in DMEM/F-12. (b) Evaluation of pH values.

To further analyze the degradation products, the solid degradation particles in the extracts were analyzed by SEM-EDX. As shown in Figure 4.5a, a precipitation of insoluble degradation granules could be observed in Zn-4Ag extracts only after centrifugation. The SEM image shows that crystal-like degradation granules are visible (Figure 4.5b). The corresponding EDX spectrum revealed that the degradation granules of Zn-4Ag were mainly composed of Zn, O, C and Cl.

4. Study III

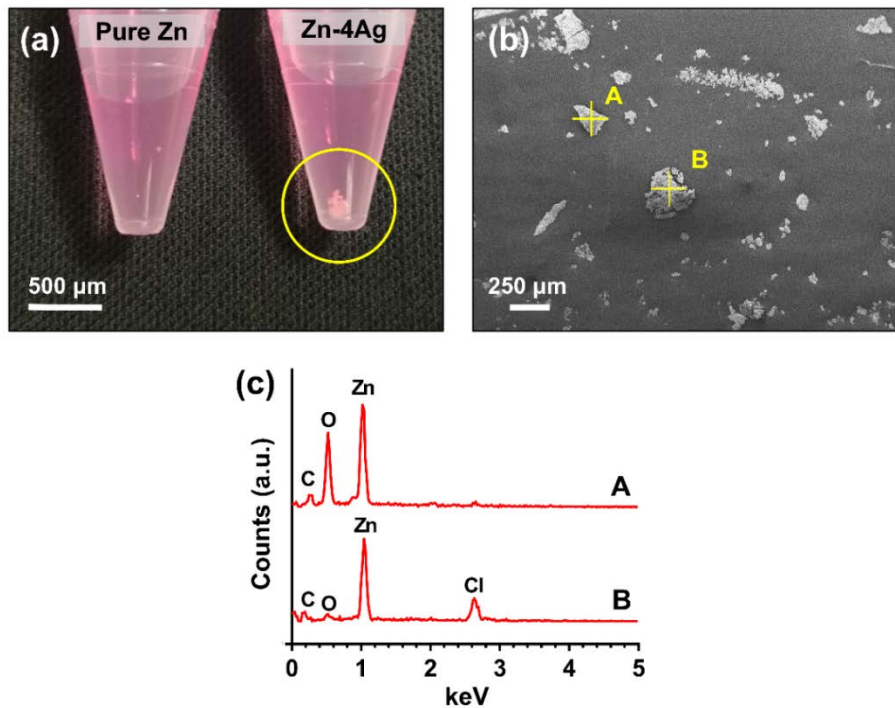


Figure 4.5. Analysis of degradation granules in Zn and Zn-4Ag alloys extracts after a 28 day period of immersion. (a) Precipitates of degradation granules in Zn-4Ag extracts (indicated by the yellow circle) after centrifugation. (b) SEM images of the degradation granules marked with yellow letters. (c) The EDX spectrum indicates the elemental composition of spots marked with yellow letters in b.

4.3.3. Examination of TAg cell functions after exposure to Zn and Zn-4Ag extracts

Figure 4.6 shows the relative metabolic activity of TAg cells after exposure to various concentrations of Zn and Zn-4Ag extracts under normal and osteogenic conditions for 12 days. An inhibition of cell metabolic activity below 70%, compared to the negative control, was regarded as a cytotoxic effect, according to ISO 10993-5: 2009 [97]. Herein, TAg cells exposed to Zn or Zn-4Ag extracts exhibited relative metabolic activities above 70%, indicating that no cytotoxic effects are emanating from Zn extracts in all concentrations tested. In contrast, in the presence of low concentrated Zn-4Ag extracts (i.e., 25%, 10% and 5%), a significant increase in metabolic activities of TAg cells under normal and osteogenic conditions was observed at day 2 compared to the controls ($p < 0.05$). With increased culture time, there were no significant increases or decreases in metabolic activities of TAg cells, independent of various Zn extract concentrations at day 12 ($p > 0.05$). Notably, significant differences were detected only in TAg

4. Study III

cells cultured in the presence of Zn-4Ag extracts.

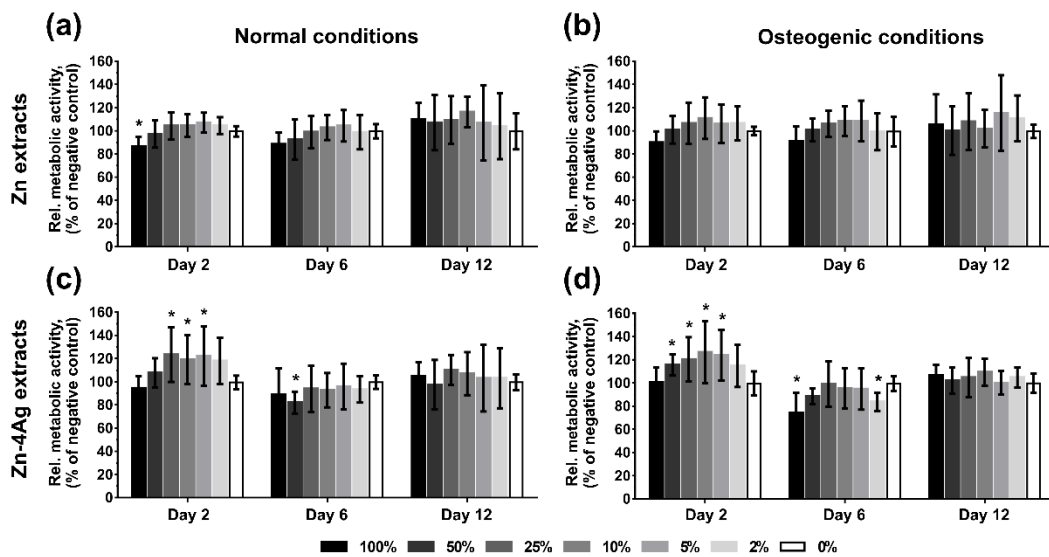
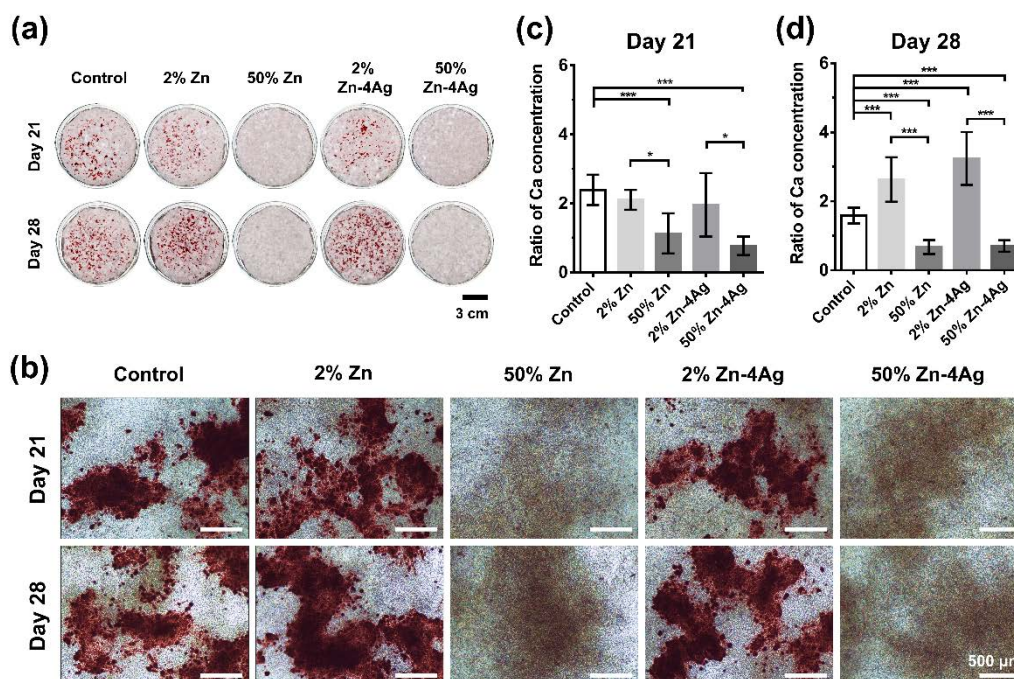


Figure 4.6. Relative metabolic activities of TAG cells cultured in the presence of Zn and Zn-4Ag extracts for up to 12 days, determined by CCK-8 assay. (a, b) cell vitalities in the presence of pure Zn extracts of various concentration, (c,d) cell vitalities in the presence of Zn-4Ag extracts of various concentration under normal conditions (a, c) and under osteogenic conditions (b, d). The DMEM/F-12 complete media (normal and osteogenic) were considered as the negative controls and set to 100%. * represent $p < 0.05$ when compared to the negative control.

For the analysis of a potential influence of Zn/Zn-4Ag extracts on osteogenic differentiation of TAG cells, one typical low (2%) and one typical high (50%) concentration of sample extracts was used. Figure 4.7a displays Alizarin red staining of TAG cells cultured in the presence of sample extracts in order to evaluate their osteogenic potential. Only weak Alizarin red staining was observed in TAG cell monolayers treated with 50% of sample extracts at day 21 and 28. In contrast, TAG cells cultivated in the presence of low concentrated (2%) sample extracts exhibited much stronger Alizarin red staining, indicating pronounced formation of calcium phosphate nodules (Figure 4.7b). For quantification of TAG cell mineralization, the ratio of Ca concentration in the extract-treated cultures was related to that determined in the control (TAG cells cultivated in the absence of Zn extracts) as illustrated in Figure 4.7 c and d. Significance tests were calculated by comparing Ca ratios of osteogenically induced TAG cells in the presence of extracts with those of cells in the absence of sample extracts. The

4. Study III

Kruskal-Wallis test showed significant differences at day 21. Dunn's multiple comparisons tests showed significantly higher Ca concentrations in the osteogenic control (ratio of 2.39 ± 0.44) compared with those cells cultivated in the presence of 50% Zn extracts (ratio of 1.13 ± 0.58 ; $p < 0.001$) and 50% Zn-4Ag extracts (0.77 ± 0.27 ; $p < 0.001$). Nevertheless, no significant differences were detected when comparing the Ca ratio of osteogenic control (without Zn extracts) with those from cells cultivated in the presence of 2% Zn (ratio of 2.10 ± 0.29 ; $p > 0.05$) or 2% Zn-4Ag extracts (ratio of 1.96 ± 0.91 ; $p > 0.05$), respectively. By comparing Ca ratios in TAg cells cultivated under 2% and 50% of sample extracts, significant differences were obtained ($p < 0.05$). In addition, ANOVA was used to confirm statistically significant differences of Ca ratios at day 28. Notably, post hoc pairwise comparisons showed significantly higher Ca concentrations in TAg cells cultivated in the presence of 2% Zn-4Ag (ratio of 3.23 ± 0.77) and 2% Zn (ratio of 2.63 ± 0.65) extracts compared with those of osteogenic control (ratio of 1.59 ± 0.23). Similarly, as already shown for Ca quantification after 21 days, significantly higher Ca ratios in TAg cells cultivated in the presence of 2% Zn extracts were detected compared to cells cultured in the presence of 50% Zn-4Ag extracts.



4. Study III

Figure 4.7. Detection of TAG cell mineralization exposed to Zn and Zn-4Ag extracts. (a) Alizarin red staining of TAG cells cultured in the presence of sample extracts under osteogenic conditions for 21 and 28 days. (b) Representative microscopic images of differentiated TAG cells cultured in the presence of sample extracts for 21 and 28 days (magnification 4x; scale bar = 500 μ m). Quantification of calcium precipitates is shown at day 21 (c) and day 28 (d). The ratio of Ca concentration (osteogenic/normal culture condition) was quantitatively analyzed by dissolving the Alizarin dye from TAG cell monolayers. Statistical differences were calculated compared to the osteogenic control without extracts. * $p < 0.05$, *** $p < 0.001$.

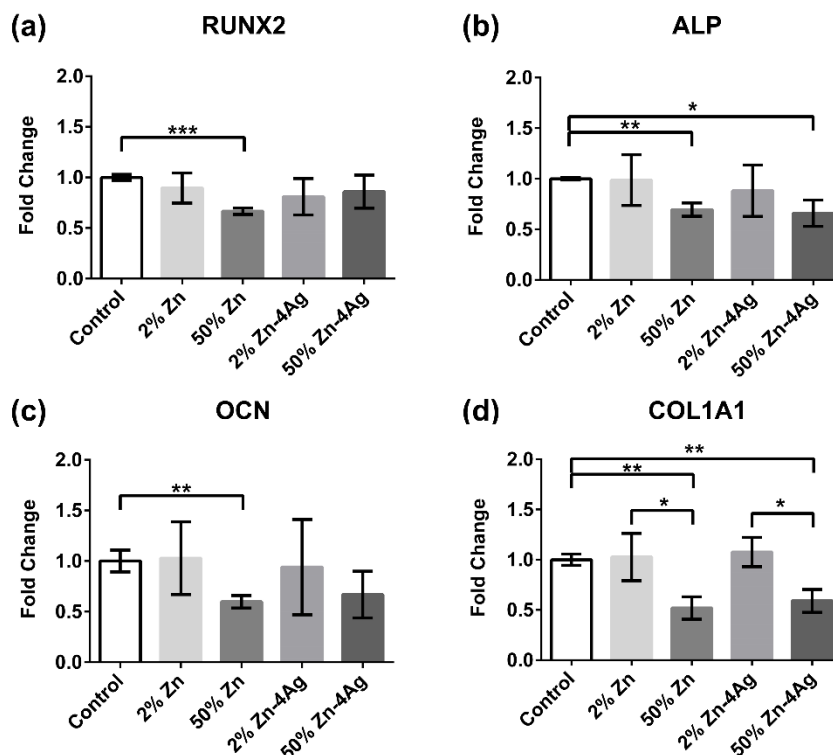


Figure 4.8. Quantitative gene expression of osteogenically induced TAG cells exposed to sample extracts for 14 days. Gene levels of osteogenically induced TAG cells in the absence of Zn extracts were set as 1 and induction indices in relation to this control were calculated. Relative expression of (a) Runt-related transcription factor-2 (RUNX2), (b) Alkaline phosphatase (ALP), (c) Osteocalcin (OCN) and (d) Alpha-1 chain of type I collagen (COL1A1) are illustrated. * $p < 0.05$, ** $p < 0.01$ and *** $p < 0.001$.

Figure 4.8 shows gene expression levels of RUNX2, ALP, OCN and COL1A1 in osteogenically induced TAG cells at day 14 of immersion with or without Zn extracts. Statistically significant differences of COL1A1 expression were confirmed by ANOVA. Post hoc pairwise comparisons showed a significantly lower COL1A1 expression in osteogenically induced TAG cells in the presence of 50% Zn-4Ag ($p < 0.05$) and 50% Zn ($p < 0.05$) extracts compared to the

4. Study III

osteogenic control (without extracts). By comparing COL1A1 expression in cells cultivated in the presence of 2% Zn (1.03 ± 0.14) and 2% Zn-4Ag (1.08 ± 0.15) extracts to that in cells cultured in the presence of 50% extracts of Zn (0.59 ± 0.11 , $p < 0.05$) and Zn-4Ag (0.52 ± 0.11 , $p = 0.014$), significant differences were obtained. In addition, RUNX2, ALP and OCN expression was shown to be significantly decreased in TAg cells cultured in the presence of 50% Zn and for ALP also in the presence of 50% Zn-4Ag extracts ($p < 0.05$). Herein, the above results coincide with the result that high concentrations of Zn and Zn-4Ag extracts (50%) significantly reduced calcium deposition of TAg cells.

4.3.4. Effects of different pH values and Zn ion concentrations on TAg cell viability

Figure 4.9 shows the results of the relative metabolic activities of TAg cells after 24 h incubation with the normal and osteogenic media adjusted to different pH values. For pH values below 9, no impact on TAg cell viabilities was detected ($p > 0.05$). In contrast, when pH values reached 10, for both media conditions the relative metabolic cell activities were significantly decreased compared to the control ($p < 0.05$).

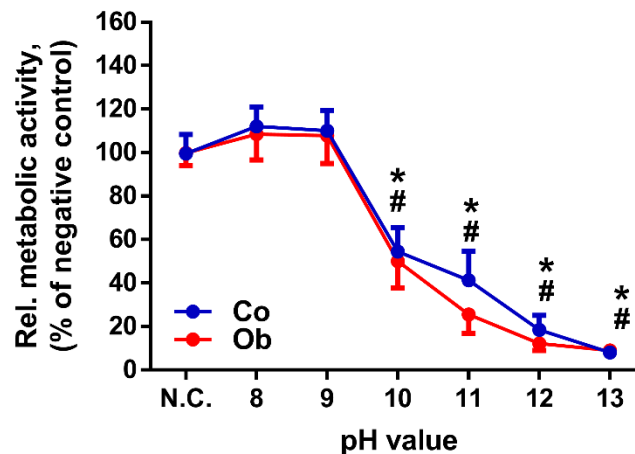


Figure 4.9. Relative metabolic activities of TAg cells after a 24 h incubation period in normal and osteogenic media of various alkaline pH values. The original media were used as negative controls (N.C.). Undifferentiated TAg cells were denoted as Co, and osteogenically induced cells as Ob. * and # represent $p < 0.05$ when compared to the respective negative controls cultured under normal and osteogenic medium, respectively.

In Figure 4.10, metabolic activities of TAg cells are plotted as a function of Zn ion

4. Study III

concentration (2-100 μM) under normal and osteogenic conditions. At day 2 of incubation (Figure 4.10a), low Zn ion concentrations (5-20 μM) significantly increased relative metabolic activities of TAG cells ($p < 0.05$) under both culture conditions. Zinc concentrations of 40-60 μM led to significantly higher cell activities only under normal conditions. If a Zn concentration of 100 μM was chosen, for both media conditions cell activities were significantly decreased compared to the control ($p < 0.05$). At day 6 of incubation, only Zn concentrations of 40 μM under normal conditions increased metabolic activity. At day 12 of incubation, TAG cell viabilities were almost comparable under normal and osteogenic conditions ($p > 0.05$). As already observed for day 2 and 6, Zn concentrations of 100 μM showed clearly cytotoxic effects.

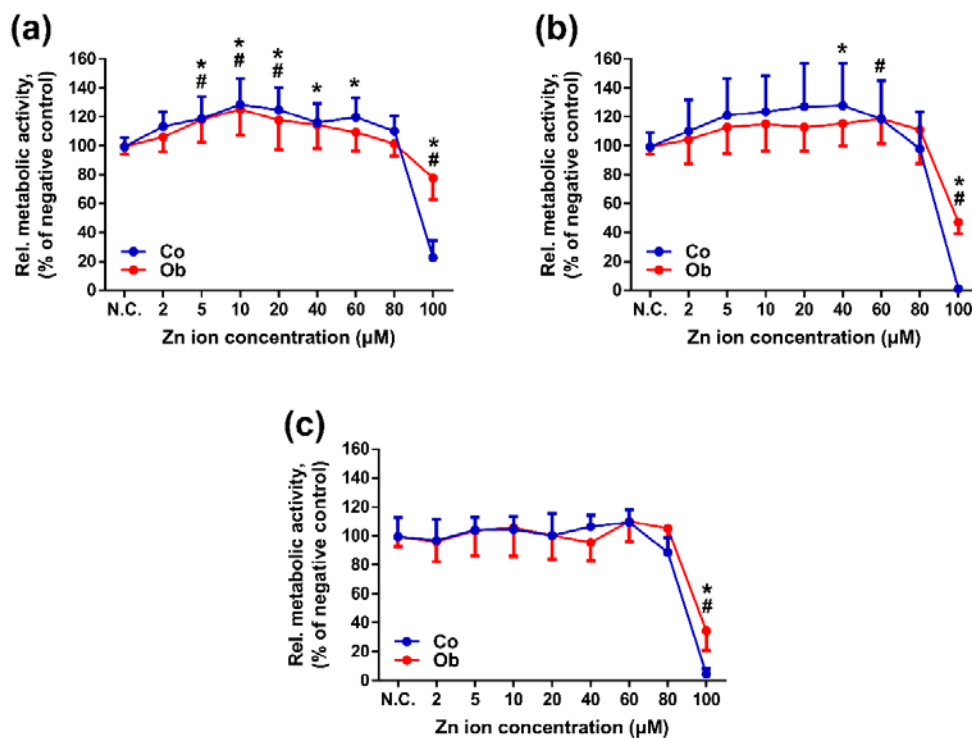


Figure 4.10. Relative metabolic activities of TAG cells treated with different Zn ion concentrations determined by CCK-8 assay. (a) 2 days of incubation, (b) 6 days of incubation and (c) 12 days of incubation. The original media served as negative controls (N.C.). * and # represent $p < 0.05$ when compared to the respective negative controls cultured under normal and osteogenic medium, respectively. Undifferentiated TAG cells were denoted as Co, and osteogenically induced cells as Ob.

To identify whether Zn ions in the medium influence the osteogenic differentiation

4. Study III

of TAg cells, one typical low (2 μM) and one typical high (40 μM) Zn ion concentration were used. As shown in Figure 4.11a, the effect of Zn ion concentration on osteogenic differentiation was assessed by Alizarin red staining. A Zn concentration of 2 μM led to a clearly stronger Alizarin red staining compared to the staining of TAg monolayers which were incubated constantly with 40 μM Zn ions for 21 and 28 days. Almost no staining was observed at this Zn concentration. After 28 days, TAg cells cultured in 2 μM Zn ion media showed significantly higher Ca concentration than those in control and 40 μM Zn ion media ($p < 0.001$). In addition, TAg cells cultured in 2 μM Zn ion was statistically higher mineralization than that in control media at day 28 ($p < 0.001$).

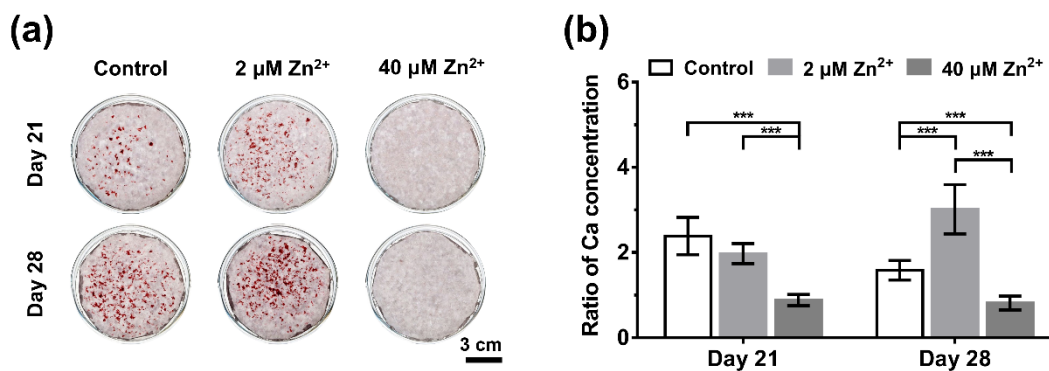


Figure 4.11. Mineralization of TAg cells treated with 2 μM and 40 μM Zn ion concentration. (a) Alizarin red staining of TAg cells under osteogenic conditions for 21 and 28 days. (b) Quantification of calcium precipitates after osteogenic induction for 21 and 28 days. The ratio of Ca concentration (osteogenically induced: untreated cells) was quantitatively analyzed by dissolving the Alizarin dye from cell monolayers, *** $p < 0.001$.

4.4. Discussion

4.4.1. *In vitro* assays for testing of absorbable metals for implants

The ideal *in vitro* tests should simulate *in vivo* conditions to the utmost, in order to accurately predict the *in vivo* performance of implants. To date, *in vitro* assays for the evaluation of degradation behavior and cytocompatibility of absorbable metals have been controversially discussed, since both aspects were considered independently [128, 145, 162]. To overcome this shortcoming, the aim of our work was to develop a modified test design in order to be able to consider and analyze *in vitro* degradation behavior and cytocompatibility at the same time.

4. Study III

The aspect of the *in vitro* degradation behavior under cell culture conditions was performed based on previously published methods [163, 164]. It has been shown that the composition of cell culture medium is close to that of human extracellular fluids [101, 163, 164]. Additionally, DMEM was recommended as appropriate fluid to obtain a comparable *in vivo* degradation behavior of Zn [165]. Herein, DMEM/F-12 has been selected, whose main constituents were compared with human extracellular fluids (Table 4.1). Previous studies on the degradation behavior of Mg alloys under cell culture conditions (37 °C, 95% rel. humidity, 5% CO₂ and 20% O₂) reported on comparable conditions to physiological environments [127, 128]. The main reason was attributed to the fact that the bicarbonate buffer system in the medium requires triggering by active CO₂, regulating pH values of the degradation medium, which is similar to the physiological conditions [166].

Table 4.1. Main composition of human extracellular fluids and the used medium.

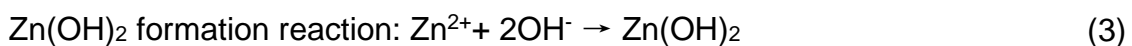
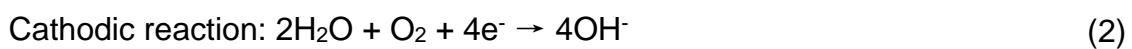
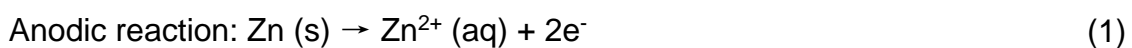
Composition	Human extracellular fluid		DMEM/F-12 [167]
	Blood plasma [101, 125]	Interstitial fluid [125]	
Inorganic ions (mM)			
Na ⁺	142.0	139.0	150.6
K ⁺	4.2	4.0	4.2
Mg ²⁺	0.8	0.7	0.7
Ca ²⁺	1.3	1.2	1.1
Cl ⁻	106.0	108.0	126.1
SO ₄ ²⁻	0.5	0.5	0.4
HPO ₄ ²⁻	2.0	2.0	0.5
HCO ₃ ⁻	24.0	28.3	29.0
Organic components			
Protein	1.2 (mM)	0.2 (mM)	-
Glucose (mM)	5.6	5.6	17.5
Amino acids	2.0 (mM)	2.0 (mM)	1.3 (g/L)
Concentrations of buffering agents (mM)			
HCO ₃ ⁻	24.0	28.3	29.0
HPO ₄ ²⁻	2.0	2.0	0.5
Tris-HCl	-	-	-
Human protein	16.0-18.0 [101]	-	-
Total	42.0-44.0	30.3	29.5

4. Study III

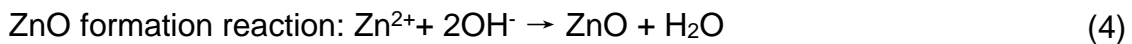
Standardized cytocompatibility evaluation tests for absorbable metals based on the ISO 10993-5 and -12 standards are not satisfactory based on the fact that they were developed for intentionally bioinert materials, neglecting the properties of absorbable materials [67, 145]. Attempts to improve the efficacy of *in vitro* evaluation methods for absorbable Mg-based and Zn-based metals, including the dilution of extracts [92, 168], the selection of extraction medium [102, 156], and the surface pretreatment [94, 169], have been reported. Considering the degradation properties of Zn and its alloys, various degradation products during long-term degradation process all participate in tissue healing *in vivo* [44, 45, 52]. Thus, in our test model, sample extracts were repeatedly collected during the degradation process and given to cultivated cells for cytocompatibility evaluation.

4.4.2. Degradation behavior under cell culture conditions

The *in vitro* degradation behavior of pure Zn and Zn-4Ag alloys in DMEM/F-12 was analyzed under common cell culture conditions. According to our results, the following degradation mechanism in DMEM/F-12 can be proposed. Immersion in DMEM/F-12 (slightly alkaline solutions, pH value: 8.06) leads to anodic and cathodic reactions as described by Eq (1) and Eq (2), respectively [145]. With the dissolution of Zn, a rapid increase in Zn ion concentration and pH value can be detected in DMEM/F-12 (Figure 4.4). According to the Pourbaix diagram, Zn trends to be passivated in slightly alkaline solutions, while the chemical reactions as described in Eq (3) and Eq (4) take place. The accumulation of zincite (ZnO) and zinc hydroxide (Zn(OH)₂) on the surfaces tends to form the passivation layers [156, 165]. On the other hand, the released Zn ions can spontaneously react with phosphate ions and carbonate ions contained in DMEM/F-12 to form Zn phosphate (Zn₃(PO₄)₂·4H₂O) and Zn carbonate (ZnCO₃) [145, 165]. According to our EDX analysis, we detected the elements Zn, O, C and P on sample surfaces, as expected (Figure 4.2).



4. Study III



Generally, the formation of Zn degradation layers can retard the degradation process [145, 170]. However, no obvious decrease in Zn ion release could be detected by ICP-OES measurements (Figure 4.4). It can be assumed that some organic components contained in DMEM/F-12 can interfere with the surface passivation, probably similar to the effect of protein adsorption on Zn surfaces [131]. Further on, more complex degradation products, such as hydrozincite ($\text{Zn}_5(\text{CO}_3)_2(\text{OH})_6$) and simonkolleite ($\text{Zn}_5(\text{OH})_8\text{Cl}_2 \cdot \text{H}_2\text{O}$) can be formed on the surfaces, as previously reported [145]. The formed degradation layers can be dissolved by chloride ion attack and transformed into zinc chloride salts, as confirmed by our EDX analysis from Zn-4Ag degradation granules, as illustrated in Figure 4.5.

Our results revealed significantly higher degradation rates of Zn-4Ag alloys compared to those of pure Zn, probably due to the occurrence of a secondary phase ($\epsilon\text{-AgZn}_3$) within the microstructure [122]. A recent study reported on micro-galvanic effect between the Zn matrix and the secondary $\epsilon\text{-AgZn}_3$ phase, leading to high degradation rates [89]. Notably, the cumulative Zn ion release of pure Zn was significantly higher than that of Zn-4Ag alloy, which is inconsistent with our obtained degradation rates. We postulate that a fraction of free Zn ions released from Zn-4Ag surfaces rapidly binds to zinc degradation granules, which is not the case with those of pure Zn. As a consequence, a higher formation of degradation granules was observed in Zn-4Ag extracts (Figure 4.5). Thus, released Zn ion concentration in the sample extracts is not directly related to the degradation rates determined in our test.

4.4.3. Assessment of cytocompatibility of Zn and Zn-4Ag alloys using immortalized periosteal cells

Viabilities of TAg cells cultured in the presence of Zn and Zn-4Ag alloy extracts for up to 12 days were shown to be unaffected, indicating no obvious cell cytotoxic effects (Figure 4.6). Zn ion concentrations analyzed in all extracts were below 90 μM after supplementation with 10% FBS (Figure 4.4a), indicating cell tolerance

4. Study III

for this concentration. This is in accordance with the tolerance level determined for TAg cells in this study by testing different extracellular Zn ion concentration between 2-100 μM , adjusted by the addition of a ZnCl_2 solution (Figure 4.10). A significant improvement of TAg cell viabilities was achieved by low concentrations of either Zn-4Ag extracts or Zn ions at day 2 of examination (Figure 4.6 and Figure 4.10). This result coincides with findings from previous studies describing the activation of vascular muscle or endothelial cell viabilities in the presence of low Zn ion concentrations [137, 138]. Ag ion concentration in the extracts from Zn-4Ag alloys was under the detection limit of ICP-OES ($< 0.5 \mu\text{M}$). This Ag ion concentration remained under the previously reported cell tolerance limit (approx. $4.25 \mu\text{M}$), indicating that limited Ag ion release does not cause the toxic effects [139]. Due to the buffering effect of the DMEM/F-12 medium, pH values in all extracts were below 8.9 (Figure 4.4b). Under pH 9, we did not detect any significant decrease of metabolic activities of TAg cells (Figure 4.9).

In our study, we detected fourfold higher degradation rates of Zn-4Ag alloys, but no higher cytotoxic effects emerged from them as compared to those of pure Zn. This finding contradicts the conclusion that cytotoxicity of Zn and its alloys is consistent with the variation of degradation rates [171, 172]. We postulate that during degradation of Zn-4Ag, free Zn ions were bound to degradation granules, leading to relatively low Zn ion concentrations in the analyzed extracts (Figure 4.4). Therefore, we conclude that cytotoxicity of Zn and its alloys is mainly determined by available Zn ions. Previously, studies have reported on obvious cytotoxicity of undiluted extracts of Zn and its alloys towards bone-related cells [45, 122, 173]. DMEM/F-12 medium without FBS was chosen for the generation of Zn extracts. The presence of FBS in the extraction medium can increase Zn ion release, leading to additional cytotoxicity [156].

Periosteum derived mesenchymal stromal cells can differentiate into multiple cell lineages and play a critical role in bone regeneration [148, 149, 174]. We explored potential effects of long-term Zn degradation products on the mineralization potential of TAg cells considering the potential application of Zn-based alloys as suitable osteosynthesis materials. Our results showed that extracts of low

4. Study III

concentrations promote the osteogenic differentiation of TAg cells, in contrast to high concentrated extracts, indicating a dose-dependent effect (Figure 4.7). Similar effects on the mineralization potential of TAg cells were detected by using Zn ion concentrations of 2 μM and 40 μM in osteogenic media (Figure 4.11). In coincidence, other studies reported on osteogenic induction caused by Zn ion release from Zn-containing biomaterials [175, 176]. Zn-mediated cellular response seems to involve GPR39/ZnR and TRPM7 receptors for Zn-entry into MSCs, thus triggering the intracellular cAMP and PKA pathway, leading to the activation of MAPK [177]. Our qPCR data revealed no obvious increase in RUNX2, ALP and OCN gene expression at day 14, when TAg cells were cultured in the presence of low concentrated extracts (Figure 4.8) in comparison to TAg cells without extract supplementation. On the other hand, we observed a significant decrease in gene expression of the osteogenesis-relevant genes in the presence of high concentrated Zn extracts. A delayed osseointegration of pure Zn, characterized by less new bone formation directly on Zn surfaces, was observed in *in vivo* studies, which might be caused by the local accumulation of excessive Zn ion concentrations [45, 63]. Our data also verify the *in vivo* performances of Zn-based implants, indicating that the Zn ion concentration should be controlled in order to not disturb the bone tissue healing process. Nevertheless, the mechanisms of Zn modulated osteogenesis are still not fully understood and should be further investigated.

4.5. Conclusions

A modified extraction method was established for better correlation of Zn/Zn-4Ag alloy degradation behavior and cytocompatibility. Both Zn and Zn-4Ag exhibited predictable *in vitro* degradation behavior under cell culture conditions. Compared with pure Zn, a Zn-4Ag alloy with higher degradation rates seemed to exhibit no adverse cytotoxic effects on TAg cells. Concerning the degradation behavior, Zn ion concentrations in the extracts were not related to the calculated degradation rates of samples. This discrepancy is probably caused by formation of insoluble precipitates of degradation products, leading to a decreased concentration of free Zn ions in the extracts. This implies that cytotoxicity cannot be predicted by

4. Study III

calculated degradation rates, determined by e. g. sample weight loss, since it is correlated with released free ions rather than with degradation rates. In addition, osteogenic differentiation of TAg cells was significantly induced in the presence of low concentrated Zn extracts and significantly inhibited after supplementation of medium with high concentrated Zn extracts. Therefore, optimized Zn-based implants should produce low Zn ion concentrations in the local tissue to avoid interference with new bone formation.

5. Discussion

The development of absorbable Zn-based CMF osteosynthesis implants requires a multidisciplinary approach to evaluate material properties and biological response. In our previous study, a novel Zn-4Ag alloy with improved mechanical properties was fabricated and developed [69]. Herein, this thesis highlighted the major material properties related to cytotoxicity, degradation behavior, antibacterial properties and osteoinductivity of Zn-based alloys as CMF osteosynthesis implants.

5.1. Evaluation of cytotoxicity

Predicting biocompatibility is of primary significance when assessing and screening the candidate implant materials. The *in vitro* standardized cytotoxicity test is a rapid, simple, sensitive method to determine whether a novel biomaterial does perform physiologically at a cellular level, without the release of any toxic substances [67, 135]. The cytotoxicity evaluation of Zn and its alloys is mainly performed by two methods, namely a direct contact test and an extract test, based on the current ISO standards.

The *in vitro* direct contact test might be limited for Zn-based alloys due to the rapid surface change during the degradation process of Zn-based alloys. Considering most physiological conditions, cells have no chance to directly grow on the original surface of implants (without any protein adsorption and initial degradation layer formation) [68]. Previous studies have demonstrated that osteoblasts can grow directly on the degraded interface of Zn alloy [94] and on a gelatin modified Zn surface [178]. Notably, the comparison of results between *in vivo* and *in vitro* results have shown that the initial degradation layers formed on pure Zn *in vivo*, especially the zinc phosphate layer, can significantly enhance its biocompatibility [68]. Herein, we focused on extract tests to evaluate the cytotoxicity of Zn and its alloys in the thesis.

In study I, the cytotoxicity of a novel Zn-4Ag alloy was evaluated with L929 and Saos-2 cells. The results indicated obvious toxic effects in the original extracts while the toxic effect was decreased in the diluted extracts (10% and 16.7%), as

5. Discussion

shown in Figure 2.7 and Figure 2.8. The possible reason is the fact that the released Zn ion concentration in the original extracts is far beyond the cellular tolerance level for Zn ions, while L929 and Saos-2 cells can survive in the diluted extracts due to the decreased Zn ion concentration. Nevertheless, these cytotoxicity results should not be overestimated. The current ISO standard is derived from the evaluation of bioinert materials, such as titanium and ceramic, without consideration of the degradability of bioresorbable materials [67, 135]. Thereby, the use of the extract test for evaluating cytotoxicity of absorbable metals has been controversially discussed.

In study II, we further explored the extraction conditions of an extract tests for Zn and its alloys. Different extraction media were compared. The outcomes revealed that relative metabolic activities of L929 cells and Saos-2 cells were significantly decreased in the extraction media containing fetal bovine serum (Figure 3.6), indicating an FBS-mediated cytotoxic effect. The probable explanation is that FBS significantly increases Zn ion release (Table 3.3), leading to Zn ion concentrations beyond cellular tolerance. Coincidentally, serum-free cell culture media were used as extraction vehicle in some previous studies, and no obvious cytotoxic effects in the original extracts of Zn alloys were observed as well [53, 144] (Table 3.4). These results verify our finding of the FBS-mediated cytotoxic effect. Thus, our results can provide significant information for choosing an appropriate extraction medium to optimize the extract test.

In study III, we modified an extraction method to correlate the degradation rate and related cytotoxicity. The results showed that the degradation rate of Zn-4Ag was almost four-fold higher than that of pure Zn under cell culture conditions. However, the relative cytotoxic effects were not significantly increased (Figure 4.6). This can be explained by the finding that the released free Zn ion concentration in the extracts was not significantly different between pure Zn and the Zn-4Ag alloy (Figure 4.4). We assume that part of the free Zn ions was bound to degradation particles during the Zn-4Ag degradation process, leading to relatively low free Zn ion concentrations released from the Zn-4Ag alloy (Figure 4.5). The result effectively denies the previous conclusion that cytotoxicity of Zn-

5. Discussion

based alloys is consistent with the variation of degradation rates [171, 172]. Therefore, we can conclude that cytotoxicity was determined by the released free Zn ions, not directly correlated with the degradation rate calculated by weight loss.

Table 5.1. Summary of cytotoxicity evaluation of Zn-based alloys with bone-related cell lines.

Samples	Incubation time, d	Key findings	Ref.
Murine osteoblast precursor cells (MC3T3-E1)			
Zn Zn-HA composite Zn-0.5Al	1, 2 and 4	Zn-HA composite had better cell viability compare with the cytotoxic effect of pure Zn	[44]
Zn-0.5Al-0.1Mg Zn-0.5Al-0.3Mg Zn-0.5Al-0.5Mg (C) Zn-0.5Al-0.5Mg Zn-0.5Al-0.5Mg-XBi where X = 0.1, 0.3, 0.5 (C)	2 and 7	Zn-0.5Al-0.5Mg alloy exhibited higher cell viability compared with the Zn-0.5Al alloy. All alloys extracts showed no cytotoxicity while cell viability decreased with increasing Bi content	[113] [143]
Pure Zn with ZnP, ZnO and Zn(OH) ₂ layers	3	ZnP had highly biocompatible, which might be the key controlling biocompatibility of Zn	[68]
Human osteosarcoma cells and osteoblasts (including MG63, U-2 OS, HOS, NHOst and Saos-2)			
Zn and Zn-4Ag	1	Zn-4Ag had obvious toxicity effect in the original extracts while cytotoxicity decreased with diluted	Study I
Zn, Zn-4Ag and Zn-2Ag-1.8Au-0.2V	1	FBS-mediated cytotoxic effect	Study II
Zn (SLM) and Zn-xMg (x=1,2,3,4)	1, 3 and 5	SLM Zn induced cytotoxicity for MG63 in 100% extracts, but Zn-xMg had good cytocompatibility	[172]
Zn-0.8Mg (E)	1	Alloy was cytotoxic effects to U-2 OS in 100% extracts but non-cytotoxic in 50% dilution.	[93]
Zn-1.2Mg (C,E)	3	As-cast Zn-1.2Mg had no toxicity to MG63	[88]
Zn-1.5Mg (E)	1	Pretreatment improved cytocompatibility	[94]
Zn-1Mg, Zn-1Ca, Zn-1Sr (HR)	1, 3 and 5	Extracts had good viability using serum-free media	[53]
Zn-1Mg-Ca, Zn-1Mg-1Sr Zn-1Ca-1Sr (C, HR)	1, 3 and 5	Cell viability and morphology of MG63 showed excellent cytocompatibility	[87]
Zn-1Mg, Zn-1Mg-0.5Ca (C)	1 and 2	Saos-2 cells tolerated 100% sample extracts	[141]
Zn-3Mg (C)	1, 3 and 7	Sample extracts showed cytotoxicity after 1 day, while cell viability was improved at 3 day	[111]

5. Discussion

Human mesenchymal stem cells (including BMSCs and TAg cells)			
Zn and Zn-4Ag	2, 6 and 12	Cytotoxicity of TAg cells mainly determined by degradation products	Study III
Pure Zn (W)	1, 3 and 5	No cytotoxicity was detected in the 50% extracts, and confluent cell densities on Zn was observed	[63]
Pure Zn pretreated by serum (W)	1, 7 and 14	hMSC proliferation on Zn was increased after 1 and 7 days while was decreased after 14 days compared with AZ31	[177]

The metallurgy techniques are indicated as follows: C: casting, E: hot extrusion, HR: hot rolling SLM, selective laser melting, W: commercial wrought product.

For cytotoxicity evaluation, the proper choice of bone-related cell lines is deemed crucial to provide significant information on the applicability of the respective osteosynthesis implants. Table 5.1 lists the cytotoxicity results of Zn-based alloys using different bone-related cell lines, according to previous studies and our results. In study III, we first reported cytotoxicity results of Zn-4Ag alloys with human periosteal cells and found that no obvious toxicity effects. However, there are conflicting reports on the cytotoxicity of Zn and based alloys. These discrepancies can be explained by the different *in vitro* test methodologies, such as alloy systems, cell lines, exposure time, pretreatment, extract concentration, extraction medium etc. In summary, the current standardized cytotoxicity test should be further optimized to better evaluate and predict *in vivo* biocompatibility.

5.2. Determination of degradation behavior

Biodegradation behavior of absorbable Zn and its alloys not only influences the maintenance of mechanical strength but determines biocompatibility as well. Current standardized tests for evaluating *in vitro* degradation behavior are still lacking. In the thesis, the degradation behavior was investigated using an immersion test model (an extraction model with cell culture medium) under cell culture conditions, (37 °C, 5% CO₂, 20% O₂ and 95% rel. humidity). Numerous previous studies on Mg degradation have been demonstrated the *in vitro* degradation test under cell culture conditions is closer to the physiological environments [127, 128].

In study I, a novel Zn-4Ag alloy was performed to estimate the *in vitro* initial degradation rate through detecting the concentration of released metallic ions in

5. Discussion

the cell culture medium. As shown in Figure 2.5, we observed higher degradation rates in DMEM medium than in McCoy's medium, suggesting that the Zn degradation behavior is influenced by different components of the media. One main reason can be that the high concentration of HPO_4^{2-} in McCoy's medium formed a zinc-phosphate layer (passivation layer), inhibiting the initial degradation rates, as depicted in Figure 5.1. In addition, the initial degradation particles on the surfaces were detected by SEM (Figure 2.6). The EDX analysis indicates the products containing Zn, O, C, P and Cl derive mainly from chemical reactions with components of the cell culture media, probably composed of hydroxides, phosphate, carbonate compounds [43, 88, 106].

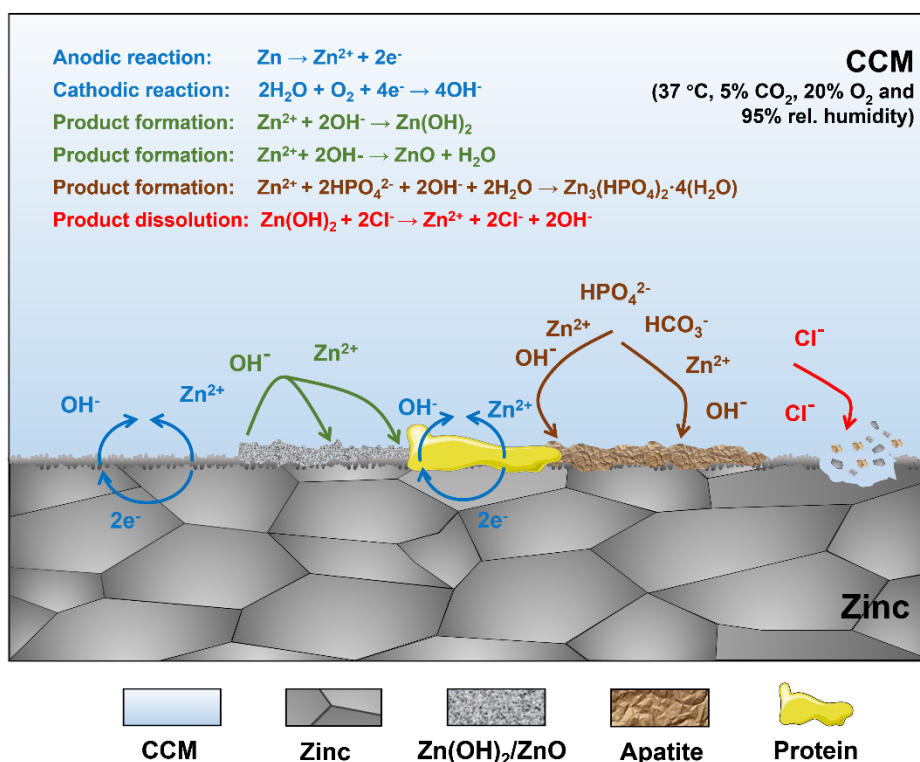


Figure 5.1. Schematic diagram of the degradation mechanism of Zn and its alloys under cell culture conditions (own image).

In study II, we further investigate the effect of FBS on the initial degradation process under cell culture conditions. According to the results of ICP-OES, FBS can significantly increase the initial Zn ion released from pure Zn and its alloys (Figure 3.2). It can be hypothesized that serum protein interferes with the passivation layer formation (Zn-P layer), leading to increased Zn ion release, as

5. Discussion

shown in Figure 5.1. Similarly, rapid protein adsorption on surfaces can prevent the initial passivation layer and increase the degradation rate when pure Zn is immersed in whole blood [131]. On the contrary, Liu et al. [179] reported that the Zn degradation process had three stages in artificial plasma. At the initial 24 h stage, Zn degradation can be retarded by the rapid albumin absorption on the surface. After 3 days, the degradation rate of Zn is increased mainly due to metal matrix dissolution. Whereas, the complex accumulation on the surface can decrease the degradation process again after 7 days. Additionally, a previous study also reported that the rapid protein adsorption on Zn surfaces can exacerbate the localized corrosion [165]. The conflicting results above can be found to reveal the complexity of the corrosion mechanisms. Hence, the effect of organic components on Zn degradation should be further explored.

In study III, a Zn-4Ag alloy was immersed in the DMEM/F-12 under cell culture conditions for 28 days. A consensus is widely recognized that a long-term immersion test under cell culture conditions closely mimics the physiological environment [163-165]. Firstly, our results indicated an inconsistency between degradation rates calculated by weight loss and free metallic ion release detected by ICP-OES (Figure 4.4). This can be attributed to the formation of degradation particles in the extracts, leading to metallic ions bound to the particles (Figure 4.5). In other words, the approach to estimate the degradation rates by detecting metallic ion release might be not suitable for a long-term degradation test. Moreover, the degradation rates of Zn-4Ag alloy ($17.38 \pm 0.78 \mu\text{m}/\text{year}$) in the DMEM/F-12 is higher than that of pure Zn ($4.80 \pm 0.82 \mu\text{m}/\text{year}$) caused by the micro-galvanic effect [89, 122]. Whereas, the degradation rates in DMEM/F-12 are slightly lower than those in the standard salt solutions such as SBF and HBBS, as shown in the Figure 5.2 a. Additionally, Liu et al. [165] proposed that the Zn degradation process can be retarded in DMEM compared to that in SBF and HBBS, due to the synergy effect of both organic components and insoluble salt formation on the Zn surface.

5. Discussion

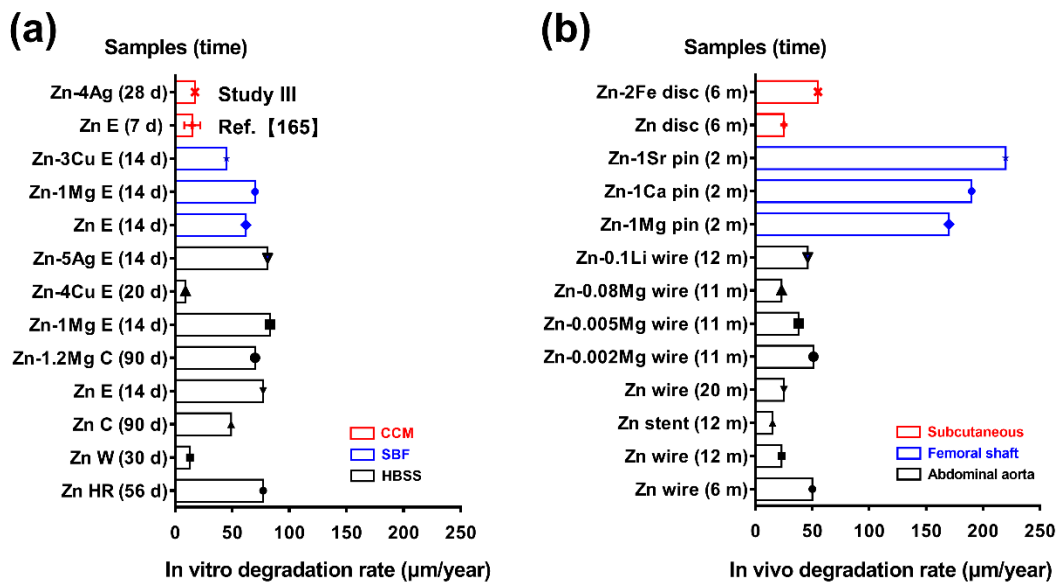


Figure 5.2. Reported degradation rates of Zn and Zn alloys. (a) *In vitro* degradation rates calculated from immersion test with different solutions: cell culture medium (CCM), simulated body fluid (SBF) and Hank's Balanced Salt Solution (HBSS). (b) In degradation rates in the different implantation sites. The metallurgy techniques are indicated as follows: C: casting, E: hot extrusion, W: commercial wrought product and HR: hot rolling. Most data gathered from the literature [24].

Though the specific degradation rates of CMF implants should depend on the clinical application, mechanical integrity needs to be maintained for at least 3-6 months. Also, the implants should be fully degraded within 2 years to avoid the interference of bone remodeling. Thereby, the suggested optimal degradation rate is $500 \mu\text{m}/\text{year}$ [24]. In the thesis, the *in vitro* degradation rate of the Zn-4Ag alloy was approximately $20 \mu\text{m}/\text{year}$, which is probably insufficient for the requirements of CMF osteosynthesis implants. As shown in Figure 5.2 b, most previous *in vivo* studies reported that pure Zn and Zn-based alloys implanted in different sites showed relatively slow degradation rates, all below $500 \mu\text{m}/\text{year}$. Consequently, it is required to adjust the degradation rates of Zn-based osteosynthesis implants in further studies.

5.3. Investigation of biofunctionality features

5.3.1. Antibacterial properties of a Zn-4Ag alloy

Antibacterial properties of CMF osteosynthesis implants can prevent post-

5. Discussion

operative infections. An intraoral surgical approach is the main trend for management of maxillofacial trauma. For transoral maxillofacial surgery, the infection risk with oral bacteria is increased [76]. Admittedly, the antibacterial properties should be effective against the related microorganisms. A previous study reported that salivary microbial species mainly include *Streptococcus*, *Rothia*, *Fusobacterium*, *Haemophilus*, *Prevotella*, and *Neisseria* [180]. In that, *S. gordonii* plays a critical role in initial colonization through creating a biofilm for adhesion of other colonizers in the oral environment [181]. Therefore, we used *S. gordonii* to evaluate the antibacterial properties of a Zn-4Ag alloy potentially used for CMF osteosynthesis implants.

In study I, the Zn-4Ag surface exhibited effective inhibition of initial *S. gordonii* adhesion and biofilm formation compared to the Ti-6Al-4V surface (Figure 2.9). Nonetheless, the potential antibacterial mechanism of Zn-4Ag is not completely understood and might be explained by several aspects as follows. Firstly, the released Zn ions from the Zn-4Ag alloy might potentially interact with *S. gordonii* on the surface. A previous study reported that Zn ions can alter charge balance, leading to cell deformation and bacteriolysis [182]. In principle, all zinc-based biodegradable materials possess potential antibacterial properties [48]. Secondly, the limited Ag ion release from a Zn-4Ag alloy might be useful for the inhibition of *S. gordonii* adhesion. Although Ag is considered as an effective antibacterial agent, the exact mechanism is still not completely understood. The effect is probably related to interaction with the cell membrane and interference with electron transport binding to DNA [183]. Additionally, released Ag ions can interact with DNA to promote pyrimidine dimerization via the photodynamic reaction, probably inhibiting DNA replication [184]. Finally, the antibacterial effect might be contributed by the cathodic reaction of Zn-4Ag in the medium, increasing hydroxide ion release on the surfaces (pH value increased). It has been reported that a magnesium alloy (AZ91) exhibited the *in vitro* antimicrobial properties mainly owing to the rapid degradation process, increasing in pH value in the culture medium. Nevertheless, the antibacterial effect is obviously diminished *in vivo* due to the buffering effect of body fluids [185]. Hence, the exact antibacterial mechanism of the Zn-4Ag alloy should be further investigated.

5. Discussion

5.3.2. Osteoinductivity of Zn and Zn-4Ag alloy

As an ideal osteosynthesis material, osteoinductivity can promote new bone formation, leading to shortening at the healing time. During the degradation process of Zn-based implants, the released Zn degradation products directly affect periosteal reaction and participate in tissue regeneration. Undoubtedly, periosteal stem cells not only can directly form bone tissue via the intramembranous pathway but induce endochondral ossification after trauma as well [147, 148]. Thus, we investigated the effect of degradation products of Zn and Zn-4Ag on the osteogenesis of a human immortalized cranial periosteal cell line (TAg cells).

In study III, our key finding is that a high concentration of Zn degradation products can significantly inhibit the osteogenesis while a low concentration induces the osteogenic differentiation of TAg cells, indicating a dose-dependent effect (Figure 4.7). Also, we used the related concentration of ZnCl₂ to verify the dose-dependent effect, suggesting that low Zn ion concentrations (2 μM) can induce osteogenesis but the osteogenesis inhibition by high Zn ion concentrations (40 μM). Previously, Li et. al [53] reported that Zn-based pins (Zn-1Mg, -1Ca, -1Sr) implanted into a femur cavity can induce new bone formation under the periosteum, probably implying that zinc ions can promote periosteum-mediated bone formation. Similarly, an *in vitro* study demonstrated that the Zn-mediated cellular response seems to involve GPR39/ZnR and TRPM7 receptors for Zn-entry into MSCs, thus triggering the intracellular cAMP and PKA pathway, leading to the activation of MAPK [177]. Admittedly, numerous studies substantiated that osteogenic induction can be caused by a low concentration of Zn ion release from Zn-containing biomaterials [175, 176]. Nevertheless, a phenomenon of delayed osseointegration around pure Zn implants was observed, probably caused by the local accumulation of excessive Zn ion concentrations [45, 63]. Thus, our results indicate that an appropriate Zn²⁺ release is essential for cellular reaction and function. Although the underlying *in vivo* mechanism remains unknown, controlling initial Zn²⁺ release should be of outstanding significance to improve biocompatibility, osteoinductivity and even osseointegration ability of Zn-based

5. Discussion

alloys as osteosynthesis implants.

6. Summary

6. Summary

The thesis focuses on *in vitro* evaluation of a Zn-4Ag alloy as a potential biomaterial for CMF osteosynthesis implants, mainly including cytotoxicity, degradation behavior, antibacterial properties and osteoinductivity.

Concerning the cytotoxicity test, obvious cytotoxic effects were observed in the original extracts. Nonetheless, we further demonstrated that the toxic effects were influenced by the presence of fetal bovine serum in the extraction medium mainly due to the FBS-mediated rapid Zn ion release. Moreover, the cytotoxicity is mainly determined by the degradation products released from Zn and a Zn-4Ag alloy rather than by their degradation rates.

The degradation behavior of Zn and Zn-4Ag alloy was evaluated under cell culture conditions. According to the calculation of weight loss, the degradation rate of Zn-4Ag in the DMEM/F-12 was approximately $17.38 \pm 0.78 \mu\text{m}/\text{year}$, which is significantly higher than that of pure Zn ($4.80 \pm 0.82 \mu\text{m}/\text{year}$). In addition, our results indicated that FBS can accelerate the initial degradation process of Zn and Zn alloys.

The antibacterial evaluation showed that the Zn-4Ag alloy has the potential to inhibit biofilm formation of *S. gordonii*. Additionally, a modified extraction method revealed a dose-dependent effect on the osteogenic differentiation of human periosteal cells. Specifically, high concentration of sample extracts significantly reduced calcium deposition, while a low concentration can induce calcium deposition.

In summary, the thesis indicates that Zn-4Ag possessed predictable cytotoxicity, relatively slow *in vitro* degradation behavior, effective antibacterial properties and potential osteoinduction capability, and thus could be a potential material for CMF osteosynthesis implants. However, further systematic studies are required.

7. German summary

Die Arbeit konzentriert sich auf die *In-vitro*-Bewertung einer Zn-4Ag-Legierung als potentiell Biomaterial für CMF-Osteosyntheseimplantate verwendet wird. Unters Dabei geht es hauptsächlich um Zytotoxizität, Abbauverhalten, antibakterielle Eigenschaften und Osteoinduktivität.

Für den Zytotoxizitätstest wurden in den ursprünglichen Extrakten offensichtliche zytotoxische Wirkungen beobachtet. Wir konnten jedoch weiterhin nachweisen, dass die toxischen Effekte durch das Vorhandensein von fötalem Rinderserum im Extraktionsmedium beeinflusst wurden, was hauptsächlich auf die durch FBS vermittelte schnelle Freisetzung von Zn-Ionen zurückzuführen ist. Darüber hinaus wird die Zytotoxizität hauptsächlich durch die Abbauprodukte bestimmt, die aus Zn und der Zn-4Ag-Legierung freigesetzt werden, und nicht durch deren Abbauraten.

Das Abbauverhalten von Zn und Zn-4Ag-Legierung wurde unter Zellkulturbedingungen evaluiert. Gemäß der Berechnung des Gewichtsverlusts betrug die Abbaurate von Zn-4Ag im DMEM / F-12 ungefähr $17,38 \pm 0,78 \mu\text{m}/\text{Jahr}$, was signifikant höher ist als die von reinem Zn ($4,80 \pm 0,82 \mu\text{m}/\text{Jahr}$). Zusätzlich zeigten unsere Ergebnisse, dass FBS den anfänglichen Abbauprozess von Zn und Zn-Legierungen beschleunigen kann.

Die antibakterielle Bewertung zeigte, dass die Zn-4Ag-Legierung das Potenzial besitzt, die Biofilmbildung von *S. gordonii* zu hemmen. Zusätzlich zeigte eine modifizierte Extraktionsmethode einen dosisabhängigen Effekt auf die osteogene Differenzierung menschlicher Periostzellen. Insbesondere die hohe Konzentration an Probenextrakten verringerte die Kalziumablagerung signifikant, während eine niedrige Konzentration eine Kalziumablagerung induzieren kann.

Zusammenfassend lässt sich sagen, dass Zn-4Ag eine vorhersagbare Zytotoxizität, ein relativ langsames Abbauverhalten *in vitro*, wirksame antibakterielle Eigenschaften und eine potenzielle Osteoinduktionsfähigkeit aufweist, und somit ein potenzielles Material für CMF-Osteosyntheseimplantate sein könnte. Weitere systematische Studien sind jedoch erforderlich.

8. Bibliography

- [1] M. Champy, F. Härle, B.C. Terry, Atlas of craniomaxillofacial osteosynthesis: microplates, miniplates, and screws, Thieme 2009.
- [2] S.C. Cifuentes, R. Benavente, M. Lieblich, J.L. González-Carrasco, Biodegradable and bioabsorbable materials for osteosynthesis applications: state-of-the-art and future perspectives, Handbook of Composites from Renewable Materials, Biodegradable Materials 5 (2017) 109-144.
- [3] K. Trajanoska, J.D. Schoufour, E.A. de Jonge, B.C. Kieboom, M. Mulder, B.H. Stricker, T. Voortman, A.G. Uitterlinden, E.H. Oei, M.A. Ikram, Fracture incidence and secular trends between 1989 and 2013 in a population based cohort: The Rotterdam Study, Bone 114 (2018) 116-124.
- [4] E. Hernlund, A. Svedbom, M. Ivergård, J. Compston, C. Cooper, J. Stenmark, E.V. McCloskey, B. Jönsson, J.A. Kanis, Osteoporosis in the European Union: medical management, epidemiology and economic burden, Archives of osteoporosis 8(1-2) (2013) 136.
- [5] P. Schumann, D. Lindhorst, M.E. Wagner, A. Schramm, N.-C. Gellrich, M. Rücker, Perspectives on resorbable osteosynthesis materials in craniomaxillofacial surgery, Pathobiology 80(4) (2013) 211-217.
- [6] R.A. Zwahlen, Internal Fixation in Oral and Maxillofacial Surgery, Handbook of Oral Biomaterials (2014) 435.
- [7] H.-S. Han, S. Loffredo, I. Jun, J. Edwards, Y.-C. Kim, H.-K. Seok, F. Witte, D. Mantovani, S. Glyn-Jones, Current status and outlook on the clinical translation of biodegradable metals, Materials Today 23 (2019) 57-71.
- [8] D. Zhao, F. Witte, F. Lu, J. Wang, J. Li, L. Qin, Current status on clinical applications of magnesium-based orthopaedic implants: A review from clinical translational perspective, Biomaterials 112 (2017) 287-302.
- [9] R. Alexander, L. Theodos, Fracture of the bone-grafted mandible secondary to stress shielding: Report of a case and review of the literature, Journal of oral and maxillofacial surgery 51(6) (1993) 695-697.
- [10] J. Nagels, M. Stokdijk, P.M. Rozing, Stress shielding and bone resorption in shoulder arthroplasty, Journal of shoulder and elbow surgery 12(1) (2003) 35-39.
- [11] M.C. Kennady, M.R. Tucker, G.E. Lester, M.J. Buckley, Stress shielding effect of rigid internal fixation plates on mandibular bone grafts. A photon absorption densitometry and quantitative computerized tomographic evaluation, International journal of oral and maxillofacial surgery 18(5) (1989) 307-310.
- [12] C. Lhotka, T. Szekeres, I. Steffan, K. Zhuber, K. Zweymüller, Four-year study of cobalt and chromium blood levels in patients managed with two different metal-on-metal total hip replacements, Journal of Orthopaedic Research 21(2) (2003) 189-195.
- [13] Q. Chen, G.A. Thouas, Metallic implant biomaterials, Materials Science and Engineering R 87 (2015) 1-57.

8. Bibliography

- [14] B. Alpert, D. Seligson, Removal of asymptomatic bone plates used for orthognathic surgery and facial fractures, *Journal of oral and maxillofacial surgery* 54(5) (1996) 618-621.
- [15] M.L. Busam, R.J. Esther, W.T. Obremsky, Hardware removal: indications and expectations, *JAAOS-Journal of the American Academy of Orthopaedic Surgeons* 14(2) (2006) 113-120.
- [16] T. Schepers, E.M. Van Lieshout, M.R. de Vries, M. Van der Elst, Complications of syndesmotic screw removal, *Foot & ankle international* 32(11) (2011) 1040-1044.
- [17] F. ASTM, Standard Specification for Unalloyed Titanium for Surgical Implant Applications, American Society for Testing and Materials, Philadelphia, PA.
- [18] M. Semlitsch, F. Staub, H. Weber, Development of a Vital, High-Strength Titanium--Aluminium--Niobium Alloy for Surgical Implants, *Biological and Biomechanical Performance of Biomaterials* (1985) 69-74.
- [19] P.K. Bowen, E.R. Shearier, S. Zhao, R.J. Guillory, F. Zhao, J. Goldman, J.W. Drelich, Biodegradable metals for cardiovascular stents: from clinical concerns to recent Zn-Alloys, *Advanced healthcare materials* 5(10) (2016) 1121-1140.
- [20] K. Van de Velde, P. Kiekens, Biopolymers: overview of several properties and consequences on their applications, *Polymer testing* 21(4) (2002) 433-442.
- [21] M. Jamshidian, E.A. Tehrany, M. Imran, M. Jacquot, S. Desobry, Poly-lactic acid: production, applications, nanocomposites, and release studies, *Comprehensive Reviews in Food Science and Food Safety* 9(5) (2010) 552-571.
- [22] H. Gong, K. Wang, R. Strich, J.G. Zhou, In vitro biodegradation behavior, mechanical properties, and cytotoxicity of biodegradable Zn–Mg alloy, *Journal of Biomedical Materials Research Part B: Applied Biomaterials* 103(8) (2015) 1632-1640.
- [23] Y. Zheng, X. Gu, F. Witte, Biodegradable metals, *Materials Science and Engineering: R: Reports* 77 (2014) 1-34.
- [24] J. Venezuela, M. Dargusch, The Influence of Alloying and Fabrication Techniques on the Mechanical Properties, Biodegradability and Biocompatibility of Zinc: A Comprehensive Review, *Acta biomaterialia* 87 (2019) 1-40.
- [25] M. Heiden, E. Walker, L. Stanciu, Magnesium, iron and zinc alloys, the trifecta of bioresorbable orthopaedic and vascular implantation-a review, *Journal of Biotechnology & Biomaterials* 5(2) (2015) 1.
- [26] D.E. Cutright, E. Hunsuck, J. Beasley, Fracture reduction using a biodegradable material, polylactic acid, *Journal of oral surgery* 29(6) (1971) 393-397.
- [27] T. Kanno, S. Sukegawa, Y. Furuki, Y. Nariai, J. Sekine, Overview of innovative advances in bioresorbable plate systems for oral and maxillofacial surgery, *Japanese Dental Science Review* 54(3) (2018) 127-138.
- [28] F.A. Barber, W.D. Dockery, Long-term absorption of poly-L-lactic acid interference screws, *Arthroscopy: The Journal of Arthroscopic & Related Surgery*

8. Bibliography

22(8) (2006) 820-826.

[29] K. Marumo, Y. Sato, H. Suzuki, D. Kurosaka, MRI study of bioabsorbable poly-L-lactic acid devices used for fixation of fracture and osteotomies, *Journal of Orthopaedic Science* 11(2) (2006) 154-158.

[30] N. Van Bakelen, G. Buijs, J. Jansma, J. de Visscher, T.J. Hoppenreijns, J. Bergsma, B. Stegenga, R. Bos, Comparison of biodegradable and titanium fixation systems in maxillofacial surgery: a two-year multi-center randomized controlled trial, *Journal of dental research* 92(12) (2013) 1100-1105.

[31] Y. Liu, Y. Zheng, X.H. Chen, J.A. Yang, H. Pan, D. Chen, L. Wang, J. Zhang, D. Zhu, S. Wu, Fundamental Theory of Biodegradable Metals—Definition, Criteria, and Design, *Advanced Functional Materials* (2019) 1805402.

[32] S. Pina, J.M. Ferreira, Bioresorbable plates and screws for clinical applications: a review, *Journal of Healthcare Engineering* 3(2) (2012) 243-260.

[33] F. Witte, The history of biodegradable magnesium implants: a review, *Acta biomaterialia* 6(5) (2010) 1680-1692.

[34] H. Windhagen, K. Radtke, A. Weizbauer, J. Diekmann, Y. Noll, U. Kreimeyer, R. Schavan, C. Stukenborg-Colsman, H. Waizy, Biodegradable magnesium-based screw clinically equivalent to titanium screw in hallux valgus surgery: short term results of the first prospective, randomized, controlled clinical pilot study, *Biomedical engineering online* 12(1) (2013) 62.

[35] H. Leonhardt, A. Franke, N. McLeod, G. Lauer, A. Nowak, Fixation of fractures of the condylar head of the mandible with a new magnesium-alloy biodegradable cannulated headless bone screw, *British Journal of Oral and Maxillofacial Surgery* 55(6) (2017) 623-625.

[36] J.-W. Lee, H.-S. Han, K.-J. Han, J. Park, H. Jeon, M.-R. Ok, H.-K. Seok, J.-P. Ahn, K.E. Lee, D.-H. Lee, Long-term clinical study and multiscale analysis of in vivo biodegradation mechanism of Mg alloy, *Proceedings of the National Academy of Sciences* 113(3) (2016) 716-721.

[37] Y. Zheng, X. Xu, Z. Xu, J. Wang, H. Cai, Development of Fe-based degradable metallic biomaterials, *Metallic biomaterials: new directions and technologies*. Wiley-VCH Verlag GmbH & Co, KGaA, Weinheim (2017) 113-160.

[38] M. Peuster, P. Wohlsein, M. Brüggemann, M. Ehlerding, K. Seidler, C. Fink, H. Brauer, A. Fischer, G. Hausdorf, A novel approach to temporary stenting: degradable cardiovascular stents produced from corrodible metal—results 6–18 months after implantation into New Zealand white rabbits, *Heart* 86(5) (2001) 563-569.

[39] T. Kraus, F. Moszner, S. Fischerauer, M. Fiedler, E. Martinelli, J. Eichler, F. Witte, E. Willbold, M. Schinhammer, M. Meischel, Biodegradable Fe-based alloys for use in osteosynthesis: Outcome of an in vivo study after 52 weeks, *Acta biomaterialia* 10(7) (2014) 3346-3353.

[40] J. Zhou, Y. Yang, M. Alonso Frank, R. Detsch, A.R. Boccaccini, S. Virtanen, Accelerated degradation behavior and cytocompatibility of pure iron treated with sandblasting, *ACS applied materials & interfaces* 8(40) (2016) 26482-26492.

8. Bibliography

- [41] Č. Donik, A. Kocijan, I. Paulin, M. Hočevar, P. Gregorčič, M. Godec, Improved biodegradability of Fe–Mn alloy after modification of surface chemistry and topography by a laser ablation, *Applied Surface Science* 453 (2018) 383-393.
- [42] Y. Qi, X. Li, Y. He, D. Zhang, J. Ding, Mechanism of Acceleration of Iron Corrosion by a Polylactide Coating, *ACS applied materials & interfaces* 11(1) (2018) 202-218.
- [43] D. Vojtěch, J. Kubásek, J. Šerák, P. Novák, Mechanical and corrosion properties of newly developed biodegradable Zn-based alloys for bone fixation, *Acta Biomaterialia* 7(9) (2011) 3515-3522.
- [44] H. Yang, X. Qu, W. Lin, C. Wang, D. Zhu, K. Dai, Y. Zheng, In vitro and in vivo studies on zinc-hydroxyapatite composites as novel biodegradable metal matrix composite for orthopedic applications, *Acta Biomater.* 71 (2018) 200-214.
- [45] H. Yang, X. Qu, W. Lin, D. Chen, D. Zhu, K. Dai, Y. Zheng, Enhanced Osseointegration of Zn-Mg Composites by Tuning the Release of Zn Ions with Sacrificial Mg-Rich Anode Design, *ACS Biomaterials Science & Engineering* 5(2) (2019) 453–467.
- [46] P. Li, W. Zhang, J. Dai, A.B. Xepapadeas, E. Schweizer, D. Alexander, L. Scheideler, C. Zhou, H. Zhang, G. Wan, Investigation of zinc-copper alloys as potential materials for craniomaxillofacial osteosynthesis implants, *Materials Science and Engineering: C* (2019) 109826.
- [47] X. Wang, X. Shao, T. Dai, F. Xu, J.G. Zhou, G. Qu, L. Tian, B. Liu, Y. Liu, In vivo study of the efficacy, biosafety, and degradation of a zinc alloy osteosynthesis system, *Acta biomaterialia* 92 (2019) 351-361.
- [48] Y. Su, I. Cockerill, Y. Wang, Y.-X. Qin, L. Chang, Y. Zheng, D. Zhu, Zinc-Based Biomaterials for Regeneration and Therapy, *Trends in biotechnology* 37(4) (2018) 428-441.
- [49] E. O' Neill, G. Awale, L. Daneshmandi, O. Umerah, K.W.-H. Lo, The roles of ions on bone regeneration, *Drug discovery today* 23(4) (2018) 879-890.
- [50] J. Cheng, B. Liu, Y. Wu, Y. Zheng, Comparative in vitro study on pure metals (Fe, Mn, Mg, Zn and W) as biodegradable metals, *Journal of Materials Science & Technology* 29(7) (2013) 619-627.
- [51] G. Katarivas Levy, J. Goldman, E. Aghion, The Prospects of Zinc as a Structural Material for Biodegradable Implants—A Review Paper, *Metals* 7(10) (2017) 402.
- [52] H. Yang, C. Wang, C. Liu, H. Chen, Y. Wu, J. Han, Z. Jia, W. Lin, D. Zhang, W. Li, Evolution of the degradation mechanism of pure zinc stent in the one-year study of rabbit abdominal aorta model, *Biomaterials* 145 (2017) 92-105.
- [53] H. Li, X. Xie, Y. Zheng, Y. Cong, F. Zhou, K. Qiu, X. Wang, S. Chen, L. Huang, L. Tian, Development of biodegradable Zn-1X binary alloys with nutrient alloying elements Mg, Ca and Sr, *Scientific reports* 5 (2015).
- [54] P.K. Bowen, J. Drelich, J. Goldman, Zinc exhibits ideal physiological corrosion behavior for bioabsorbable stents, *Advanced materials* 25(18) (2013)

8. Bibliography

2577-2582.

- [55] P.K. Bowen, R.J. Guillory, E.R. Shearier, J.-M. Seitz, J. Drelich, M. Bocks, F. Zhao, J. Goldman, Metallic zinc exhibits optimal biocompatibility for bioabsorbable endovascular stents, *Materials Science and Engineering: C* 56 (2015) 467-472.
- [56] S. Zhao, J.-M. Seitz, R. Eifler, H.J. Maier, R.J. Guillory, E.J. Earley, A. Drelich, J. Goldman, J.W. Drelich, Zn-Li alloy after extrusion and drawing: Structural, mechanical characterization, and biodegradation in abdominal aorta of rat, *Materials Science and Engineering: C* 76 (2017) 301-312.
- [57] A. Drelich, S. Zhao, R.J. Guillory, J.W. Drelich, J. Goldman, Long-term surveillance of zinc implant in murine artery: surprisingly steady biocorrosion rate, *Acta Biomaterialia* 58 (2017) 539-549.
- [58] A.A. Shomali, R.J. Guillory, D. Seguin, J. Goldman, J.W. Drelich, Effect of PLLA coating on corrosion and biocompatibility of zinc in vascular environment, *Surface Innovations* 5(4) (2017) 211-220.
- [59] H. Jin, S. Zhao, R. Guillory, P.K. Bowen, Z. Yin, A. Griebel, J. Schaffer, E.J. Earley, J. Goldman, J.W. Drelich, Novel high-strength, low-alloys Zn-Mg (< 0.1 wt% Mg) and their arterial biodegradation, *Materials Science and Engineering: C* 84 (2018) 67-79.
- [60] R.J. Guillory, P.K. Bowen, S.P. Hopkins, E.R. Shearier, E.J. Earley, A.A. Gillette, E. Aghion, M. Bocks, J.W. Drelich, J. Goldman, Corrosion characteristics dictate the long-term inflammatory profile of degradable zinc arterial implants, *ACS Biomaterials Science & Engineering* 2(12) (2016) 2355-2364.
- [61] P.K. Bowen, J.M. Seitz, R.J. Guillory, J.P. Braykovich, S. Zhao, J. Goldman, J.W. Drelich, Evaluation of wrought Zn–Al alloys (1, 3, and 5 wt% Al) through mechanical and in vivo testing for stent applications, *Journal of Biomedical Materials Research Part B: Applied Biomaterials* 106(1) (2018) 245-258.
- [62] C. Hehrlein, B. Schorch, N. Kress, A. Arab, C. von zur Mühlen, C. Bode, T. Epting, J. Haberstroh, L. Mey, H. Schwarzbach, Zn-alloy provides a novel platform for mechanically stable bioresorbable vascular stents, *PloS one* 14(1) (2019) e0209111.
- [63] D. Zhu, I. Cockerill, Y. Su, Z. Zhang, J. Fu, K.-W. Lee, J. Ma, C. Okpokwasili, L. Tang, Y. Zheng, Mechanical Strength, Biodegradation, and In Vitro and In Vivo Biocompatibility of Zn Biomaterials, *ACS applied materials & interfaces* 11(7) (2019) 6809-6819.
- [64] A. Kafri, S. Ovadia, G. Yosafovich-Doitch, E. Aghion, In vivo performances of pure Zn and Zn–Fe alloy as biodegradable implants, *Journal of Materials Science: Materials in Medicine* 29(7) (2018) 94.
- [65] A. Kafri, S. Ovadia, G. Yosafovich-Doitch, E. Aghion, The Effects of 4% Fe on the Performance of Pure Zinc as Biodegradable Implant Material, *Annals of biomedical engineering* (2019) 1-9.
- [66] A. Kafri, S. Ovadia, J. Goldman, J. Drelich, E. Aghion, The suitability of Zn–1.3% Fe alloy as a biodegradable implant material, *Metals* 8(3) (2018) 153.

8. Bibliography

- [67] P. Li, N. Zhou, H. Qiu, M.F. Maitz, J. Wang, N. Huang, In vitro and in vivo cytocompatibility evaluation of biodegradable magnesium-based stents: a review, *Science China Materials* 61(4) (2018) 501-515.
- [68] Y. Su, H. Yang, J. Gao, Y.X. Qin, Y. Zheng, D. Zhu, Interfacial Zinc Phosphate is the Key to Controlling Biocompatibility of Metallic Zinc Implants, *Advanced Science* (2019) 1900112.
- [69] U.E.K.c. Claudia Legner, Alexander Heiss c, Production and characterization of zinc-based bioresorbable alloys, *Pforzheimer Werkstofftag Conference* (2014) 85-94.
- [70] T.J. Cahill III, R. Gandhi, A.C. Allori, J.R. Marcus, D. Powers, D. Erdmann, S.T. Hollenbeck, H. Levinson, Hardware removal in craniomaxillofacial trauma: a systematic review of the literature and management algorithm, *Annals of plastic surgery* 75(5) (2015) 572.
- [71] M. Xiao, Y. Chen, M. Biao, X. Zhang, B. Yang, Bio-functionalization of biomedical metals, *Materials Science and Engineering: C* 70 (2017) 1057-1070.
- [72] K. Yang, C. Zhou, H. Fan, Y. Fan, Q. Jiang, P. Song, H. Fan, Y. Chen, X. Zhang, Bio-functional design, application and trends in metallic biomaterials, *International journal of molecular sciences* 19(1) (2017) 24.
- [73] J. Niu, Z. Tang, H. Huang, J. Pei, H. Zhang, G. Yuan, W. Ding, Research on a Zn-Cu alloy as a biodegradable material for potential vascular stents application, *Materials Science and Engineering: C* 69 (2016) 407-413.
- [74] Z. Tang, J. Niu, H. Huang, H. Zhang, J. Pei, J. Ou, G. Yuan, Potential biodegradable Zn-Cu binary alloys developed for cardiovascular implant applications, *Journal of the mechanical behavior of biomedical materials* 72 (2017) 182-191.
- [75] J.S. Schenkel, J. Obwegeser, W. Zemmann, C. Rostetter, R. Tandon, P. Metzler, Outcome of comminuted mandibular fracture repair using an intraoral approach for osteosynthesis, *Journal of Craniofacial Surgery* 25(6) (2014) 2033-2037.
- [76] Y.J. Spaey, R.M. Bettens, M.Y. Mommaerts, J. Adriaens, H.W. Van Landuyt, J.V. Abeloos, C.A. De Clercq, P.R. Lamoral, L.F. Neyt, A prospective study on infectious complications in orthognathic surgery, *Journal of Cranio-Maxillofacial Surgery* 33(1) (2005) 24-29.
- [77] Y. Zheng, X. Xu, Z. Xu, J. Wang, H. Cai, Development of Zn-Based Degradable Metallic Biomaterials, *Metallic Biomaterials: New Directions and Technologies* (2017) 161-188.
- [78] M. Moravej, D. Mantovani, Biodegradable metals for cardiovascular stent application: interests and new opportunities, *International journal of molecular sciences* 12(7) (2011) 4250-4270.
- [79] T. Kraus, S.F. Fischerauer, A.C. Hänzi, P.J. Uggowitzer, J.F. Löffler, A.M. Weinberg, Magnesium alloys for temporary implants in osteosynthesis: in vivo studies of their degradation and interaction with bone, *Acta biomaterialia* 8(3) (2012) 1230-1238.

8. Bibliography

- [80] J. Geis-Gerstorfer, C. Schille, E. Schweizer, F. Rupp, L. Scheideler, H.-P. Reichel, N. Hort, A. Nolte, H.-P. Wendel, Blood triggered corrosion of magnesium alloys, *Materials Science and Engineering: B* 176(20) (2011) 1761-1766.
- [81] D. Pierson, J. Edick, A. Tauscher, E. Pokorney, P. Bowen, J. Gelbaugh, J. Stinson, H. Getty, C.H. Lee, J. Drelich, A simplified in vivo approach for evaluating the bioabsorbable behavior of candidate stent materials, *Journal of Biomedical Materials Research Part B: Applied Biomaterials* 100(1) (2012) 58-67.
- [82] A. Drynda, T. Hassel, F.W. Bach, M. Peuster, In vitro and in vivo corrosion properties of new iron–manganese alloys designed for cardiovascular applications, *Journal of Biomedical Materials Research Part B: Applied Biomaterials* 103(3) (2015) 649-660.
- [83] D. Beyersmann, H. Haase, Functions of zinc in signaling, proliferation and differentiation of mammalian cells, *Biometals* 14(3-4) (2001) 331-341.
- [84] A.S. Prasad, Zinc in human health: effect of zinc on immune cells, *MOLECULAR MEDICINE-CAMBRIDGE MA THEN NEW YORK-* 14(5/6) (2008) 353.
- [85] J.F. Schenck, The role of magnetic susceptibility in magnetic resonance imaging: MRI magnetic compatibility of the first and second kinds, *Medical physics* 23(6) (1996) 815-850.
- [86] J. Kubasek, D. Vojtěch, Zn-based alloys as an alternative biodegradable materials, *Proc Metal* 5 (2012) 23-25.
- [87] H. Li, H. Yang, Y. Zheng, F. Zhou, K. Qiu, X. Wang, Design and characterizations of novel biodegradable ternary Zn-based alloys with IIA nutrient alloying elements Mg, Ca and Sr, *Materials & Design* 83 (2015) 95-102.
- [88] C. Shen, X. Liu, B. Fan, P. Lan, F. Zhou, X. Li, H. Wang, X. Xiao, L. Li, S. Zhao, Mechanical properties, in vitro degradation behavior, hemocompatibility and cytotoxicity evaluation of Zn–1.2 Mg alloy for biodegradable implants, *RSC Advances* 6(89) (2016) 86410-86419.
- [89] M. Sikora-Jasinska, E. Mostaed, A. Mostaed, R. Beanland, D. Mantovani, M. Vedani, Fabrication, mechanical properties and in vitro degradation behavior of newly developed Zn Ag alloys for degradable implant applications, *Materials Science and Engineering: C* 77 (2017) 1170-1181.
- [90] D. Tie, F. Feyerabend, W.-D. Mueller, R. Schade, K. Liefeth, K.U. Kainer, R. Willumeit, Antibacterial biodegradable Mg-Ag alloys, *European cells & materials* 25 (2012) 284-98; discussion 298.
- [91] ISO 10993-12: 2012. Biological Evaluation of Medical Devices–Part 12: Sample Preparation and Reference Materials; International Organization for Standardization: Geneva, Switzerland, 2012.
- [92] J. Wang, F. Witte, T. Xi, Y. Zheng, K. Yang, Y. Yang, D. Zhao, J. Meng, Y. Li, W. Li, Recommendation for modifying current cytotoxicity testing standards for biodegradable magnesium-based materials, *Acta biomaterialia* 21 (2015) 237-249.

8. Bibliography

- [93] J. Kubásek, D. Vojtěch, E. Jablonská, I. Pospíšilová, J. Lipov, T. Ruml, Structure, mechanical characteristics and in vitro degradation, cytotoxicity, genotoxicity and mutagenicity of novel biodegradable Zn–Mg alloys, *Materials Science and Engineering: C* 58 (2016) 24-35.
- [94] E. Jablonská, D. Vojtěch, M. Fousová, J. Kubásek, J. Lipov, J. Fojt, T. Ruml, Influence of surface pre-treatment on the cytocompatibility of a novel biodegradable ZnMg alloy, *Materials Science and Engineering: C* 68 (2016) 198-204.
- [95] J. Čapek, E. Jablonská, J. Lipov, T.F. Kubatík, D. Vojtěch, Preparation and characterization of porous zinc prepared by spark plasma sintering as a material for biodegradable scaffolds, *Materials Chemistry and Physics* 203 (2018) 249-258.
- [96] B. Liu, Y. Zheng, Effects of alloying elements (Mn, Co, Al, W, Sn, B, C and S) on biodegradability and in vitro biocompatibility of pure iron, *Acta biomaterialia* 7(3) (2011) 1407-1420.
- [97] ISO 10993–5: 2009. Biological Evaluation of Medical Devices–Part 5: Tests for In Vitro Cytotoxicity; International Organization for Standardization: Geneva, Switzerland, 2009.
- [98] X.-N. Gu, Y.-F. Zheng, A review on magnesium alloys as biodegradable materials, *Frontiers of Materials Science in China* 4(2) (2010) 111-115.
- [99] M.S.-J. E. Mostaed, A. L. Ramirez-Ledesma, L. Levesque, D. Mantovani,, M. Vedani, Development of Zn-Ag-Mn alloys for future bioabsorbable vascular stents, 9th Symposium on Biodegradable Metals; , Metals: Bertinoro, Italy, 2017.
- [100] N. Kirkland, J. Lespagnol, N. Birbilis, M. Staiger, A survey of bio-corrosion rates of magnesium alloys, *Corrosion Science* 52(2) (2010) 287-291.
- [101] Y. Xin, T. Hu, P. Chu, In vitro studies of biomedical magnesium alloys in a simulated physiological environment: a review, *Acta biomaterialia* 7(4) (2011) 1452-1459.
- [102] L. Scheideler, C. Füger, C. Schille, F. Rupp, H.-P. Wendel, N. Hort, H. Reichel, J. Geis-Gerstorfer, Comparison of different in vitro tests for biocompatibility screening of Mg alloys, *Acta biomaterialia* 9(10) (2013) 8740-8745.
- [103] A.H.M. Sanchez, B.J. Luthringer, F. Feyerabend, R. Willumeit, Mg and Mg alloys: how comparable are in vitro and in vivo corrosion rates? A review, *Acta biomaterialia* 13 (2015) 16-31.
- [104] M.K. Patterson, R.T. Dell'orco, Preparation of McCoy's medium 5A, *Methods in Cell Science* 4(1) (1978) 737-740.
- [105] X. Liu, J. Sun, Y. Yang, Z. Pu, Y. Zheng, In vitro investigation of ultra-pure Zn and its mini-tube as potential bioabsorbable stent material, *Materials Letters* 161 (2015) 53-56.
- [106] Y. Chen, W. Zhang, M.F. Maitz, M. Chen, H. Zhang, J. Mao, Y. Zhao, N. Huang, G. Wan, Comparative corrosion behavior of Zn with Fe and Mg in the

8. Bibliography

course of immersion degradation in phosphate buffered saline, *Corrosion Science* 111 (2016) 541-555.

[107] J. Fischer, M.H. Prosenč, M. Wolff, N. Hort, R. Willumeit, F. Feyerabend, Interference of magnesium corrosion with tetrazolium-based cytotoxicity assays, *Acta Biomaterialia* 6(5) (2010) 1813-1823.

[108] K.M. Hambidge, N.F. Krebs, Zinc deficiency: a special challenge, *The Journal of nutrition* 137(4) (2007) 1101-1105.

[109] L.M. Plum, L. Rink, H. Haase, The essential toxin: impact of zinc on human health, *International journal of environmental research and public health* 7(4) (2010) 1342-1365.

[110] N. Hadrup, H.R. Lam, Oral toxicity of silver ions, silver nanoparticles and colloidal silver—a review, *Regulatory Toxicology and Pharmacology* 68(1) (2014) 1-7.

[111] N. Murni, M. Dambatta, S. Yeap, G. Froemming, H. Hermawan, Cytotoxicity evaluation of biodegradable Zn–3Mg alloy toward normal human osteoblast cells, *Materials Science and Engineering: C* 49 (2015) 560-566.

[112] C. Wang, H. Yang, X. Li, Y. Zheng, In Vitro Evaluation of the Feasibility of Commercial Zn Alloys as Biodegradable Metals, *Journal of Materials Science & Technology* 32(9) (2016) 909-918.

[113] H. Bakhsheshi-Rad, E. Hamzah, H. Low, M. Kasiri-Asgarani, S. Farahany, E. Akbari, M. Cho, Fabrication of biodegradable Zn-Al-Mg alloy: mechanical properties, corrosion behavior, cytotoxicity and antibacterial activities, *Materials Science and Engineering: C* 73 (2017) 215-219.

[114] C. Misch, *Vertical Alveolar Ridge Augmentation in Implant Dentistry: A Surgical Manual*, LWW, 2017.

[115] O.-M. Goudouri, E. Kontonasaki, U. Lohbauer, A.R. Boccaccini, Antibacterial properties of metal and metalloid ions in chronic periodontitis and peri-implantitis therapy, *Acta biomaterialia* 10(8) (2014) 3795-3810.

[116] V.T. Noronha, A.J. Paula, G. Durán, A. Galembeck, K. Cogo-Müller, M. Franz-Montan, N. Durán, Silver nanoparticles in dentistry, *Dental Materials* 33(10) (2017) 1110-1126.

[117] S. Shafeeq, O.P. Kuipers, T.G. Kloosterman, The role of zinc in the interplay between pathogenic streptococci and their hosts, *Molecular microbiology* 88(6) (2013) 1047-1057.

[118] H. Hu, W. Zhang, Y. Qiao, X. Jiang, X. Liu, C. Ding, Antibacterial activity and increased bone marrow stem cell functions of Zn-incorporated TiO₂ coatings on titanium, *Acta biomaterialia* 8(2) (2012) 904-915.

[119] E. Mostaed, M. Sikora-Jasinska, J.W. Drelich, M. Vedani, Zinc-based alloys for degradable vascular stent applications, *Acta biomaterialia* 71 (2018) 1-23.

[120] C. Schille, M. Braun, H. Wendel, L. Scheideler, N. Hort, H.-P. Reichel, E. Schweizer, J. Geis-Gerstorfer, Corrosion of experimental magnesium alloys in blood and PBS: A gravimetric and microscopic evaluation, *Materials Science and*

8. Bibliography

Engineering: B 176(20) (2011) 1797-1801.

[121] I. Johnson, W. Jiang, H. Liu, The effects of serum proteins on magnesium alloy degradation in vitro, *Scientific reports* 7(1) (2017) 14335.

[122] P. Li, C. Schille, E. Schweizer, F. Rupp, A. Heiss, C. Legner, U.E. Klotz, J. Geis-Gerstorfer, L. Scheideler, Mechanical Characteristics, In Vitro Degradation, Cytotoxicity, and Antibacterial Evaluation of Zn-4.0 Ag Alloy as a Biodegradable Material, *International journal of molecular sciences* 19(3) (2018) 755.

[123] X. Tong, D. Zhang, X. Zhang, Y. Su, Z. Shi, K. Wang, J. Lin, Y. Li, J. Lin, C. Wen, Microstructure, mechanical properties, biocompatibility, and in vitro corrosion and degradation behavior of a new Zn–5Ge alloy for biodegradable implant materials, *Acta Biomaterialia* 82 (2018) 197-204.

[124] P.S. Bagha, S. Khaleghpanah, S. Sheibani, M. Khakbiz, A. Zakeri, Characterization of nanostructured biodegradable Zn-Mn alloy synthesized by mechanical alloying, *Journal of Alloys and Compounds* 735 (2018) 1319-1327.

[125] J.E. Hall, Guyton and Hall textbook of medical physiology e-Book, Elsevier Health Sciences 2015.

[126] P.J. Price, E.A. Gregory, Relationship between in vitro growth promotion and biophysical and biochemical properties of the serum supplement, *In vitro* 18(6) (1982) 576-584.

[127] J. Gonzalez, R.Q. Hou, E.P. Nidadavolu, R. Willumeit-Römer, F. Feyerabend, Magnesium degradation under physiological conditions—Best practice, *Bioactive Materials* 3(2) (2018) 174-185.

[128] S. Johnston, M. Dargusch, A. Atrens, Building towards a standardised approach to biocorrosion studies: a review of factors influencing Mg corrosion in vitro pertinent to in vivo corrosion, *Science China Materials* 61(4) (2018) 1-26.

[129] X. Liu, J. Sun, K. Qiu, Y. Yang, Z. Pu, L. Li, Y. Zheng, Effects of alloying elements (Ca and Sr) on microstructure, mechanical property and in vitro corrosion behavior of biodegradable Zn–1.5Mg alloy, *Journal of Alloys and Compounds* 664 (2016) 444-452.

[130] T. Yao, Y. Asayama, Animal-cell culture media: History, characteristics, and current issues, *Reproductive medicine and biology* 16(2) (2017) 99-117.

[131] K.B. Törne, A. Örnberg, J. Weissenrieder, Characterization of the protective layer formed on zinc in whole blood, *Electrochimica Acta* 258 (2017) 1476-1483.

[132] A. Yamamoto, S. Hiromoto, Effect of inorganic salts, amino acids and proteins on the degradation of pure magnesium in vitro, *Materials Science and Engineering: C* 29(5) (2009) 1559-1568.

[133] C. Liu, Y. Xin, X. Tian, P.K. Chu, Degradation susceptibility of surgical magnesium alloy in artificial biological fluid containing albumin, *Journal of Materials Research* 22(7) (2007) 1806-1814.

[134] X. Gu, Y. Zheng, L. Chen, Influence of artificial biological fluid composition on the biocorrosion of potential orthopedic Mg–Ca, AZ31, AZ91 alloys, *Biomedical Materials* 4(6) (2009) 065011.

8. Bibliography

- [135] A. Bruinink, R. Luginbuehl, Evaluation of biocompatibility using in vitro methods: Interpretation and limitations, *Tissue Engineering III: Cell-Surface Interactions for Tissue Culture*, Springer 2011, pp. 117-152.
- [136] Z. Zhen, X. Liu, T. Huang, T. Xi, Y. Zheng, Hemolysis and cytotoxicity mechanisms of biodegradable magnesium and its alloys, *Materials Science and Engineering: C* 46 (2015) 202-206.
- [137] J. Ma, N. Zhao, D. Zhu, Endothelial cellular responses to biodegradable metal zinc, *ACS biomaterials science & engineering* 1(11) (2015) 1174-1182.
- [138] J. Ma, N. Zhao, D. Zhu, Bioabsorbable zinc ion induced biphasic cellular responses in vascular smooth muscle cells, *Scientific reports* 6 (2016) srep26661.
- [139] A. Yamamoto, R. Honma, M. Sumita, Cytotoxicity evaluation of 43 metal salts using murine fibroblasts and osteoblastic cells, *Journal of Biomedical Materials Research* 39(2) (1998) 331-340.
- [140] C. Xiao, L. Wang, Y. Ren, S. Sun, E. Zhang, C. Yan, Q. Liu, X. Sun, F. Shou, J. Duan, Indirectly extruded biodegradable Zn-0.05 wt% Mg alloy with improved strength and ductility: In vitro and in vivo studies, *Journal of Materials Science & Technology* (2018).
- [141] G.K. Levy, A. Leon, A. Kafri, Y. Ventura, J.W. Drelich, J. Goldman, R. Vago, E. Aghion, Evaluation of biodegradable Zn-1% Mg and Zn-1% Mg-0.5% Ca alloys for biomedical applications, *Journal of Materials Science: Materials in Medicine* 28(11) (2017) 174.
- [142] Z. Tang, H. Huang, J. Niu, L. Zhang, H. Zhang, J. Pei, J. Tan, G. Yuan, Design and characterizations of novel biodegradable Zn-Cu-Mg alloys for potential biodegradable implants, *Materials & Design* 117 (2017) 84-94.
- [143] H. Bakhsheshi-Rad, E. Hamzah, H. Low, M. Cho, M. Kasiri-Asgarani, S. Farahany, A. Mostafa, M. Medraj, Thermal Characteristics, Mechanical Properties, In Vitro Degradation and Cytotoxicity of Novel Biodegradable Zn-Al-Mg and Zn-Al-Mg-xBi Alloys, *Acta Metallurgica Sinica (English Letters)* 30(3) (2017) 201-211.
- [144] C. Xiao, L. Wang, Y. Ren, S. Sun, E. Zhang, C. Yan, Q. Liu, X. Sun, F. Shou, J. Duan, Indirectly extruded biodegradable Zn-0.05 wt% Mg alloy with improved strength and ductility: In vitro and in vivo studies, *Journal of Materials Science & Technology* 34(9) (2018) 1618-1627.
- [145] J. Venezuela, M. Dargusch, The Influence of Alloying and Fabrication Techniques on the Mechanical Properties, Biodegradability and Biocompatibility of Zinc: A Comprehensive Review, *Acta biomaterialia* (2019).
- [146] R. Marsell, T.A. Einhorn, The biology of fracture healing, *Injury* 42(6) (2011) 551-555.
- [147] Z. Lin, A. Fateh, D. Salem, G. Intini, Periosteum Biology and Applications in Craniofacial Bone Regeneration, *Journal of dental research* 93(2) (2014) 109-116.
- [148] S. Debnath, A.R. Yallowitz, J. McCormick, S. Lalani, T. Zhang, R. Xu, N. Li,

8. Bibliography

- Y. Liu, Y.S. Yang, M. Eiseman, Discovery of a periosteal stem cell mediating intramembranous bone formation, *Nature* 562(7725) (2018) 133.
- [149] D. Alexander, M. Rieger, C. Klein, N. Ardjomandi, S. Reinert, Selection of osteoprogenitors from the jaw periosteum by a specific animal-free culture medium, *PloS one* 8(12) (2013) e81674.
- [150] J. Dai, D. Rottau, F. Kohler, S. Reinert, D. Alexander, Effects of Jaw Periosteal Cells on Dendritic Cell Maturation, *Journal of clinical medicine* 7(10) (2018) 312.
- [151] D. Alexander, F. Schäfer, M. Olbrich, B. Friedrich, H.-J. Bühring, J. Hoffmann, S. Reinert, MSCA-1/TNAP selection of human jaw periosteal cells improves their mineralization capacity, *Cellular Physiology and Biochemistry* 26(6) (2010) 1073-1080.
- [152] Y. Wanner, F. Umrath, M. Waidmann, S. Reinert, D. Alexander, Platelet Lysate: The Better Choice for Jaw Periosteal Cell Mineralization, *Stem cells international* 2017 (2017).
- [153] N. Kirkland, N. Birbilis, M. Staiger, Assessing the corrosion of biodegradable magnesium implants: a critical review of current methodologies and their limitations, *Acta biomaterialia* 8(3) (2012) 925-936.
- [154] A.F. Cipriano, A. Sallee, R.-G. Guan, Z.-Y. Zhao, M. Tayoba, J. Sanchez, H. Liu, Investigation of magnesium–zinc–calcium alloys and bone marrow derived mesenchymal stem cell response in direct culture, *Acta biomaterialia* 12 (2015) 298-321.
- [155] A.F. Cipriano, A. Sallee, M. Tayoba, M.C.C. Alcaraz, A. Lin, R.-G. Guan, Z.-Y. Zhao, H. Liu, Cytocompatibility and early inflammatory response of human endothelial cells in direct culture with Mg-Zn-Sr alloys, *Acta biomaterialia* 48 (2017) 499-520.
- [156] P. Li, C. Schille, E. Schweizer, E. Kimmerle-Müller, F. Rupp, A. Heiss, C. Legner, U.E. Klotz, J. Geis-Gerstorfer, L. Scheideler, Selection of extraction medium influences cytotoxicity of zinc and its alloys, *Acta Biomaterialia* (2019) doi.org/10.1016/j.actbio.2019.03.013.
- [157] B.J. Luthringer, R. Willumeit-Römer, Effects of magnesium degradation products on mesenchymal stem cell fate and osteoblastogenesis, *Gene* 575(1) (2016) 9-20.
- [158] D. Maradze, D. Musson, Y. Zheng, J. Cornish, M. Lewis, Y. Liu, High magnesium corrosion rate has an effect on osteoclast and mesenchymal stem cell role during bone remodelling, *Scientific reports* 8 (2018).
- [159] D. Alexander, R. Biller, M. Rieger, N. Ardjomandi, S. Reinert, Phenotypic characterization of a human immortalized cranial periosteal cell line, *Cell Physiol Biochem* 35(6) (2015) 2244-54.
- [160] ISO 8407: 2009. Corrosion of metals and alloys–Removal of corrosion products from corrosion test specimens; International Organization for Standardization: Geneva, Switzerland, 2009.

8. Bibliography

- [161] ASTM G31-12a. Standard Guide for Laboratory Immersion Corrosion Testing of Metals; American Section of the International Association for Testing Materials: West Conshohocken, PA, USA, 2017.
- [162] H. Hermawan, Updates on the research and development of absorbable metals for biomedical applications, *Progress in biomaterials* 7(2) (2018) 93-110.
- [163] R.-Q. Hou, N. Scharnagl, R. Willumeit-Römer, F. Feyerabend, Different effects of single protein vs. protein mixtures on magnesium degradation under cell culture conditions, *Acta biomaterialia* (2019) doi.org/10.1016/j.actbio.2019.02.013.
- [164] R. Hou, R. Willumeit-Römer, V.M. Garamus, M. Frant, J. Koll, F. Feyerabend, Adsorption of Proteins on Degradable Magnesium—Which Factors are Relevant?, *ACS applied materials & interfaces* 10(49) (2018) 42175-42185.
- [165] X. Liu, H. Yang, Y. Liu, P. Xiong, H. Guo, H.-H. Huang, Y. Zheng, Comparative Studies on Degradation Behavior of Pure Zinc in Various Simulated Body Fluids, *JOM* 71(4) (2019) 1414-1425.
- [166] M. Schinhammer, J. Hofstetter, C. Wegmann, F. Moszner, J.F. Löffler, P.J. Uggowitzer, On the immersion testing of degradable implant materials in simulated body fluid: active pH regulation using CO₂, *Advanced engineering materials* 15(6) (2013) 434-441.
- [167] G.T. Technical Resources - Media Formulations: DMEM/F-12, Available online: <https://www.thermofisher.com/de/de/home/technical-resources/media-formulation.216.html> (accessed on 22 October 2018).
- [168] J. Fischer, D. Pröfrock, N. Hort, R. Willumeit, F. Feyerabend, Improved cytotoxicity testing of magnesium materials, *Materials Science and Engineering: B* 176(20) (2011) 1773-1777.
- [169] O. Jung, R. Smeets, P. Hartjen, R. Schnettler, F. Feyerabend, M. Klein, N. Wegner, F. Walther, D. Stangier, A. Henningsen, Improved In Vitro Test Procedure for Full Assessment of the Cytocompatibility of Degradable Magnesium Based on ISO 10993-5/-12, *International journal of molecular sciences* 20(2) (2019) 255.
- [170] Y. Zhang, Y. Yan, X. Xu, Y. Lu, L. Chen, D. Li, Y. Dai, Y. Kang, K. Yu, Investigation on the microstructure, mechanical properties, in vitro degradation behavior and biocompatibility of newly developed Zn-0.8% Li-(Mg, Ag) alloys for guided bone regeneration, *Materials Science and Engineering: C* 99 (2019) 1021-1034.
- [171] T. Ren, X. Gao, C. Xu, L. Yang, P. Guo, H. Liu, Y. Chen, W. Sun, Z. Song, Evaluation of as-extruded ternary Zn–Mg–Zr alloys for biomedical implantation material: In vitro and in vivo behavior, *Materials and Corrosion* 70(6) (2019) 1056-1070.
- [172] Y. Yang, F. Yuan, C. Gao, P. Feng, L. Xue, S. He, C. Shuai, A combined strategy to enhance the properties of Zn by laser rapid solidification and laser alloying, *Journal of the mechanical behavior of biomedical materials* 82 (2018) 51-60.

8. Bibliography

- [173] W. Yuan, B. Li, D. Chen, D. Zhu, Y. Han, Y. Zheng, Formation Mechanism, Corrosion Behavior, and Cytocompatibility of Microarc Oxidation Coating on Absorbable High-Purity Zinc, *ACS Biomaterials Science & Engineering* 5(2) (2018) 453-467.
- [174] Y. Zhang, J. Xu, Y.C. Ruan, M.K. Yu, M. O'Laughlin, H. Wise, D. Chen, L. Tian, D. Shi, J. Wang, Implant-derived magnesium induces local neuronal production of CGRP to improve bone-fracture healing in rats, *Nature Medicine* 22(10) (2016) 1160-1169.
- [175] K. Yusa, O. Yamamoto, M. Fukuda, S. Koyota, Y. Koizumi, T. Sugiyama, In vitro prominent bone regeneration by release zinc ion from Zn-modified implant, *Biochemical and biophysical research communications* 412(2) (2011) 273-278.
- [176] W. Liu, J. Li, M. Cheng, Q. Wang, K.W. Yeung, P.K. Chu, X. Zhang, Zinc-Modified Sulfonated Polyetheretherketone Surface with Immunomodulatory Function for Guiding Cell Fate and Bone Regeneration, *Advanced Science* 5(10) (2018) 1800749.
- [177] D. Zhu, Y. Su, M.L. Young, J. Ma, Y. Zheng, L. Tang, Biological responses and mechanisms of human bone marrow mesenchymal stem cells to Zn and Mg biomaterials, *ACS Applied Materials & Interfaces* 9(33) (2017) 27453-27461.
- [178] E.R. Shearier, P.K. Bowen, W. He, A. Drelich, J. Drelich, J. Goldman, F. Zhao, In vitro cytotoxicity, adhesion, and proliferation of human vascular cells exposed to zinc, *ACS biomaterials science & engineering* 2(4) (2016) 634-642.
- [179] L. Liu, Y. Meng, A.A. Volinsky, H.-J. Zhang, L.-N. Wang, Influences of albumin on in vitro corrosion of pure Zn in artificial plasma, *Corrosion Science* 153 (2019) 341-356.
- [180] M.W. Hall, N. Singh, K.F. Ng, D.K. Lam, M.B. Goldberg, H.C. Tenenbaum, J.D. Neufeld, R.G. Beiko, D.B. Senadheera, Inter-personal diversity and temporal dynamics of dental, tongue, and salivary microbiota in the healthy oral cavity, *NPJ biofilms and microbiomes* 3(1) (2017) 2.
- [181] C. Loo, D. Corliss, N. Ganeshkumar, *Streptococcus gordonii* biofilm formation: identification of genes that code for biofilm phenotypes, *Journal of bacteriology* 182(5) (2000) 1374-1382.
- [182] Y.-W. Wang, A. Cao, Y. Jiang, X. Zhang, J.-H. Liu, Y. Liu, H. Wang, Superior antibacterial activity of zinc oxide/graphene oxide composites originating from high zinc concentration localized around bacteria, *ACS applied materials & interfaces* 6(4) (2014) 2791-2798.
- [183] M. Rai, A. Yadav, A. Gade, Silver nanoparticles as a new generation of antimicrobials, *Biotechnology advances* 27(1) (2009) 76-83.
- [184] A. Russell, W. Hugo, Antimicrobial activity and action of silver, *Progress in medicinal chemistry*, Elsevier 1994, pp. 351-370.
- [185] E.K. Brooks, R. Ahn, M.E. Tobias, L.A. Hansen, N.R. Luke-Marshall, L. Wild, A.A. Campagnari, M.T. Ehrensberger, Magnesium alloy AZ91 exhibits antimicrobial properties in vitro but not in vivo, *Journal of Biomedical Materials Research Part B: Applied Biomaterials* 106(1) (2018) 221-227.

9. Declaration of contribution of others

9. Declaration of contribution of others



Medizinische Fakultät

Version April 2019

Declaration of contribution of all authors:

Herewith I, Ping Li declare, that I have contributed to the major part of the following publication: Mechanical characteristics, in vitro degradation, cytotoxicity, and antibacterial evaluation of Zn-4.0 Ag alloy as a biodegradable material. International journal of molecular sciences, (2018) 19(3), 755.

The authors contributed to the publications as indicated in the following table (indicated in %):

Contribution	Research concept	Selection of methods	Data acquisition	Results interpretation	Manuscript preparation
Ping Li	15	15	30	30	25
Christine Schille	5	10	10	5	5
Ernst Schweizer	5	10	10	5	5
Frank Rupp	10	5	5	5	5
Alexander Heiss	15	15	20	20	20
Claudia Legner	5	5	5	5	5
Ulrich E. Klotz	10	10	5	10	5
Jürgen Geis-Gerstorfer	20	15	5	10	10
Lutz Scheideler	15	15	10	10	20

Signature of the doctoral candidate

Ping Li

As supervisor, I agree with the declarations by the candidate:

J. Geis

As corresponding author, agree with the declarations by the candidate:

L. Scheideler

As co-authors, we agree to the declarations above:

C. Schille

[Christine Schille]

E. Schweizer

[Ernst Schweizer]

F. Rupp

[Frank Rupp]

A. Heiß

[Alexander Heiss]

C. Legner

[Claudia Legner]

U. Klotz

[Ulrich E. Klotz]

J. Geis-Gerstorfer

[Jürgen Geis-Gerstorfer]

L. Scheideler

[Lutz Scheideler]

9. Declaration of contribution of others



Declaration of contribution of all authors:

Herewith I, Ping LI declare, that I have contributed to the major part of the following publication: Selection of extraction medium influences cytotoxicity of zinc and its alloys. Acta Biomaterialia (2019) Accepted, DOI: 10.1016/j.actbio.2019.03.013.

The authors contributed to the publications as indicated in the following table (indicated in %):

Contribution	Research concept	Selection of methods	Data acquisition	Results Interpretation	Manuscript preparation
Ping Li	20	25	35	30	25
Christine Schille	5	5	5	5	5
Ernst Schweizer	5	15	15	5	5
Evi Kimmerte-Müller	10	10	10	5	5
Frank Rupp	15	10	5	10	5
Alexander Heiss	5	5	10	5	10
Claudia Legner	5	5	5	5	5
Ulrich E. Klotz	5	5	5	5	5
Jürgen Geis-Gerstorfer	15	10	5	10	15
Lutz Scheideler	15	10	5	20	20

Signature of the doctoral candidate

Ping Li

As supervisor, I agree with the declarations by the candidate:

J. Geis

As corresponding author, agree with the declarations by the candidate:

L. Scheideler

As co-authors, we agree to the declarations above:

C. Schille

[Christine Schille]

Ernst Schweizer

[Ernst Schweizer]

Evi Kimmerte-Müller

[Evi Kimmerte-Müller]

F. Rupp

[Frank Rupp]

A. Heiss

[Alexander Heiss]

Claudia Legner

[Claudia Legner]

U. Klotz

J. Geis

L. Scheideler

9. Declaration of contribution of others

Declaration of contribution of all authors:

Herewith I, Ping Li declare, that I have contributed to the major part of the following publication: Response of human periosteal cells to degradation products of zinc and its alloy, under review.

The authors contributed to the publications as indicated in the following table (indicated in %):

Contribution	Research concept	Selection of methods	Data acquisition	Results interpretation	Manuscript preparation
Ping Li	15	20	35	20	20
Jingtao Dai	10	15	20	10	10
Ernst Schweizer	5	5	10	5	5
Frank Rupp	10	5	5	5	5
Alexander Heiss	10	5	5	10	10
Ulrich E. Klotz	5	5	5	5	5
Jürgen Geis-Gerstorfer	15	15	5	15	15
Lutz Scheideler	15	15	10	15	15
Dorothea Alexander	15	15	5	15	15

Signature of the doctoral candidate

Ping Li

As supervisor, I agree with the declarations by the candidate:

J. Geis

As corresponding author, agree with the declarations by the candidate:

Alexander Heiss

As co-authors, we agree to the declarations above:

Jingtao Dai

[Jingtao Dai]

Ernst Schweizer

[Ernst Schweizer]

Frank Rupp

[Frank Rupp]

A Heiss

[Alexander Heiss]

U. Klotz

[Ulrich E. Klotz]

J. Geis

[Jürgen Geis-Gerstorfer]

Lutz Scheideler

[Lutz Scheideler]

Alexander Heiss

[Dorothea Alexander]

Acknowledgements

Acknowledgements

I would like to express my deep gratitude to my supervisor, Prof. Dr. Jürgen Geis-Gerstorfer, for giving me a great opportunity to be his student, for his great guidance and constructive suggestions with me so generously. I would also like to appreciate my doctoral committee members, Prof. Dr. Dorothea Alexander and Prof. Dr. Katja Schenke-Layland, for the so precious time and professional advice. My sincere gratitude to Prof. Dr. Dorothea Alexander for your help and support with the investigation of Zn osteoinductivity.

I am particularly grateful for the continuous support given by Dr. Lutz Scheideler, for fruitful discussions and helpful guidance in my scientific writing. I would like to thank Prof. Dr. Frank Rupp for his willingness to share his innovative ideas and scientific insight.

I acknowledge my sincere gratitude to all of my colleagues in the MWT Ms. Christine Schille, Mr. Ernst Schweizer, Mr. Sebastian Spintzyk, and Ms. Evi Kimmerle-Müller, who patiently give me the help in the technical assistance. I also wish to thank my Chinese colleagues, Mr. Yichen Xu, Ms. Xingting Han and Ms. Zeqian Xu, for the fun and memorable time we had in the MWT.

I would also like to thank Dr. Alexander Heiss, Dr. Ulrich E. Klotz and Ms. Claudia Legner from the fem Forschungsinstitut Edelmetalle & Metallchemie for their co-initiate the research project and fruitful cooperation.

I am deeply grateful to my beloved wife, Jingtao Dai, for her unconditional love and endless support. I am also grateful to my parents, my sister and my young brother for their encouragement and understanding in every way.

Curriculum Vitae

Curriculum vitae

Personal Information:

Name: Ping Li

Gender: Male

Date of birth: August 1988

Nationality: Chinese

Education:

June 2012 Bachelor's degree, Anhui Medical University, China.

June 2015 Master's degree, Jinan University, China.

Since October 2016 PhD degree, University of Tübingen, Germany.

Scholarships:

Scholarship from the Jinan University, 2015.

Scholarship from the Chinese Scholarship Council, 2016-2019.

Scholarship from the German Academic Exchange Service (DAAD), 2018-2019.

Certificates:

Dental practitioner's qualification certificate of China (licensed since 2012).

Full list of publications:

Ping Li, Christine Schille, Ernst Schweizer, Frank Rupp, Alexander Heiss, Claudia Legner, Ulrich E. Klotz, Jürgen Geis-Gerstorfer, Lutz Scheideler. *Mechanical characteristics, in vitro degradation, cytotoxicity, and antibacterial evaluation of Zn-4.0 Ag alloy as a biodegradable material*. International journal of molecular sciences, (2018) 19(3), 755.

Ping Li, Christine Schille, Ernst Schweizer, Evi Kimmerle-Müller, Frank Rupp, Alexander Heiss, Claudia Legner, Ulrich E. Klotz, Jürgen Geis-Gerstorfer, Lutz Scheideler. *Selection of extraction medium influences cytotoxicity of zinc and its alloys*. Acta Biomaterialia 98 (2019): 235-245.

Curriculum Vitae

Ping Li, Jingtao Dai, Ernst Schweizer, Frank Rupp, Alexander Heiss, Ulrich E. Klotz, Jürgen Geis-Gerstorfer, Lutz Scheideler, Dorothea Alexander. *Response of human periosteal cells to degradation products of zinc and its alloy*, Materials Science and Engineering: C 108 (2020): 110208.

Ping Li, Wentai Zhang, Jingtao Dai, Alexander Basileos Xepapadeas, Ernst Schweizer, Dorothea Alexander, Lutz Scheideler, Chao Zhou, Haijun Zhang, Guojiang Wan, Jürgen Geis-Gerstorfer. *Investigation of zinc-copper alloys as potential materials for craniomaxillofacial osteosynthesis implants*. Materials Science and Engineering: C, 2019 (103) : 109826..

Ping Li, Christine Schille, Ernst Schweizer, Evi Kimmerle-Müller, Frank Rupp, Xingting Han, Alexander Heiss, Andreas Richter, Claudia Legner, Ulrich E. Klotz, Jürgen Geis-Gerstorfer, Lutz Scheideler. *Evaluation of a Zn-2Ag-1.8 Au-0.2 V Alloy for Absorbable Biocompatible Materials*. Materials, 2020, 13(1): 56.

Academic Activities:

Oral presentation of “Effect of fetal bovine serum on *in vitro* degradation behaviour and cytotoxicity of Zn and Zn alloys” 10th Symposium on Biodegradable Metals, Oxford, UK, 2018.

Poster presentation of “*In vitro* corrosion behavior, cytotoxicity and antibacterial properties of Zn-2Ag-1.8Au-0.2V alloy” 10th Symposium on Biodegradable Metals, Oxford, UK, 2018.

Poster presentation of “Cytotoxicity evaluation of biodegradable Zn-4Cu alloy using L929, Saos-2 and TAg cell lines” 5th Euro BioMAT, Weimar, Germany, 2019.

Oral presentation of “Response of human periosteal cells on zinc or zinc-silver alloy extracts” 11th Symposium on Biodegradable Metals, Alicante, Spain, 2019.

Oral presentation of “Effect of sandblasting treatment on *in vitro* degradation behavior and cytotoxicity of zinc and its alloys” 30th Annual Conference of the European Society for Biomaterials, Dresden, Germany, 2019.